Investigations on microwave-assisted freeze-drying

Zur Erlangung des akademischen Grades eines

DOKTORS DER INGENIEURWISSENSCHAFTEN
(Dr.-Ing.)

von der KIT-Fakultät für Chemieingenieurwesen und Verfahrenstechnik des Karlsruher Instituts für Technologie (KIT)

genehmigte

DISSERTATION

von

M.Sc. Till Alexander Kaysan
aus Hamm

Tag der mündlichen Prüfung:	14.11.2025
Erstgutachter:	PD Dr. rer. nat. Volker Gaukel
Zweitgutachterin:	apl. Prof. Dr. Gisela Guthausen

“No man is an island.”
— *John Donne*

Abstract

Freeze-drying (FD) is a well-established process for preserving heat-sensitive materials. FD is widely used in the food and pharmaceutical industries because it provides high-quality products. However, conventional freeze-drying (CFD) is characterized by lengthy drying times and high energy consumption, which lead to elevated production costs. These limitations have prompted the exploration of process intensification techniques to increase efficiency without compromising product quality.

Microwave-assisted freeze-drying (MFD) emerges as a promising alternative to CFD. In MFD, microwave energy is used to supply the sublimation enthalpy directly within the product through interactions between the microwaves and the material to be dried. This direct energy input can potentially reduce drying durations and energy usage. However, MFD is a process that faces several major challenges. The electromagnetic field is inherently inhomogeneous, leading to the formation of hot spots that have the potential to cause damage to the product. The low operating pressures that are characteristic of MFD promote arcing within the process chamber. This has the potential to result in both energy waste and damage to both the product and the equipment. Furthermore, as drying progresses in MFD, the dielectric properties of the material being dried decrease. This relation renders the coupling of microwave power to the product progressively inefficient, particularly in the later stages of MFD.

Solid-state microwave generators (SSGs) provide a potential solution to these challenges through the precise and fast modulation of the microwave parameters frequency, power, and phase shift. The precise microwave control may be used to optimize the process.

This thesis investigates the optimization of the MFD process based on the use of SSGs. The research focuses on process development, understanding, and optimization. Process optimization aims to increase energy efficiency and drying homogeneity and to shorten drying duration. At the same time, MFD must yield product quality comparable to that of CFD. The work is structured into four main chapters, each addressing different aspects of MFD.

Chapter 2 details the design and construction of a laboratory-scale drying system capable of performing MFD and CFD within the same process chamber. The modular setup includes an SSG that allows for precise control over microwave parameters, enabling the exploration of frequency-based control concepts. The system is equipped with sensors to monitor critical process parameters, such as product temperature, chamber pressure, and microwave power.

Successful MFD and CFD commissioning experiments validated the design and functionality of the system. In MFD, the integration of an SSG enabled the application of microwaves at well-defined frequencies. The extensive process monitoring provided valuable data on sample weight and energy utilization during MFD, laying a solid foundation for subsequent process optimization. One limitation of the system is the frequency-dependent forward power of the SSG, which must be considered when evaluating the results. The constraint can be addressed by analyzing the energy efficiency of converting electromagnetic energy into heat as a normalized parameter.

Resonant frequencies (RFs) are associated with local maxima in the frequency-dependent energy efficiency and distinct patterns of the microwave field. The results from the MFD commissioning experiment revealed a shift of RFs to higher frequencies during drying, indicating changes in the electromagnetic field distribution due to the changing product state. These findings underscore the importance of adjusting microwave frequencies throughout MFD to maintain high energy efficiency. Characterizations of the microwave reflections at progressive drying states confirmed the shift of RFs to higher frequencies.

In Chapter 3, electromagnetic simulations were performed to investigate frequency-based control concepts for MFD. The simulations were decoupled from solving

thermodynamic equations by representing discrete drying states. This approach allowed for analyzing how different frequencies affect energy efficiency and power distribution among and within the samples.

Four control concepts with the application of different frequencies were evaluated:

1. **Single Minimum Frequency (1MF):** Frequency with the lowest energy efficiency,
2. **Single Resonant Frequency (1RF):** Resonant frequency with the highest energy efficiency,
3. **Six Equidistant Frequencies (6EF):** Six frequencies evenly spaced between 2400 MHz and 2500 MHz, and
4. **Six Resonant Frequencies (6RF or $6RF_{max}$):** Six resonant frequencies with the highest local maxima of energy efficiency.

The simulation results indicate that the application of RFs (1RF and 6RF) increases the energy efficiency throughout drying. The use of multiple frequencies (6EF and 6RF) achieves a more homogeneous power distribution among the samples, indicating an increasing drying homogeneity. The validation of the simulations with measurements of the frequency-dependent energy efficiency resulted in quantitative differences. However, qualitative similarities were observed regarding the number and energy efficiency of RFs, making the simulations a valuable tool for process development. MFD experiments of the initial drying stage with constant frequencies confirmed increased energy efficiency when applying RFs and increased drying homogeneity at similar dissipated power when using multiple frequencies.

Chapter 4 introduces a time-saving approach for parameter studies of MFD using partial drying. By terminating the drying process after removing 20% of the initial water content, the time required for an MFD experiment was reduced by approximately 92% compared to complete drying. This approach enables efficient investigation of process parameters, focusing on their influence on drying kinetics and homogeneity.

Parameter studies with partial MFD revealed the following effects:

- **Microwave frequency:** Targeted application of energy-efficient RFs shortened the process duration and increased energy efficiency, as expected from the literature.
- **Microwave power:** Increasing the specific dissipated microwave power reduced process duration in accordance with expectations from existing literature.
- **Chamber pressure:** Contrary to some reports in literature, reducing the chamber pressure in partial MFD led to shorter process durations due to increased sublimation before microwave application and higher drying rates.

The use of multiple frequencies increased drying homogeneity among samples, while neither chamber pressure nor microwave power notably affected it. The study confirms that partial MFD is an effective tool for investigating the influence of microwave power and frequency on drying kinetics and homogeneity. On the other hand, partial MFD may not fully capture the effects of chamber pressure since mass transfer limitations through the thin dried layer are not representative of complete drying. Partial MFD remains a potent tool for fast process investigation when the limitations of its application are considered.

Chapter 5 focuses on optimizing MFD by implementing real-time frequency modulation based on the product state. An algorithm was developed to continuously identify and apply multiple RFs throughout drying. This procedure enabled adaptive control that maintained high energy efficiency.

Comparative experiments between CFD and MFD using the previously introduced control concepts 6EF and $6RF_{max}$ as well as $6RF_{min}$, in which the six RFs with the lowest energy efficiency were applied, and 1CF, in which 2460 MHz was applied, yielded the following results:

- The application of multiple real-time adjusted RFs in MFD with $6RF_{max}$ resulted in the highest average energy efficiency and drying rate.

- MFD using $6RF_{max}$ reduced the process duration by 24.2% compared to CFD and by 38.4% compared to MFD with 6EF.
- Each frequency adjustment during MFD directly affected energy efficiency, sample temperature, and drying rate.

Product quality assessment showed that all MFD control concepts achieved similar levels of residual moisture content and ascorbic acid retention compared to CFD. However, the formation of large pores observed in some MFD samples underscores the need for further optimization to minimize product damage. Nonetheless, MFD using RFs demonstrated its potential as a rapid and energy-efficient alternative to commonly used CFD.

The research successfully demonstrates that targeted modulation of microwave frequency, particularly through the application of multiple RFs adjusted in real-time, can intensify MFD by increasing energy efficiency, reducing process duration, and increasing drying homogeneity. The intensified MFD process shows promise as an efficient method for drying heat-sensitive materials while maintaining product quality comparable to that of CFD.

Future work could focus on refining frequency control algorithms. Artificial intelligence could be used to optimize control strategies based on extensive experimental data sets. Integrating additional input variables, such as real-time sample temperature and weight measurements, could further increase the adaptability of the process and help to prevent product damage.

Expanding the system capabilities by installing multiple SSGs would enable studies on phase shifts and simultaneous application of multiple frequencies, offering more extensive control over the electromagnetic field. In addition, investigating the applicability of optimized MFD processes for industrially relevant products and addressing scale-up challenges are essential steps toward industrial implementation.

In conclusion, this work provides valuable insights into the optimization of MFD through targeted frequency modulation. These results pave the way for future advances in MFD technology, offering potential benefits such as energy savings

and reduced process durations while achieving product quality that meets the high standards of products from CFD.

Kurzfassung

Die Gefriertrocknung (engl. *freeze-drying*, FD) ist ein etabliertes Verfahren zur Konservierung wärmeempfindlicher Produkte und wird aufgrund der hohen Produktqualität häufig in der Lebensmittel- und Pharmaindustrie eingesetzt. Die konventionelle Gefriertrocknung (engl. *conventional freeze-drying*, CFD) ist jedoch mit langen Trocknungszeiten und einem hohen Energieverbrauch verbunden, was zu erhöhten Produktionskosten führt. Diese Einschränkungen der FD machen die Forschung zur Prozessintensivierung relevant. Das Ziel besteht darin, die Prozesseffizienz zu steigern, ohne die Produktqualität zu beeinträchtigen.

Die mikrowellenunterstützte Gefriertrocknung (engl. *microwave-assisted freeze-drying*, MFD) stellt eine vielversprechende Alternative zur CFD dar. In der MFD wird Mikrowellenenergie eingesetzt, um die Sublimationsenthalpie durch Wechselwirkungen zwischen den Mikrowellen und dem Trockengut direkt im Produkt einzubringen. Diese direkte Energiezufuhr hat das Potenzial die Trocknungsdauer und den Energieverbrauch zu reduzieren. Allerdings ist die MFD mit mehreren Herausforderungen verbunden. Das elektromagnetische Feld ist von Natur aus inhomogen, was zur Bildung von thermischen Hot Spots führt, die das Produkt beschädigen können. Die für die MFD charakteristischen niedrigen Betriebsdrücke begünstigen die Entstehung von Lichtbögen in der Prozesskammer. Dies kann sowohl zu einem überflüssigen Energieverbrauch als auch zu Schäden am Produkt und an der Anlage führen. Zudem nehmen mit fortschreitender Trocknung die dielektrischen Eigenschaften des getrockneten Materials ab. Dies führt dazu, dass die Einkopplung der Mikrowellenleistung in das Produkt zunehmend ineffizient wird, insbesondere in den späteren Phasen der MFD.

Halbleiterbasierte Mikrowellengeneratoren (engl. *solid-state microwave generators*, SSGs) bieten eine potenzielle Lösung für diese Herausforderungen, indem sie eine präzise und schnelle Modulation der Mikrowellenparameter Frequenz, Leistung und Phasenverschiebung ermöglichen. Die genaue Mikrowellensteuerung kann zur Prozessoptimierung genutzt werden.

Diese Arbeit untersucht die Optimierung der MFD auf der Grundlage der Verwendung von SSGs. Die Forschungsarbeit fokussiert sich auf die Themen Prozessentwicklung, Prozessverständnis und Prozessoptimierung. Die Prozessoptimierung zielt darauf ab, die Energieeffizienz und die Trocknungshomogenität zu erhöhen und die Trocknungsdauer zu verkürzen. Gleichzeitig muss mittels der MFD eine Produktqualität erzielen, die mit der Qualität aus der CFD vergleichbar ist. Die Arbeit gliedert sich in vier Hauptkapitel, die sich jeweils mit verschiedenen Aspekten der MFD befassen.

Kapitel 2 beschreibt das Design und den Aufbau einer Trocknungsanlage im Labormaßstab, in der sowohl MFD als auch CFD innerhalb derselben Prozesskammer durchgeführt werden können. Die modulare Anlage ist mit einem SSG ausgestattet, der eine präzise Steuerung der Mikrowellenparameter und die Untersuchung frequenzbasierter Regelkonzepte ermöglicht. Die Anlage ist mit einer Reihe von Sensoren ausgestattet, die eine Überwachung kritischer Prozessparameter, wie Produkttemperatur, Kammerdruck und Mikrowellenleistung, ermöglichen.

In erfolgreichen MFD- und CFD-Experimenten zur Inbetriebnahme wurde die Funktionalität der Anlage validiert. Die Integration eines SSG ermöglichte in der MFD die Anwendung von Mikrowellen mit definierten Frequenzen. Die umfassende Sensorik lieferte Daten zum Probengewicht und Energienutzung in der MFD. Dies stellt eine Grundlage für die anschließende Prozessoptimierung dar. Eine Einschränkung des Systems ist die frequenzabhängige Vorwärtsleistung des SSG, die bei der Auswertung der Ergebnisse berücksichtigt werden muss. Dies kann durch die Analyse der Energieeffizienz als normierten Parameter umgesetzt werden.

Resonanzfrequenzen (engl. *resonant frequencies*, RFs) sind mit lokalen Maxima der frequenzabhängigen Energieeffizienz und charakteristischen Mustern des Mikrowellenfeldes verbunden. Die Ergebnisse aus der Inbetriebnahme der MFD zeigen eine Verschiebung der RFs zu höheren Frequenzen während der MFD, was auf Änderungen in der elektromagnetischen Feldverteilung aufgrund des zeitlich variablen Produktzustands hinweist. Diese Erkenntnisse unterstreichen die Bedeutung der Anpassung der Mikrowellenfrequenzen während der MFD zur Erzielung einer durchgängig hohen Energieeffizienz. Die Verschiebung der RFs zu höheren Frequenzen wurde durch Charakterisierungen der Mikrowellenreflexionen bei fortschreitenden Trocknungszuständen bestätigt.

In Kapitel 3 wurden frequenzbasierte Regelkonzepte für die MFD mittels elektromagnetischer Simulationen untersucht. Die Simulationen wurden durch die getrennte Simulation diskreter Trocknungszustände von der Lösung thermodynamischer Gleichungen entkoppelt. Dieser Ansatz ermöglichte eine Analyse des Einflusses der Frequenzen auf die Energieeffizienz und Leistungsverteilung zwischen und innerhalb den Proben.

Vier Regelkonzepte mit der Anwendung verschiedener Frequenzen wurden untersucht:

1. **Single Minimum Frequency (1MF):** Frequenz mit der geringsten Energieeffizienz,
2. **Single Resonant Frequency (1RF):** Resonante Frequenz mit der höchsten Energieeffizienz,
3. **Six Equidistant Frequencies (6EF):** Sechs gleichmäßig verteilte Frequenzen in konstanten Intervallen zwischen 2400 MHz und 2500 MHz und
4. **Six Resonant Frequencies (6RF oder $\mathbf{6RF_{max}}$):** Sechs resonante Frequenzen mit den höchsten lokalen Maxima der Energieeffizienz.

Die Simulationsergebnisse zeigen einer Erhöhung der Energieeffizienz während des gesamten Trocknungsprozesses durch die Anwendung der RFs (1RF und 6RF). Durch den Einsatz mehrerer Frequenzen (6EF und 6RF) wurde eine homogenere

Leistungsverteilung unter den Proben erzielt, was auf eine erhöhte Trocknungshomogenität hinweist. Die Validierung der Simulationen mittels der frequenzabhängigen Energieeffizienz ergab quantitative Diskrepanzen. Es wurden jedoch qualitative Ähnlichkeiten hinsichtlich der Anzahl und Energieeffizienz der RFs festgestellt. Dies macht die Simulationen zu einem nützlichen Werkzeug für die Prozessentwicklung. Experimentelle Ergebnisse aus der Anfangsphase der MFD bei konstanten Frequenzen bestätigten eine höhere Energieeffizienz bei der Applikation von RFs und eine höhere Homogenität der Trocknung unter Verwendung mehrerer Frequenzen bei ähnlicher Verlustleistung.

In Kapitel 4 wird die Partialtrocknung als ein zeitsparender Ansatz für die Durchführung von Parameterstudien zur MFD vorgestellt. Durch das Beenden des Trocknungsprozesses nach der Entfernung von 20 % des anfänglichen Wassergehalts wird die erforderliche Zeit für ein MFD-Experiment im Vergleich zur vollständigen Trocknung um etwa 92 % reduziert. Dieser Ansatz ermöglicht eine effiziente Untersuchung einflussreicher Prozessparametern. Der Fokus der Untersuchungen liegt auf dem Einfluss der Parameter auf die Trocknungskinetik und -homogenität.

Die Parameterstudien zeigten die folgenden Effekte unter Einsatz der partiellen MFD:

- **Mikrowellenfrequenz:** Die gezielte Anwendung energieeffizienter RFs verkürzte die Prozessdauer und erhöhte die Energieeffizienz, wie aus der Literatur erwartet wurde.
- **Mikrowellenleistung:** Die Erhöhung der spezifisch dissipierten Mikrowellenleistung verkürzte die Prozessdauer entsprechend den Erwartungen aus der bestehenden Literatur.
- **Kammerdruck:** In Widerspruch zur Literatur führte die Verringerung des Kammerdrucks in der partiellen MFD zu kürzeren Prozessdauern aufgrund erhöhter Sublimation vor der Mikrowellenapplikation und höherer Trocknungsraten.

Der Einsatz mehrerer Frequenzen erhöhte die Trocknungshomogenität unter den Proben, während weder Kammerdruck noch Mikrowellenleistung die Trocknungshomogenität beeinflussten. Die partielle MFD ist ein effektives Mittel zur Untersuchung des Einflusses von Mikrowellenleistung und -frequenz auf Trocknungskinetik und -homogenität. Andererseits kann die partielle MFD die Auswirkungen des Kammerdrucks nicht vollständig erfassen, da die Limitierungen des Massentransfers durch die dünne Schicht getrockneten Produkts nicht repräsentativ für die vollständige Trocknung sind. Die partielle MFD ist dennoch ein wirksames Werkzeug für schnelle Prozessuntersuchungen, sofern die Grenzen ihrer Anwendbarkeit berücksichtigt werden.

Kapitel 5 konzentriert sich auf die Optimierung der MFD durch Implementierung einer Frequenzmodulation in Echtzeit basierend auf dem Produktzustand. Es wurde ein Algorithmus zur Prozesssteuerung entwickelt, um während des Trocknungsprozesses kontinuierlich mehrere RFs automatisiert zu identifizieren und anzuwenden. Dieses Verfahren ermöglichte eine adaptive Steuerung zur Erzielung einer hohen Energieeffizienz.

Vergleichende Experimente zwischen CFD und MFD unter Verwendung der zuvor vorgestellten Steuerungskonzepte 6EF und $6RF_{max}$ sowie $6RF_{min}$, bei dem die sechs RFs mit der geringsten Energieeffizienz angewendet wurden, und 1CF, bei dem 2460 MHz angewendet wurde, ergaben folgende Ergebnisse:

- Die Anwendung mehrerer, in Echzeit angepasster RFs in der MFD mit $6RF_{max}$ führte zur höchsten durchschnittlichen Energieeffizienz und Trocknungsrate.
- Die MFD unter Verwendung von $6RF_{max}$ reduzierte die Prozessdauer um 24,2 % im Vergleich zur CFD und um 38,4 % im Vergleich zur MFD mit 6EF.
- Jede Frequenzanpassung während der MFD zeigte einen direkten Einfluss auf die Energieeffizienz, Probentemperatur und Trocknungsrate.

Die Auswertung der Produktqualität zeigte ähnliche Restfeuchtegehalte und Retention von Ascorbinsäure für MFD mit allen Regelkonzepten im Vergleich zur

CFD. Allerdings unterstreicht die Bildung großer Poren, die in einigen Proben aus der MFD detektiert wurde, die Notwendigkeit einer weiteren Optimierung zur Vermeidung von Produktschäden. Nichtsdestotrotz demonstrierte die MFD unter Verwendung von RFs ihr Potenzial als schnelle und energieeffiziente Alternative zur CFD.

In dieser Dissertation wird die erfolgreiche Intensivierung der MFD durch die gezielte Modulation der Mikrowellenfrequenz demonstriert. Insbesondere die Anwendung mehrerer in Echtzeit angepasster RFs resultierte in einer erhöhten Energieeffizienz, einer verkürzten Prozessdauer und einer erhöhten Trocknungshomogenität. Die intensivierte MFD ist eine effektive Methode zur schnellen Trocknung wärmeempfindlicher Materialien, während gleichzeitig eine Produktqualität erzielt wird, die mit Produkten aus der CFD vergleichbar ist.

Zukünftige Arbeiten könnten eine Verfeinerung der Algorithmen zur Frequenzsteuerung untersuchen. So könnte künstliche Intelligenz eingesetzt werden, um die Steuerungsstrategien basierend auf umfangreichen experimentellen Datensätzen zu optimieren. Die Integration zusätzlicher Eingangsvariablen, wie Echtzeitmessungen von Probentemperatur und -gewicht, könnte die Anpassungsfähigkeit des Prozesses erhöhen und zu einer Vermeidung von Produktschäden genutzt werden.

Die Erweiterung der konstruierten Anlage durch die Installation mehrerer SSGs würde Studien zu Phasenverschiebungen und der gleichzeitigen Anwendung mehrerer Frequenzen ermöglichen. Die entsprechende Steuerung könnte zu einer Erweiterung der Kontrolle über das elektromagnetische Feld eingesetzt werden. Darüber hinaus sind die Untersuchung der Anwendbarkeit der optimierten MFD für industriell relevante Produkte und der Maßstabübertragung wesentliche Schritte für eine industrielle Implementation des Verfahrens.

Zusammenfassend liefert diese Arbeit wertvolle Einblicke in die Optimierung der MFD durch gezielte Frequenzmodulation. Diese Ergebnisse ebnen den Weg für zukünftige Fortschritte in der Anwendung der MFD und bieten potenzielle Vorteile wie Energieeinsparungen und verkürzte Prozessdauern, während gleichzeitig eine Produktqualität erreicht wird, die den hohen Standards der Produkte aus der CFD entspricht.

Danksagung

Eine Promotion ist immer eine Gruppenleistung. Hinter jeder Arbeit steht nicht eine einzelne Person, sondern Interaktionen, große und kleine, erwartete und unerwartete. Diese Gespräche und Begegnungen lassen eine Reise entstehen. Sie sind es, die Ideen entstehen, formen und reifen lassen. Und manchmal wird bei einer einzigen Begegnung viel mehr Wissen vermittelt, als man es selbst in einer ganzen Promotion lernen könnte. Diese Arbeit wäre in dieser Form nie ohne eine ganze Reihe von Personen möglich gewesen.

Für die Betreuung meiner Arbeit möchte ich mich bei PD Dr. Volker Gaukel bedanken. Von dir habe ich alle Möglichkeiten bekommen, diese Arbeit gestalten zu können. Vielen Dank für alle Diskussionen vom Piezoelement bis zum Vakuumtrockner und für dein Vertrauen.

Vielen Dank an Prof. Dr. Gisela Guthausen für die Übernahme der Zweitkorrektur dieser Arbeit und die Zusammenarbeit während meiner Promotion. Ich bedanke mich auch bei Prof. Dr.-Ing. Heike Karbstein für die Möglichkeit zur Promotion an Ihrem Institut und die vielen spannenden Diskussionen.

Danke an meine Kolleg*innen am KIT, insbesondere an Markus Fischer und Max Renaud, die so viel Arbeit in die Konstruktion der Versuchsanlage gesteckt haben. Vielen Dank auch an Dr.-Ing. Mario Pauli, ohne dessen Unterstützung im Bereich Mikrowellentechnik große Teile dieser Arbeit nicht möglich gewesen wären. Danke an alle Studierenden, mit denen ich während ihrer Abschlussarbeiten oder als Hilfswissenschaftler*innen zusammenarbeiten durfte: Michel, Maximilian, Lukas, Sebastian, Eric, Lena, Gabriel, Franco, Malte, Judith, Jana, Richy, Xiaoqi, Nils, Nico, Tobias, Anisa, Chiara und Katharina. Ihr habt diese Dissertation durch eure Arbeit mit ermöglicht und so viele Denkanstöße gegeben.

Vielen Dank auch an Isabel Kalinke und Prof. Dr.-Ing. Petra Först für die immer angenehme Zusammenarbeit in unserem gemeinsamen Projekt.

Vielen Dank auch an meine Freunde aus Hamm und Karlsruhe. Es waren die kleinen Momente, Wochenenden unterwegs und großen Urlaube mit euch, die mir auch in der stressigsten Phase der Promotion gezeigt haben, dass es doch nur eine kleine Welt ist, in der man sich im Alltag bewegt.

Danke, Gina. Danke für deine positive, fröhliche und wunderbare Art, die mir jeden Tag zeigt, wie schön das Leben ist. Danke, dass ich mich immer auf dich verlassen kann. Danke für die Unterstützung in Momenten, in denen ich vor lauter Bäumen den Wald nicht mehr gesehen habe. Und nicht zuletzt danke für die Korrekturen und Diskussionen dieser Dissertation.

Vielen Dank an meine Eltern, Gabi und Stefan. Ihr habt mir den Freiraum gegeben, das zu tun, was ich gerne machen möchte, finanziell, bei der Studienwahl und an vielen anderen Stellen. Teilweise hat mich diese Freiheit überfordert und auch in falsche Richtungen geführt. Aber es ist die schönste Art der Überforderung, aus eigenen Fehlern zu lernen und daran wachsen zu können. Danke an meine Brüder, Moritz und Leonard. Ihr seid beide eine Inspiration in eurer Art, wie ihr euer Leben angeht. Auch wenn alle immer sagen, dass wir gleich aussehen, sind es die Unterschiede zwischen uns, aus denen ich so viel mitnehme.

Contents

Acronyms and symbols

Acronyms

1CF	single constant frequency
1MF	single minimum frequency
1RF	single resonant frequency
6EF	six equidistant frequencies
6RF	six resonant frequencies
AA	ascorbic acid
ANOVA	analysis of variance
CFD	conventional freeze-drying
DPs	dielectric properties
FD	freeze-drying
GUI	graphical user interface
IQR	interquartile range
ISM	industrial, medical, and scientific
MFD	microwave-assisted freeze-drying
PEEK	polyether ether ketone
rpm	rounds per minute

RF	resonant frequency
SSG	solid-state microwave generator
SSPA	solid-state power amplifier
TE	transverse electric
TM	transverse magnetic
wt	weight
$\mu - \mathbf{CT}$	micro-computed tomography

Constants

$\mathbf{c}$	speed of light: $299\,792\,458\,\mathrm{m\,s^{-1}}$
$\mathbf{e}$	Euler's number: $2.71828\ldots$
ε_0	vacuum permittivity: $8.85418 \times 10^{-12}\,\mathrm{F\,m^{-1}}$
η_0	vacuum permeability: $1.25664 \times 10^{-6}\,\mathrm{N\,A^{-2}}$
π	Pi: $3.14159\ldots$

Latin symbols and variables

$\vec{\mathbf{B}}$	magnetic flux density (T)
$\mathbf{c}_{\mathrm{spec}}$	molar concentration for species spec (mol m^{-3})
$\mathbf{d}_{\mathrm{p}}$	penetration depth (m)
$\vec{\mathbf{D}}$	electric flux density (A s m^{-2})
$\vec{\mathbf{E}}$	electric field (V m^{-1})
$\mathbf{f}$	frequency (s^{-1})

$\mathbf{f}_{\mathrm{co}}$	cutoff frequency (s^{-1})
$\vec{\mathbf{H}}$	magnetic field (A m^{-1})
$\boldsymbol{i}$	imaginary number (-)
$\vec{\mathbf{I}}$	current density (A m^{-2})
$\mathbf{k}$	sample position (-)
$\mathbf{l}_{\mathbf{mode}}$	number half-sinusoidal variations standing wave along z-axis (-)
$\mathbf{L}$	length (m)
$\mathbf{m}$	mass (kg)
$\boldsymbol{\Delta}\mathbf{m}$	mass difference (kg)
$\dot{\mathbf{m}}$	drying rate (kg s^{-1})
$\mathbf{m}_{\mathbf{mode}}$	number half-sinusoidal variations standing wave along y-axis (-)
$\dot{\mathbf{m}}_{\mathrm{std}}$	standardized drying rate (kg kg^{-1} s^{-1})
$\dot{\mathbf{m}}_{\mathrm{v}}$	mass flow (kg s^{-1})
$\tilde{\mathbf{M}}$	molar mass (kg mol^{-1})
$\mathbf{n}$	total integer number (-)
$\mathbf{n}_{\mathbf{mode}}$	number half-sinusoidal variations standing wave along x-axis (-)
$\mathbf{NPA}$	normalized power absorption (-)
$\mathbf{p}$	pressure (Pa)
$\mathbf{P}$	power (W)
$\mathbf{P}_{\mathrm{A}}$	absorbed power per unit volume (W m^{-3})
$\dot{\mathbf{Q}}$	heat flow (W)
$\mathbf{r}$	radius (m)

$\mathbf{r}_{\mathrm{on}}$	activation ratio (-)
$\mathbf{R}$	mass-transfer resistance (Pa s kg^{-1})
$\mathbf{R^2}$	coefficient of determination (-)
$\Re$	real-part operator (-)
$\mathbf{S}_{11}$	scattering parameter (-)
$\mathbf{S}_{\mathrm{LC}}$	load-cell signal (-)
$\mathbf{t}$	time (s)
$\mathbf{U}$	voltage (V)
$\mathbf{V}$	volume (m^3)
$\mathbf{X}$	water content (kg kg^{-1})
$\mathbf{X}_{\mathrm{res}}$	residual moisture, dry basis (kg kg^{-1})
$\mathbf{y}$	proportion or ratio (-)
$\mathbf{z}$	drying state (-)

Greek symbols and variables

$\tan\delta$	loss tangent (-)
ε_{r}	relative permittivity (-)
$\varepsilon_{\mathrm{r}}'$	dielectric constant (-)
$\varepsilon_{\mathrm{r}}''$	dielectric loss factor (-)
ζ	heating homogeneity factor (-)
η	energy efficiency (-)
ϑ	temperature (°C)

θ	phase angle (-)
λ_0	wavelength in air (m)
ρ	electric charge density (C m^{-3})
ω	angular frequency (s^{-1})

General deep indexes

0	initial
av	average
c	chamber
C	capacitive
d	dissipated
dry	dry
eff	effective
f	forward
frozen	frozen
H_2O	water
i	integer index
j	integer index
max	maximum
min	minimum
nml	mode indices
on	on

pause	pause
pow	power application
pre	before
proc	averaged over process
P	Pirani
r	reflected
rms	root mean square
s	specific
set	set
smp	samples
std	standardized
sub	sublimation front
surf	surface
total	total
T	thermostat
x	x-axis
y	y-axis
z	z-axis

1 Introduction

1.1 Motivation

Freeze-drying (FD), also known as lyophilization, is widely used in process engineering. The particular product-preserving characteristic of FD can be attributed to the absence of liquid water and low temperatures [1] as well as the exclusion of oxygen [2]. Thus, FD is used mainly to dry heat-sensitive products. FD has been investigated not only for high-value foods, such as strawberries [3] or blueberries [4], but also for other products, such as active pharmaceutical ingredients [5] or microorganisms [6]. Comprehensive reviews show the advantages of FD in the drying of food [2, 7]. A major drawback of FD is its long drying time compared to other drying processes, such as hot-air drying [1, 8] or microwave-assisted vacuum drying [9]. In addition, FD is a costly process compared to the widely used hot-air drying [1]. Therefore, there is great interest in intensifying the FD process to achieve an economically competitive and fast process that yields high-quality products.

Using complementary technologies is one option to intensify the FD process. These technologies include the use of microwaves in microwave-assisted freeze-drying (MFD) [8, 10–14], ultrasound [15], and infrared radiation [16]. MFD, in particular, has recently been the subject of increased scientific research. The availability of solid-state microwave generators (SSGs) enables precise adjustment of frequency, power, and phase shift between multiple SSGs based on electrical control, which is not possible with conventionally used magnetrons [17]. Furthermore, SSGs can measure the reflected power and forward power of microwaves. This combination opens up new possibilities for process control and monitoring.

For microwave-assisted heating, control strategies have already been developed to intensify the process in terms of energy efficiency [18–22] and temperature uniformity [18–24]. Electromagnetic simulations of microwave-assisted heating support these results [23].

The occurrence of a phase change makes microwave-assisted drying, such as MFD, a thermodynamically more complex process than microwave-assisted heating. The changing material composition during drying leads to constantly changing electromagnetic field interactions with the material to be dried, as demonstrated for microwave-assisted drying [25–27]. These changes in material composition affect the microwave field patterns and the conversion of electromagnetic energy into heat. Therefore, microwaves must be continually adapted to the composition of the material to achieve an optimized process regarding energy efficiency and heating homogeneity. The ability of SSGs to precisely adjust the microwaves during drying enables customized process control. With this technology, drying can be tailored to each product and process run.

This thesis investigates the targeted adjustment of the microwave field during MFD to increase process understanding and identify opportunities for process optimization. Developing the MFD process is a necessary prerequisite for these investigations. Process development includes constructing a laboratory-scale MFD system and developing control concepts based on electromagnetic simulations. Subsequently, special emphasis is placed on investigating the effects of microwave frequency modulation, given the particularly pronounced effects observed in microwave-assisted heating [19, 21]. The research focuses on the influence of microwaves on process parameters in MFD, such as process duration and energy efficiency, and the resulting product properties, such as residual moisture and ascorbic acid retention.

1.2 Freeze-drying

FD is based on the removal of water from the material to be dried by sublimation, with the ice crystals in the material passing directly into the gaseous state without an intermediate liquid state [28]. The FD process typically consists of three phases [2]:

- Freezing,
- primary drying, and
- secondary drying.

Figure 1.1 shows a simplified overview of FD in the phase diagram of pure water. The aggregate states and phase changes of water during FD are shown as a function of pressure and temperature. Point A represents the starting point of the FD process. Liquid water is present at ambient pressure and temperature. First, water in the material is frozen by lowering the temperature below the freezing point (A $\rightarrow$ B). Then, a vacuum is applied to obtain process conditions below the triple point of water (B $\rightarrow$ C). The conditions at the triple point of water are a temperature of 0.01 °C (273.16 K) and a pressure of 6.12 mbar [29]. This is followed by primary drying (C $\rightarrow$ D). The heat supplied provides the sublimation enthalpy.

For freezing, the material must be supercooled in order to cause initial nucleation. The application of high cooling rates with high supercooling leads to a larger number of smaller ice crystals than with lower cooling rates [28]. Differences in ice crystals resulting from the process parameters during freezing influence mass transfer during subsequent drying in FD, as described in the literature [28, 30–33]. Therefore, freezing conditions must be considered as process parameters or kept constant when FD is examined.

During primary drying, the frozen water in the material to be dried is sublimated [32]. Maintaining the sublimation at process conditions below the triple point requires an energy supply. The energy provided is used to sublimate the frozen

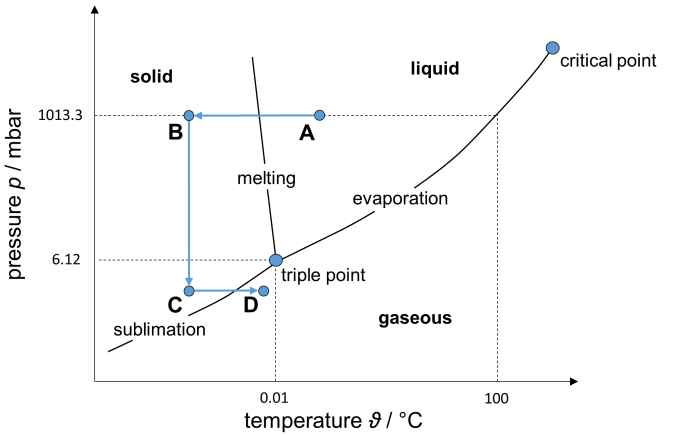

Figure 1.1: Schematic representation of freezing and primary drying in FD (A to D) in the phase diagram of water. Depiction according to [2].

water and heat the material. The enthalpy required for the sublimation of water is composed of the melting enthalpy and the vaporization enthalpy. The resulting sublimation enthalpy of water is approximately 2805 kJ/kg in the relevant temperature range [28]. In conventional freeze-drying (CFD), energy is usually supplied to the drying material with a shelf that serves as a heat exchanger. The heat transfer mechanisms associated with CFD are conduction, thermal radiation, and convection [28, 31]. Conduction is the energy transfer between neighboring molecules, in which heat is transferred in the opposite direction of a thermal gradient. Thermal radiation is energy transfer by electromagnetic waves, which does not require any material as a transfer medium. Convection describes the transportation of energy through moving fluids. [34]

The structure of a material undergoing FD is schematically depicted in Figure 1.2 with qualitative water content and temperature curves. King [31] describes the phenomena of mass transfer during FD. Drying occurs on a sublimation front that separates the frozen area in the drying material from the dry area. During drying, the sublimation front continuously retreats into the interior of the material. Water vapor is removed through the pores in the dry area, which formerly contained ice

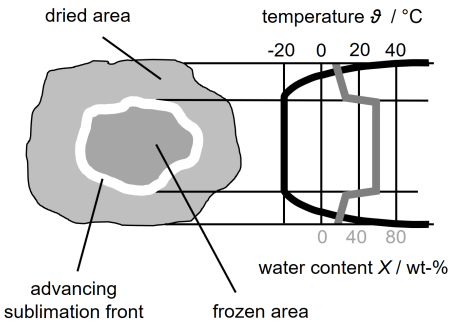

Figure 1.2: Schematic representation of local temperature and water content in a particle during CFD. Depiction according to [36].

crystals. A pressure gradient drives mass transport through the porous layer. The driving pressure gradient for the process is between the water vapor pressure at the sublimation front inside the material and the water vapor pressure at a moisture sink. The water vapor pressure at the sublimation front depends on the respective local temperature. To maintain the driving pressure gradient, a lower temperature is required at the moisture sink than at the sublimation front. Assegehegn et al. [35] describe the mass transfer during FD only with respect to the material to be dried. They describe the mass flow $\dot{m}_v$ through the dried layer as a function of the water vapor pressures on the sublimation front p_{sub} and on the surface of the material p_{surf} as

$$\dot{m}_v = \frac{p_{sub} - p_{surf}}{R}, \tag{1.1}$$

where R is the mass transfer resistance of the dried material.

As the sublimation front recedes into the interior of the material, heat and mass transfer resistances increase. The increase in resistance is caused by the formation of a dried porous layer, which generally leads to a slowdown in drying.

The control options in CFD are restricted to chamber pressure, shelf temperature, and process time as the main controllable variables [37, 38]. By increasing

chamber pressure, higher sublimation rates can be achieved due to the increase in thermal conductivity [37]. A higher drying rate can also be achieved with a higher shelf temperature, increasing the thermal gradient to the sublimation front. However, shelf temperature cannot be increased indefinitely, as critical process parameters must be considered. These include product temperature in dried and frozen areas, speed of progression of the sublimation front, as well as temperature and geometry of the sublimation front [32]. The shelf temperature and the heat transfer through the product influence the product temperature. If the energy input is too high, the water vapor produced cannot be transferred solely through the pores of the dried material. The resulting build-up of pressure can lead to the pore walls breaking open and destroying the matrix of the material [28]. In addition, ice crystals can melt at locally increased pressure above the triple point conditions, as shown in Figure 1.1.

In the FD of dissolved polymers, as they occur in drying pharmaceutical formulations, care must be taken to ensure that the glass transition temperature of the material is not exceeded [37]. Exceeding the glass transition temperature leads to a viscous rubbery state in which the material loses its macroscopic and microscopic structure. The collapse temperature describes the temperature at which the structure of a material collapses and is closely related to the glass transition temperature [32]. As a rule, the collapse temperature is a few kelvin above the glass transition temperature [39]. The glass transition temperature has also been applied to food drying, as explained in a review by Ratti [1]. It is not clear why the concept of a polymeric glass transition temperature applies to complex biological systems such as food. However, it is clear that the quality of these products can be compromised at excessive temperatures. For example, the preservation of valuable ingredients can decrease with increasing temperature, as has been shown for ascorbic acid and anthocyanins in the CFD of black currant juice [40].

In secondary drying, bound water is removed from the product by desorption until an equilibrium between the product and the process environment is reached. This drying stage is characterized by a lower drying rate than primary drying and a residual moisture plateau at a desorption equilibrium. [28] The occurrence of secondary drying cannot be completely separated from primary drying, as

the processes overlap in time. Secondary drying can occur in areas that have already been dried at the same time as the primary drying of the frozen area. [32] Secondary drying is not dominated by energy supply, but is limited by diffusional processes [37]. During secondary drying, only a small percentage of water is removed from the product, usually less than 10 wt% dry basis [28].

1.3 Microwave-assisted processing

This section covers the foundations of microwave technology and its use in process engineering. First, the basic principles of microwaves and how they interact with processed materials are explained. The following section discusses the theoretical background of microwave applicators, which are essential for the practical application of microwaves. Solid-state microwave technology that enables precise control of microwave application is covered in the subsequent section. The role of electromagnetic modeling is discussed as a tool for investigating microwave-assisted processes.

1.3.1 Microwaves

Microwaves are electromagnetic waves in the frequency range between 0.3 GHz and 300 GHz [41]. Figure 1.3 illustrates the position of microwaves in the electromagnetic spectrum compared to various types of electromagnetic waves.

Standard microwave devices for material processing operate at frequencies around 915 MHz and 2450 MHz [43]. These frequencies lie within the industrial, medical, and scientific (ISM) radio bands. The ISM bands cover frequency ranges that can be used without governmental permission. Due to the low regulatory requirements, the use of frequencies in the ISM band around 2450 MHz, ranging from 2400 MHz to 2500 MHz, is particularly suited for microwave-assisted processes. Another advantage of using the established ISM band around 2450 MHz is the availability of components for these frequencies [44]. The widespread use of

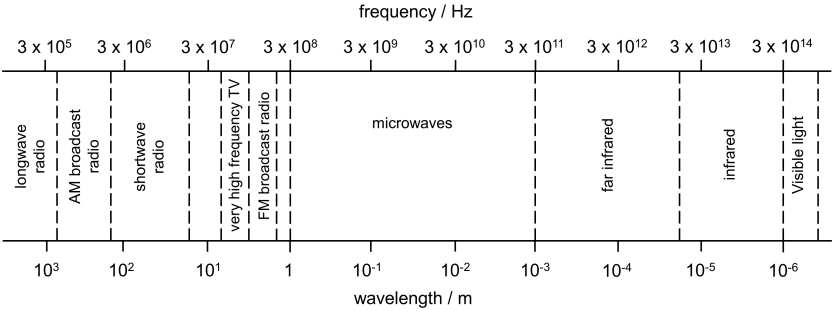

Figure 1.3: Illustration of the electromagnetic spectrum. Depiction according to [42].

frequencies from this ISM band in microwave-assisted processes in the literature [11, 14, 45] ensures a high level of comparability when using the same ISM band.

1.3.2 Microwave-material interactions

Microwave heating is based on the interaction of electromagnetic fields with a dielectric, an insulating material, leading to the dissipation of electromagnetic energy into heat [46]. Thus, microwave heating does not require a thermal gradient [47]. Concerning drying, the generation of heat within the product with microwaves can overcome the heat transfer limitations that limit the drying rate in conventional drying processes [48].

The loss mechanisms in dielectrics can be subdivided into losses because of interactions with the electric or magnetic field components. The interactions with magnetic field components can generally be neglected when processing biological materials, as they only need to be considered for magnetic materials. The electrical loss mechanisms include conductivity and dipolar losses, with dipolar losses becoming more dominant at higher frequencies. Dipolar losses can be subdivided into interactions due to dipolar polarization, electronic polarization, atomic polarization, and Maxwell-Wagner polarization. [46] Selected interaction mechanisms of dielectrics with the electric component of an electromagnetic field are schematically depicted in Figure 1.4.

Dipolar polarization and ionic conduction are two relevant interaction mechanisms in the microwave frequency range [46]. Dipolar polarization causes a charge shift due to the rotation of electric dipoles, while ionic conduction transfers charges over long distances compared to rotation [41]. According to Metaxas and Meredith [46], dipolar polarization is 'perhaps the most important type' of all loss mechanisms in industrial applications at frequencies above 1000 MHz. A prominent polar molecule present in many materials in microwave-assisted processes is water. When an electric field is applied, water and other polar molecules align in the direction of the electric field vectors. The oscillation of the microwave field causes the polar molecules to rotate. Losses due to dipolar rotation occur when the dipoles cannot restore their original orientation due to rapid field reversals [46, 49]. The energy of the electric field is converted into heat, which is the kinetic energy of molecules.

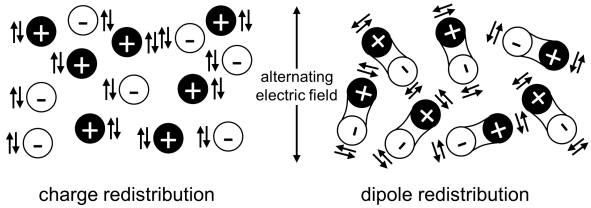

Figure 1.4: Schematic representation of the mechanisms of charge redistribution, for example, due to Maxwell-Wagner polarization, and dipole redistribution, also called dipolar polarization, when microwaves interact with a dielectric. Depiction according to [46].

The dielectric properties (DPs) describe how electromagnetic fields interact with dielectrics, making them crucial for assessing microwave-assisted processes. One of the first extensive investigations of the experimentally determined DPs of organic and inorganic materials goes back to the work of von Hippel [50]. DPs specify how dielectrics store electromagnetic energy and convert it into heat. The DPs that characterize the interactions with the electric field are summarized in the relative permittivity ε_r. The relative permittivity is a complex number. It can be subdivided into a real part, which is referred to as the dielectric constant ε'_r,

and an imaginary part, which is referred to as the dielectric loss factor ε_r'', leading to its expression according to Metaxas and Meredith [46] as

$$\varepsilon_r = \varepsilon_r' - i\varepsilon_r''. \tag{1.2}$$

Here, i denotes the imaginary unit. The relative dielectric constant ε_r' is a measure of the capacity of the material to store electric energy, while the relative dielectric loss factor ε_r'' describes the conversion of electric energy into heat. Another way to denote the DPs is the loss tangent $\tan\delta$, which, according to Chandrasekaran et al. [51], is defined as

$$\tan\delta = \frac{\varepsilon_r''}{\varepsilon_r'}. \tag{1.3}$$

The DPs influence the penetration depth d_p and the absorbed power per unit volume P_A [46]. The definition of d_p is the distance from the surface into the material at which the power drops to $1/e$ of the value on the surface and can be calculated, according to Bengtsson and Risman [52], as

$$d_p = \frac{\lambda_0}{2\sqrt{2}\pi\sqrt{\varepsilon_r'}\sqrt{\sqrt{1+(\tan\delta)^2}-1}}. \tag{1.4}$$

The parameter e is Euler's number and λ_0 represents the wavelength in air. The average absorbed power per unit volume P_A is defined as published by Metaxas and Meredith [46] with

$$P_A = 2\pi f \varepsilon_0 \varepsilon_r'' |E_{rms}|^2. \tag{1.5}$$

Here, f is the frequency of the electromagnetic field, $\varepsilon_0 = 8.85418\times10^{-12}\,\mathrm{F\,m^{-1}}$ is the vacuum permittivity, and E_{rms} the root mean square of the electric field.

According to these equations, the DPs affect the magnitude and pattern of the dissipated power inside the processed material, underlining their critical importance for microwave heating processes.

DPs themselves are influenced by the frequency of applied microwaves [53]. In addition, material properties, such as composition, moisture content, and temperature, influence the DPs [46, 53]. The material composition can influence the DPs in a variety of ways. For example, the addition of salts to aqueous solutions results in them being present in a dissociated state. Thus, the addition of salt increases the ion content and, consequently, the interaction with the microwave fields through ionic conduction [47, 53].

During microwave-assisted drying, the changes in the temperature and material composition resulting from the removal of water lead to changes in the DPs. Li et al. [25] observed a decrease in the dielectric constant and the loss factor during microwave-assisted vacuum drying of Chinese yam through online measurements. The investigations by Nakagawa and Kono [26] also indicate a decrease in DPs during CFD. Therefore, a similar trend of time-dependent material-microwave interaction is expected for MFD.

1.3.3 Microwave applicators

Figure 1.5 shows a schematic block diagram of a microwave heating system with optional components. According to Metaxas and Meredith [46], such a heating system can be subdivided into the following components:

- A microwave power unit,
- an applicator with auxiliary systems, and
- a control system.

The microwave power unit generates microwaves with a specific power and frequency from electrical energy. Magnetrons are conventionally used to generate

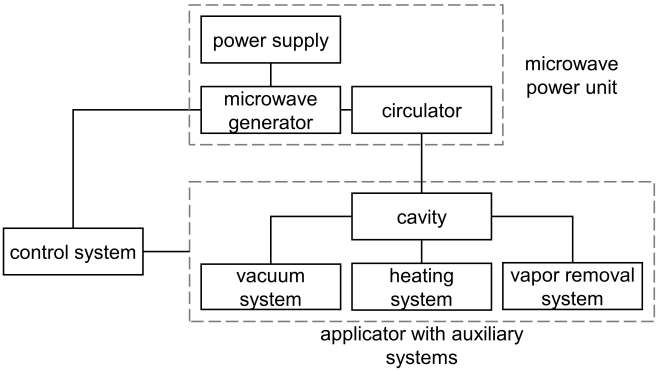

Figure 1.5: Schematic block diagram of a microwave heating system with optional devices as part of the auxiliary system. Depiction according to [46].

microwaves, but SSGs offer a superior alternative in several respects, as described in Section 1.3.4. Waveguides or coaxial cables can be used as microwave transmission lines from the microwave generator to the applicator. A circulator usually shields the microwave generator from reflected power.

The material to be processed is placed inside the applicator, also known as the cavity in the context of microwave engineering. The applicator can optionally be connected to auxiliary systems to support processing. Supplementary heating systems enable hybrid processes by supplying additional energy to the process, e.g., through infrared radiation. Vacuum systems create process conditions below atmospheric pressure to reduce the partial vapor pressure. Vapor removal systems remove excess vapor from the atmosphere, e.g., through an air stream or a condenser. The latter two systems are particularly valuable when steam is continuously generated, as in drying processes.

The control system enables control of the microwave field and additional process parameters, e.g., the chamber pressure. Automated systems can continuously adjust the microwave field, especially when using SSGs.

Conductive walls enclose the electromagnetic field in the cavity. In these walls, wall currents reduce the electric field tangential to the surface. If the walls were

perfect electrical conductors, the tangential electric field would be nullified and the electromagnetic waves would be fully reflected. If the walls of a cavity are highly conductive but not lossless, as is the case in practical applications, wall losses occur within the walls of the cavity due to dissipation of electromagnetic energy on the surface of the walls [46].

The superposition of incident and reflected waves can form standing waves inside the cavity due to constructive and destructive interference. These waves appear stationary with distinct points of minimum and maximum field amplitude. Resonant frequencies (RFs) are defined as the frequencies at which electromagnetic waves inside the cavity constructively interfere to form stable, high-amplitude standing waves. The application of RFs leads to the maximization of energy transfer to the processed material because of the maximization of the electromagnetic field, increasing the energy efficiency of the process. The specific electromagnetic field patterns within the cavity at the RFs are referred to as modes [46].

Microwave cavities can be subdivided into monomodal and multimodal resonators. Monomodal cavities can only sustain one dominant mode in the applied frequency range. Monomodal cavities are energy-efficient but lack the versatility of multimodal systems [46]. Their size is limited to dimensions in the magnitude of one wavelength of the applied microwaves [54]. This limitation makes them unusable for processing larger materials.

Multimodal systems support many modes at respective RFs in the applied frequency range. For an empty rectangular resonator, the mode equation for the RFs can be calculated according to Collin [55] as

$$f_{nml} = c\sqrt{\left(\frac{n_{mode}}{2L_x}\right)^2 + \left(\frac{m_{mode}}{2L_y}\right)^2 + \left(\frac{l_{mode}}{2L_z}\right)^2}, \tag{1.6}$$

where f_{nml} is the resonant frequency of a TE_{nml} or TM_{nml} mode, $c = 299\,792\,458\,\mathrm{m\,s^{-1}}$ is the speed of light and n_{mode}, m_{mode}, and l_{mode} are the number of half-sinusoidal variations in the standing wave pattern along the x-,

y-, and z-axes. L_x, L_y, and L_z are the cavity dimensions along the x-, y-, and z-axes.

Metaxas and Meredith [46] elaborate that partially filling a microwave cavity with a lossy dielectric results in an increased spectral density of modes, meaning there is a higher number of modes in a given frequency range. Additional effects listed are higher power absorption, a shift of modes to lower RFs, and broader response peaks around the RFs. In this context, response peaks describe the maxima observed in the frequency spectrum, indicating frequencies at which electromagnetic energy is most efficiently coupled into the cavity due to resonance. Broader response peaks reflect reduced selectivity, which enables energy absorption over a wider frequency range. Consequently, the introduction of a lossy dielectric can cause the modes to overlap in frequency as a result of their increased spatial density and the expanded width of the response peaks.

The heating effects on the microwave field depend on the DPs of the processed material, as described in Section 1.3.2. Geometric factors, such as the position, size, and shape of the material, also influence the characteristics of the RFs [56]. In microwave-assisted processes, materials are present within the cavity. Thus, developing a cavity based solely on analyzing an empty cavity is impractical.

1.3.4 Solid-state technology

Conventionally used magnetrons are the lowest-cost microwave source available because of their mass production. Magnetrons do not generate a specific frequency, but a frequency spectrum [57]. In addition, Luan et al. [58] demonstrated frequency fluctuations of magnetrons as a function of time, as well as the geometry and placement of the load in a study with household microwave ovens.

The frequencies generated by conventional magnetrons cannot be specifically adjusted [54]. This reduces the degrees of freedom to adjust the electromagnetic field to the variation of power output, which limits the potential for process control.

SSGs have several advantages over magnetrons. These include electrical control over the frequency, power, and phase shift of microwaves. In addition to the extended control options, electromagnetic waves generated by an SSG have a stable and precisely defined frequency. [17]

SSGs are based on semiconductor components that generate high-power microwaves. Figure 1.6 shows the implementation of an SSG in a microwave heating system, in contrast to a magnetron-based heating system. The main components of an SSG are a small-signal generator, a solid-state power amplifier (SSPA), and a power supply. The small-signal generator is a tuned electronic circuit that can create a low-amplitude microwave signal. This signal is transmitted to the SSPA, which uses direct current to amplify the power of the microwaves received using semiconductor technology. SSGs are capable to measure power signals in dependence on frequency. This feedback can be used for the targeted control of microwave parameters such as frequency, power, and phase to adapt the microwaves to the needs of the material being processed. [17]

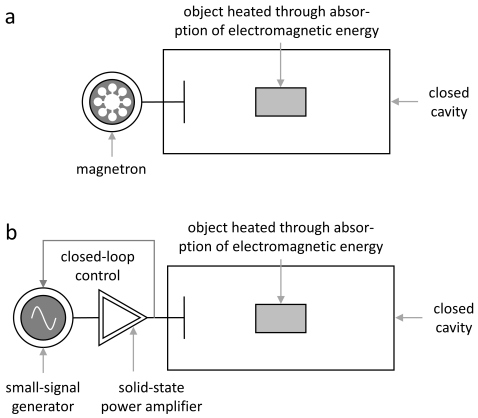

Figure 1.6: Schematics of (a) a magnetron-powered microwave heating system and (b) a solid-state-powered microwave heating system showing the possibility for feedback control. Depiction according to [17].

1.3.5 Electromagnetic modeling

Maxwell's equations are a series of coupled partial differential equations established by James Clerk Maxwell [59]. In combination with the Lorentz force law, they constitute the basis of classical electromagnetism. Maxwell's equations describe how electric and magnetic fields are generated by charges, currents, and field changes. They serve as the mathematical basis for models of microwave applications.

According to Hampshire [60], Maxwell's equations in their differential form can be written as

$$\nabla \cdot \vec{E} = \frac{\rho}{\varepsilon_0}, \tag{1.7}$$

$$\nabla \cdot \vec{B} = 0, \tag{1.8}$$

$$\nabla \times \vec{E} = -\frac{\partial \vec{B}}{\partial t}, \text{and} \tag{1.9}$$

$$\nabla \times \vec{B} = \eta_0(\varepsilon_0 \frac{\partial \vec{E}}{\partial t} + \vec{I}). \tag{1.10}$$

In these equations, $\vec{E}$ represents the electric field, $\vec{B}$ the magnetic field, t the time, ρ the electric charge density, and $\vec{I}$ the current density. The parameter $\eta_0 = 1.25664 \times 10^{-6}\,\mathrm{N\,A^{-2}}$ is the vacuum permeability. Equation 1.7 and Equation 1.8 are Gauss's law and Gauss's law for magnetism, respectively. Equation 1.9 is Faraday's law and Equation 1.10 Ampére's law with Maxwell's addition for displacement currents.

Commercial software for electromagnetic field simulation offers a variety of solvers to Maxwell's equations in dependence on the users' specific requirements. Yakovlev [61] examined the applicability of various commercial software to investigate microwave-assisted heating in 2006. Currently used software in research includes COMSOL Multiphysics (COMSOL, Stockholm, Sweden) [62, 63], QuickWave (QWED, Warsaw, Poland) [23, 64], and CST Microwave Studio (Dassault Systèmes, Vélizy-Villacoublay, France) [64, 65].

The above programs use various solvers to handle Maxwell's equations, including frequency domain solvers, time domain solvers, eigenmode solvers, integral equation solvers, and asymptotic solvers. Important factors in choosing an appropriate solver are the quality factor in resonant devices and the frequency in weakly resonant devices, as shown in Figure 1.7. In the case of microwave-assisted process engineering, microwaves are applied in resonant structures with varying quality factors. Therefore, applying the frequency domain solver is a preferable choice since its performance does not depend on the quality factor of the resonant device, as shown in Figure 1.7.

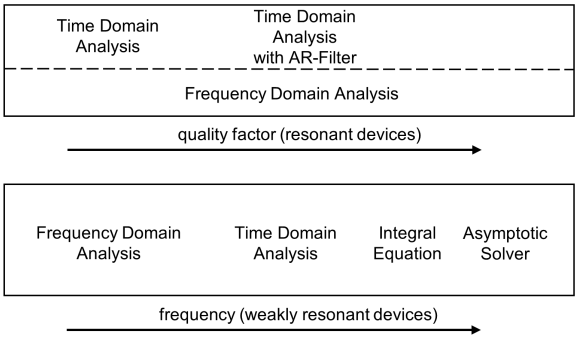

Figure 1.7: Schematic representation of the areas of optimal operation for various solvers for Maxwell's equations. Depiction according to [66].

The basis for using frequency solvers is the transformation of Maxwell's equations into the frequency domain, assuming a time-harmonic dependence of the fields and

the excitation. The fields are then represented by the real part of complex pointers multiplied by a time factor. As an example, the electric field in dependence on time can be written as

$$\vec{E}(t) = \Re\{\vec{E}(\omega) \cdot e^{i\omega t}\}, \tag{1.11}$$

where ω is the angular frequency and $\Re$ is the real-part operator for the complex number [66]. A separate system of equations must be set up and solved for each frequency in the defined domain. Special broadband frequency sweep techniques can be used to derive the full broadband spectrum from a relatively small number of frequency samples [66].

The simulation of an electromagnetic field in microwave-assisted processing begins with creating a geometric model of the respective cavity. The governing equations are derived from Maxwell's equations. In combination with boundary conditions at the geometric boundaries, they form a complete system of equations. The defined electromagnetic model is then solved in a simulation. The simulation results are post-processed to obtain the target parameters. Examples of these parameters are the energy efficiency as a function of frequency or the dissipated power in individual samples.

The details of the simulations carried out in this work are presented in Section 3.3.1. The section includes the assumptions that enable a purely electromagnetic model of MFD by solving various electromagnetic models at different drying states.

1.4 Microwave-assisted freeze-drying

MFD differs from CFD in that electromagnetic waves supply the sublimation enthalpy during drying. Microwaves generate heat directly within the product, so there are no restrictions due to heat transfer resistance through the dried layer [48]. Therefore, MFD is particularly advantageous for materials characterized by low

thermal conductivity, such as materials with high porosity. When these materials are dried with CFD, the heat transfer resistance may limit the drying rate. In addition, microwaves provide benefits such as selective heating and immediate switching of the heating source [41]. These properties lead to advantageous features of microwave-assisted processing, such as shorter processing times and economic benefits [41]. Regarding food drying, microwaves offer the advantage of fast drying in combination with increased quality of some food products [51].

MFD has increasingly become the focus of research in recent years [8, 11–14, 45, 67–73]. MFD achieved reductions in drying time of 40% to 80% in comparison to CFD [8, 11, 67, 68]. The literature even reports a reduction in the drying time of onion slices up to 96% [74]. In these works, MFD yielded products with quality attributes comparable to or higher than those obtained with CFD. More specifically, MFD was found in comparison to CFD to achieve similar characteristics regarding the stability of monoclonal antibodies [14, 68], slightly higher retention of polyphenolic compounds [73], and similar retention of ascorbic acid and anthocyanins [12]. However, structural degradation of the product was observed for excessive power levels [12] and dense product structure [73].

These results underscore the potential of MFD to yield a product with quality attributes comparable to or exceeding those obtained through CFD in a reduced amount of time. It is essential to carefully select the applied microwave power during MFD to prevent any degradation of product quality to unacceptable levels.

Goldblith [75] outlined challenges associated with MFD as early as 1966. He highlighted limitations such as the need to control the energy input to prevent melting of the frozen material, differences in the dielectric loss factors between the frozen core and the dry layer, and the cost of translating theoretical developments into practical commercial applications. Ratti [76] attributed the limited application of MFD to technical issues, such as melting and overheating of the frozen core, non-uniform heating, and dielectric breakdown inside the applicator. The technical challenges associated with using microwaves in MFD can be summarized as non-uniform heating [75, 76], dielectric breakdown inside the

applicator at high microwave power [76, 77], and efficient power delivery to the product throughout drying, as DPs decrease during drying [25, 78].

The first technical challenge is the inherently non-uniform nature of the electromagnetic field in MFD, illustrated in Figure 1.8 as the electric field pattern from an electromagnetic simulation. Standing waves in resonant microwave applicators at RFs are associated with local minima and maxima of field strength. These can lead to so-called hot and cold spots in the processed material. The material may be damaged at hot spots due to increased temperatures [12, 79, 80]. In addition, a high power density can generate large amounts of vapor within the processed material, which can lead to rupture of the material due to a local increase in pressure [46]. Furthermore, several factors intrinsic to microwaves cause non-uniform heating. These include focusing effects, corner and edge heating, as well as the shape and composition of the processed material [81]. Moreover, there is a pronounced difference in the DPs of frozen and dried areas [75], leading to inhomogeneous power dissipation between these areas. Additionally, the DPs of thawed materials are higher than of frozen materials [52], leading to highly inhomogeneous heating as soon as local thawing occurs during MFD. The effects outlined underscore the importance of taking measures to ensure uniform heating for product-friendly processing.

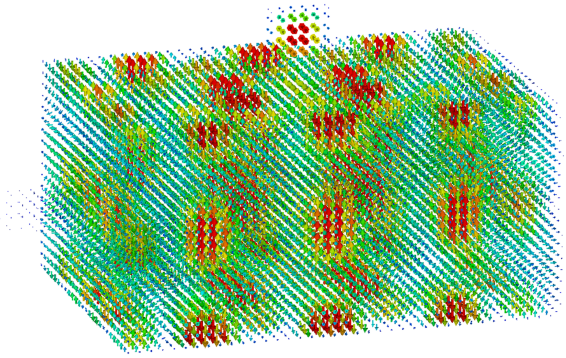

Figure 1.8: Three-dimensional pattern of the electric field from an exemplary electromagnetic simulation at a frequency of $f = 2480$ MHz and a phase angle $\theta = 30°$.

The second challenge in MFD is dielectric breakdown, a well-known phenomenon when microwaves are applied in a vacuum. The associated discharges are generally undesired during microwave-assisted processing due to wasting energy and potentially damaging processed materials and equipment [82]. The dielectric strength of insulating materials determines the maximum electric field strength that can be tolerated without dielectric breakdown [83]. A related parameter is the breakdown voltage. This parameter describes the voltage above which a dielectric breakdown occurs in a specific material, i.e., the dielectric strength is exceeded. The breakdown voltage is dependent on the pressure and the distance between the electrodes [84]. The corresponding curves are called Paschen curves [85].

Dielectric breakdown in gases is caused by collision ionization, which occurs when an electric current flows through a usually insulating gaseous medium due to its ionization [86]. Ionization involves the removal of electrons from atoms or molecules, creating positively charged ions and free electrons. The free electrons generated by ionization can gain enough energy to cause further ionization in an avalanche effect. The ionization can result in corona discharge as well as a short-lived spark or a prolonged arc to nearby objects. A corona discharge occurs when the fluid around an electrically charged conductor is ionized. During a corona discharge, the electric field surrounding a conductor is strong enough to create a conductive zone, but not strong enough to produce arcs or sparks [86].

MFD is especially prone to dielectric breakdown, as the process must be carried out at pressures below 6.12 mbar to ensure a phase transition by sublimation. At this low pressure level, dielectric breakdowns occur more frequently, which limits the applicable power density [82]. Duan et al. [8] detected the critical power at which arcing occurred in dependence on pressure. They found a minimum critical power at around 1.0 mbar to 1.5 mbar, a typical pressure range for MFD. Hence, particular care has to be taken to avoid dielectric breakdown in MFD.

The third challenge is efficient power delivery to the material to be dried throughout the entire process. Changes in moisture content and temperature during drying affect the DPs of the materials, as shown in offline [78] and online measurements [25]. Both the dielectric constant and the loss factor decrease with a lower moisture

content. In contrast, increasing temperature increases the DPs, but this effect is minor compared to changes with moisture content [78]. Therefore, efficient power delivery to the material to be dried becomes increasingly challenging as MFD progresses and the DPs decrease.

As described in Section 1.3.3, lower DPs shift the RFs of the predominant modes to higher frequencies [42, 46]. Moreover, the response peaks around the RFs are more narrow for an empty cavity than for a cavity containing a dielectric as a workload [46]. These facts indicate that the decrease in DPs during drying also causes narrower response peaks associated with specific RFs as drying progresses. Therefore, energy-efficient RFs can only be applied through the precise application of specific frequencies, especially in the later stages of drying.

All technical challenges of MFD above can be addressed by controlling the electromagnetic field. The adoption of SSGs enables the required precise control of microwaves through modulation of power, frequency, and phase shift, as described in Section 1.3.4. By definition, multiple RFs exist in a multimodal cavity for the ISM-band of 2400 MHz to 2500 MHz. The targeted excitation of energy-efficient RFs could increase energy efficiency throughout drying. The excitation of multiple individual modes at frequencies with distinct electromagnetic field patterns should increase heating uniformity compared to individual frequencies due to superposed heating patterns. Regulation of microwave power over time would allow thermal diffusion to counteract the effects of the inherently inhomogeneous dissipation of electromagnetic energy. The occurrence of dielectric breakdown could also be circumvented through a targeted power application.

Previous studies on MFD have largely left the potential of controlling the microwave field untapped. When conventional magnetrons are used, the microwave power is mostly controlled with an on-off control. This power control has been used in the literature to set the maximum temperature of the product [11, 12]. If a previously defined critical temperature value was exceeded, the magnetron was switched off intermittently. The same concept was also used with SSGs [45, 69].

Regarding MFD process control by frequency adjustment, experiments were performed with SSGs at a constant frequency of 2450 MHz [69] or with a non-targeted

frequency variation of 2430 MHz to 2480 MHz [14, 87]. Abdelraheem et al. [88] conducted MFD with a range of frequencies from 12 GHz to 18 GHz and detected effects on the drying process but also kept the frequencies constant during drying. Based on available information, no studies have used targeted frequency modulation in MFD. Wang et al. [62] coupled a thermodynamic model of MFD with an electromagnetic model but only simulated drying at a constant frequency of 2450 MHz.

In summary, controlling the microwave field during MFD is a promising approach to overcome various technical challenges. The investigation of this approach fills a research gap, as it has not yet been the focus of academic literature.

1.5 Objectives and outline of this thesis

The adjustment of microwaves during MFD is a way to overcome technical challenges, as described in Section 1.4. This work aims to generate knowledge about the effects of targeted microwave modulation during MFD and to investigate the associated possibilities for process optimization. A schematic outline of the thesis is shown in Figure 1.9.

Part (I) Process development is the first step in achieving this overarching goal by establishing a basis for further research. The part includes the construction of a modular laboratory-scale drying system for MFD and CFD, described in Chapter 2. The construction includes the installation of process equipment, consisting of the components for FD and microwave generation, as well as systems for process monitoring and process control, which include software and hardware. When the system is functional and calibrated, the process parameters in MFD and CFD should follow the expected course with respect to the literature. The expectations for the process parameters product temperature, chamber pressure, and product weight are described in detail in Chapter 2. On this basis, the following hypothesis is proposed:

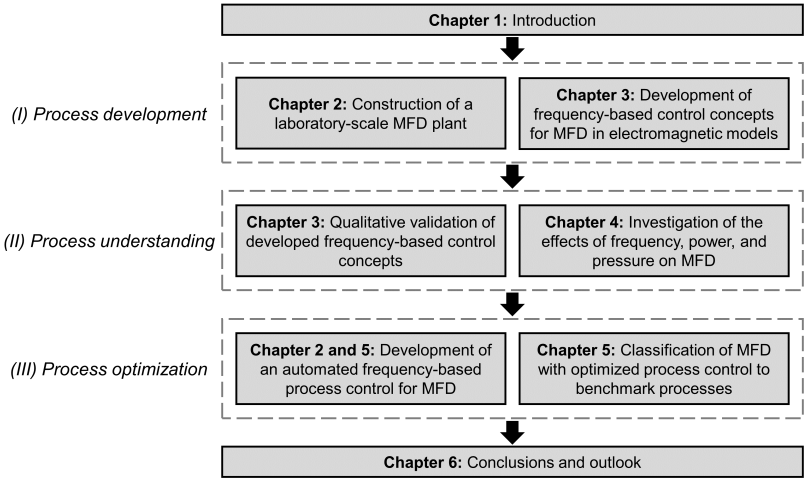

Figure 1.9: Schematic outline of this thesis.

H2.1: Commissioning experiments in a modular drying plant on a laboratory scale show the expected course of the process parameters sample temperature, chamber pressure, and sample weight for MFD and CFD in accordance with the literature.

Part (I) also includes electromagnetic simulations of MFD in Chapter 3 to provide access to a microwave field assessment. The electromagnetic simulations are based exclusively on Maxwell's equations. Thermodynamic equations are not required since the drying progress in MFD is represented by the electromagnetic simulation of discrete drying states. The commercial software CST Studio Suite (Dassault Systèmes, Vélizy-Villacoublay, France) is used to perform the electromagnetic simulations.

The goal of the simulations is to evaluate the advantages of frequency modulation in MFD with respect to energy efficiency and heating homogeneity. Assuming that the outlined advantages of frequency modulation in microwave-assisted heating can be extended to the entire duration of MFD, the following hypotheses are postulated:

H3.1: The electromagnetic simulations of MFD show that the excitation of RFs, as opposed to non-specific excitation, results in increased energy efficiency during the entire process duration due to the high energy efficiency of RFs.

H3.2: The electromagnetic simulations of MFD indicate that the excitation of multiple frequencies, as opposed to a single frequency, leads to a more uniform distribution of dissipated energy within the processed material throughout the entire drying process due to the superposition of multiple heating patterns.

In part (II) Process understanding, MFD is experimentally investigated in the constructed drying system. The simulation results of the frequency-based control concepts are validated in Chapter 3. Assuming that the microwave field is accurately simulated leads to the following hypothesis:

H3.3: The electromagnetic simulations can be validated by comparison with experimental results of the frequency-dependent energy efficiency in the range of 2400 MHz to 2500 MHz.

The experimental investigation of MFD in part (II) includes the development of partial drying in Chapter 4 as an approach to reduce the time required for parameter studies of the lengthy MFD process. Partial drying refers to terminating the process before complete drying. The time savings with partial MFD are estimated to be at least as high as the ratio of water still contained in the material to be dried since the drying rate is expected to be highest in the initial drying time. This expectation leads to the following hypothesis:

H4.1: Partial MFD, i.e., terminating the process after the removal of 20 wt% initially contained water, decreases the time required for parameter studies of MFD by more than 80%.

Another potential advantage of partial MFD is that it allows determining drying homogeneity among samples. Because the samples have not yet reached equilibrium in terms of residual moisture, differences between the drying states of individual samples should be more pronounced than for complete MFD. Accordingly, the following hypothesis is stated:

H4.2: Partial MFD enables an evaluation of the drying homogeneity among the processed samples, as the drying states of individual products do not yet approach a homogeneous equilibrium.

Several studies on MFD have already investigated the influence of process parameters such as chamber pressure [11, 89] and microwave power [8, 11, 12, 67, 89–92]. However, no study has comprehensively investigated the influential process parameters of microwave frequency, microwave power, and chamber pressure. Assuming that the initial part of drying performed in partial drying is representative of the complete process, the following hypothesis is stated:

H4.3: Performing a parameter study involving partial MFD, concluding the process before complete drying, is adequate for qualitatively examining the impact of the process parameters microwave frequency, microwave power, and chamber pressure on the MFD process.

In part (III) Process optimization, insights from parameter studies and electromagnetic simulations are used to develop an algorithm for automated real-time process control. The modular laboratory-scale drying plant enables the classification of the optimized MFD process and the respective product properties compared to the established CFD process and alternative MFD processes.

As described in Section 1.4, frequency adjustment during MFD has proven particularly promising, although it is associated with challenges in process control. An automated algorithm for frequency control is developed to monitor and apply RFs throughout MFD. The control algorithms are described in Chapter 2 and Chapter 5. The algorithms developed are applied to MFD in Chapter 5. Benchmark processes include MFD with automated real-time control applying RFs with the lowest energy efficiency, MFD with constant frequencies throughout drying, and CFD. Process parameters and product properties are analyzed to compare these processes. The following hypothesis is based on the outlined findings on frequency adjustment in microwave-assisted heating:

H5.1: The application of energy-efficient RFs throughout MFD with real-time frequency control results in increased energy efficiency and reduced drying duration compared to MFD without real-time frequency control.

Based on the studies highlighting similar or superior product properties of MFD compared to CFD [12, 14, 73], the following hypothesis is postulated:

H5.2: The application of energy-efficient RFs throughout MFD with real-time frequency modulation yields a process with similar or superior product quality compared to CFD.

In Chapter 6, the results are reviewed concerning the hypotheses, placed in the research context, and an outlook on future research perspectives is provided.

2 Construction of a laboratory-scale plant for the investigation of microwave-assisted freeze-drying

2.1 Introduction

Performing controlled freeze-drying (FD) experiments lays the foundation for achieving the overarching goals of this thesis in the investigation of microwave-assisted freeze-drying (MFD) to gain an understanding of the process and enable process optimization. The corresponding experiments should be performed on an appropriately small scale in a laboratory-scale plant. Building such a plant from scratch allows for the customized integration of all required functions. The approach also provides the opportunity to implement a flexible setup, which allows future changes to ensure that the plant can adapt to current and evolving research needs.

This chapter describes the design of a customized laboratory-scale drying system and demonstrates its suitability for controlled FD experiments. This introduction focuses on the main requirements for the design of the system, suitable sensors for process monitoring, and the expected behavior of process parameters during FD, which allow the assessment of performed experiments in comparison to the literature on FD. In the following section, the plant setup is described, including the components necessary to perform MFD and conventional freeze-drying (CFD). This part comprises a description of the process chamber, the plant layout, the sensor network, and the software of the control system. The subsequent section focuses on the setup of the FD commissioning experiments, including descriptions of the preparation of the tylose gel, which is the model product used, and the experimental procedures. The results of the commissioning experiments are presented in the next section. These results comprise the process parameters from CFD and MFD and the microwave reflections in dependence on the frequency, the material to be dried, and the microwave transmission line. Finally, the conclusion wraps up this chapter.

FD produces the highest quality products compared with other drying techniques, especially for heat-sensitive compounds and materials, like antibodies, enzymes, or peptides [93]. Microwaves can be used to supplement FD as MFD. The main benefits of MFD in the drying of foods are high drying rates and increased quality

of some products [51]. A detailed evaluation of the benefits and limitations of CFD and MFD is presented in Sections 1.2 and 1.4.

Process conditions in the plant must be suitable for FD in both CFD and MFD processes. Therefore, a similar plant design is required for both processes. Figure 2.1 shows the schematic layout of an FD system suitable for MFD and CFD. Its main components are a process chamber, a condenser, a vacuum pump, and an energy supply system.

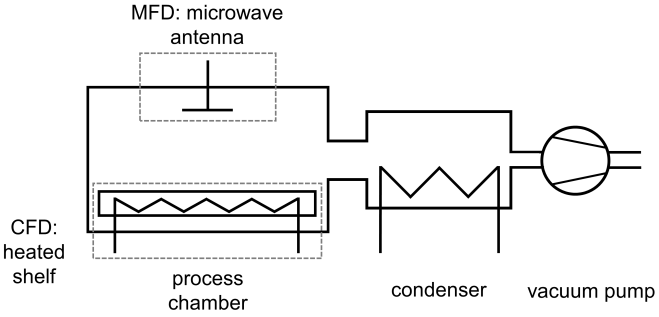

Figure 2.1: Schematic representation of an FD system. In MFD, microwave antennas are installed to supply the material to be dried with energy, while in CFD the energy is supplied with heated shelves.

The defining difference between CFD and MFD is the energy supply mechanism to the material to be dried. In CFD, the material to be dried is placed on shelves in the processing chamber, which function as heat exchangers. The shelves supply the heat required during drying and can optionally be used to freeze the products prior to drying. Alternatively, an external freezer is used to freeze the product. In MFD, heat is supplied to the material to be dried using microwaves fed into the process chamber. Solid-state microwave generators (SSGs) are particularly suitable for adjusting microwave properties because of their ability to quickly and precisely control frequency, power, and phase shift. Section 1.3.4 provides a detailed description of SSGs and their components.

During FD, water is sublimated from the material to be dried and desublimated at the cooling coil in the condenser, removing excess vapor from the process chamber. A refrigeration circuit is used in the condenser to generate the required low temperatures on the cooling coil, i.e., a high pressure gradient between the process chamber and the condenser. A vacuum pump connected to the condenser generates the vacuum required for sublimation in the process chamber. The vacuum pump is necessary to establish the initial vacuum and remove inertial gases during FD.

The laboratory-scale drying system has to fulfill all basic requirements to perform MFD. Additionally, CFD experiments should be performed in the same process chamber to enable MFD benchmarking. This requirement necessitates the integration of a heat exchanger, which can be removed for MFD experiments. For MFD experiments, the process chamber must be designed as a multimodal resonator. This design is the only way to operate with multiple resonant frequencies (RFs), which is a promising approach to increase energy efficiency and heating homogeneity, see Section 1.4. Safety aspects must also be taken into account in the design. Particular attention must be paid to shielding the environment from microwave leakage from the process chamber during MFD experiments. At least one SSG has to be incorporated into the system to generate microwaves from 2400 MHz to 2500 MHz during MFD. This frequency range is an ISM band, the benefits of which are described in Section 1.3.1. The capability of SSGs for fast and precise control of the microwave parameters frequency, power, and phase shift during MFD is essential for the control concepts to be explored in this thesis.

The plant setup must include all necessary sensors for process monitoring. For monitoring of product temperature, fiber optic temperature sensors are used, as metallic thermocouples interact with microwaves, leading to thermal instabilities and dielectric breakdown [94]. Chamber pressure is monitored using capacitive pressure sensors, which are considered particularly suitable for this application [95]. In addition, a Pirani vacuum gauge is used. The pressure signal derived from the Pirani gauges is based on thermal conductivity of the gaseous phase, which depends on the vacuum pressure and the gas composition. This dependency leads to variations in the Pirani gauge readings during primary drying as a function of the

gas composition since the thermal conductivity of water vapor is approximately 1.6 times higher than that of nitrogen [95]. Consequently, the sublimation of water and the ensuing elevation in the proportion of water vapor causes the Pirani gauge to indicate an increased chamber pressure. The equivalence of Pirani pressure with the pressure determined by the capacitive sensor can be used to determine the end of primary drying [96]. Incorporating a load cell enables continuous monitoring of the sample mass, providing real-time information regarding drying progress and residual moisture content. The temperature of the heat transfer medium is a crucial parameter in the monitoring of CFD experiments. In MFD, SSGs enable the detection of forward and reflected power by internal sensors, from which the dissipated power and energy efficiency is calculated. The dissipated power P_d is calculated as

$$P_d = P_f - P_r, \tag{2.1}$$

where P_r is the reflected power and P_f is the forward power. The energy efficiency η describes the conversion of electromagnetic energy into heat and is calculated as

$$\eta = 1 - P_r/P_f. \tag{2.2}$$

Commissioning experiments are performed to check the agreement of the results obtained with the constructed plant with results from the literature. The commissioning experiments in this chapter include frequency sweeps in the range of 2400 MHz to 2500 MHz to characterize the influence of the material within the cavity on microwave reflections. The presence of material in the process chamber will presumably increase energy efficiency as a result of power dissipation in the material. The product state is also expected to cause differences in power dissipation within the cavity. A progressing drying state in FD should lead to reduced dielectric properties (DPs) and consequently to a lower dissipation of electromagnetic energy, as can be deduced from the results of Nakagawa and Kono [26]. In addition, the effect of the connection type between the SSG and the

process chamber is investigated to evaluate the relevance of the transmission line for microwave application. Additional interfaces for microwave coupling between the SSG and the process chamber are expected to lead to lower energy efficiency due to increased reflections.

The commissioning experiments also include MFD and CFD process runs. The expectation for FD commissioning experiments is that product temperature, chamber pressure, drying kinetics, and energy efficiency will exhibit typical patterns for FD. The comparable patterns of these parameters would show the suitability of the constructed plant for performing FD experiments. Toward the end of CFD, the product temperature should asymptotically approach the shelf temperature [35, 97]. At the end of MFD, an equilibrium temperature should be reached at which the absorbed microwave energy and the heat losses to the environment are in balance [11]. During FD, the Pirani gauge should indicate a decrease in chamber pressure at the end of primary drying, although the chamber pressure is constant, as indicated by a capacitive pressure sensor. This characteristic is attributable to the diminishing proportion of water vapor in the process chamber. Härdter et al. [14] used a mass spectrometer and a comparative pressure measurement between signals indicated by a capacitive pressure sensor and a Pirani gauge to monitor MFD. Their results confirmed the possibility of detecting the end point of primary drying by comparative pressure measurement. The drying rate should be highest at the beginning of the drying process and gradually decrease throughout CFD [8, 97] as well as MFD [8, 11]. For MFD, the energy efficiency is expected to decrease throughout FD as the DPs decrease due to the removal of moisture [26].

2.2 Plant setup

The plant setup is designed to enable both MFD and CFD within the same process chamber based on its modular design. Using a single plant setup for both processes allows for direct comparisons between CFD and MFD due to eliminating influencing factors, such as differences in the performance of the process equipment or deviations in sensor calibration.

2.2.1 Process chamber

The centerpiece of the laboratory-scale plant is the process chamber, where the product is placed for FD. The stainless steel process chamber has inner dimensions of 612 mm × 400 mm × 300 mm, as depicted in the design views shown in Figure 2.2. Yakovlev [23] showed in electromagnetic simulations that an empty cavity of these dimensions with microwave sources located centrally at the top and right side is a multimodal resonator. As a multimodal resonator is intended for this work, these dimensions should be suitable.

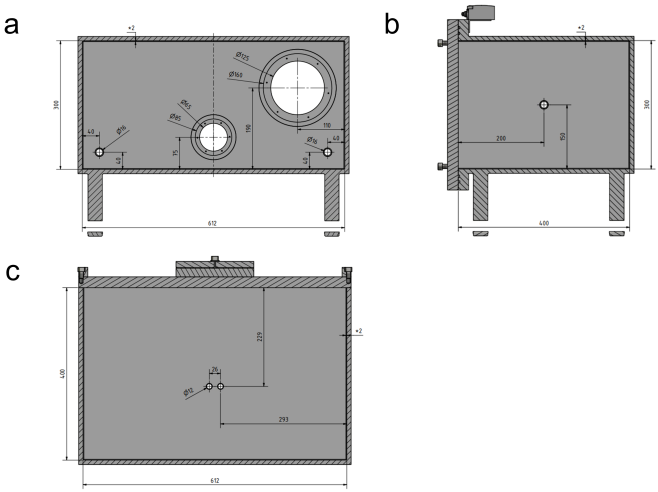

Figure 2.2: Design views of the process chamber: (a) Sectional front view, (b) sectional side view, (c) sectional top view. The dimensions are given in millimeters.

Figure 2.3 shows a three-dimensional design view of the process chamber with highlights of relevant features. The front of the process chamber is designed as a door, allowing easy access for experimental work and modifications to the inner installations. Air can be let into the chamber through a stub (A) via a manually operated valve. A connection on the back (B) links the process chamber to the peripheral devices for FD through a manually adjustable butterfly valve.

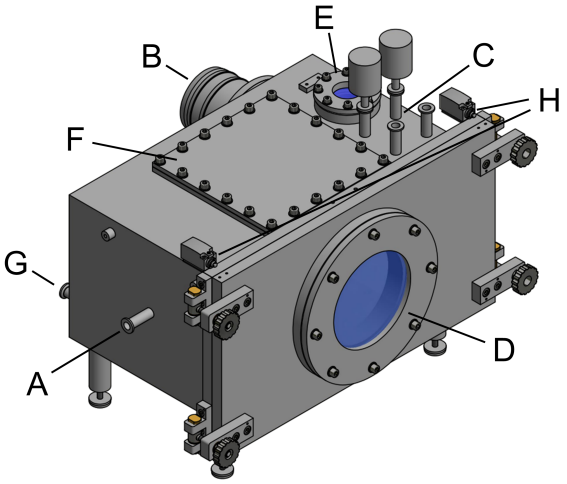

Figure 2.3: Three-dimensional design view of the process chamber. A - air inlet, B - connection to the condenser, C - stubs for sensor mounting, D - viewing window, E - illumination opening, F - exchangeable wall module, G - feed-through heat transfer medium, H - limit switches.

Connections to up to two SSGs are realized with 86 mm × 43 mm WR340 waveguides, which can be embedded in the ceiling and right side wall of the cavity. These openings are not implemented in Figure 2.3 and can be closed with metal plugs, allowing flexible microwave application through the openings. One waveguide can be embedded in the top wall and another in the shorter side wall of the process chamber, opposite to the air inlet (A). Both openings are centrally located on the walls, with the longer side of the waveguide parallel to the longer side of the wall.

Four DN 16 ISO-KF stubs are located next to each other at the top of the process chamber (C). Various compatible sensors can be mounted on those stubs, such as those for chamber pressure. Ultra-Torr 1/8 inch vacuum fittings (Swagelok, Solon, USA) for up to four individual fiberoptic temperature sensors are installed centrally in the lower back wall in an exchangeable round module. The respective opening is shown in Figure 2.2 (a). A viewing window (D) is embedded in the

front door for visibility during processing. A second opening at the top (E) enables interior illumination with a lamp.

An interchangeable rectangular wall module (F) is located at the top of the process chamber to facilitate a later modification of the connections. The opening has dimensions of 260 mm × 260 mm. Figure 2.3 shows a module without openings, while a module with a centrally embedded waveguide was used in the MFD experiments. Two DN 16 ISO-KF stubs on the lower left and lower right of the back wall (G) enable feed-through of heat transfer medium to the modular heat exchanger required in CFD. For MFD, two stubs with a diameter of 12 mm are located in the bottom wall, see Figure 2.2 (c). These openings allow the connection of a plate on which the material to be dried is placed, i.e., the product support, to a load cell that is mounted in an airtight rectangular chamber below the process chamber.

Quartz glass panes are inserted between the waveguides and the cavity to shield the vacuum while admitting microwave transmission. All remaining openings to the environment are covered with acrylic glass. The waveguide connections are sealed airtight with custom-made flat gaskets made of polytetrafluoroethylene. The remaining openings are sealed with polymeric flat gaskets and ring gaskets.

A gasket ring with a metal gauze jacket shields the narrow gap at the chamber door against microwave leakage. The microwave shielding of the remaining openings is selected on the basis of their size relative to the cutoff wavelength. The cutoff frequency f_{co} of a circular waveguide is the frequency below which electromagnetic waves cannot propagate, corresponding to a rapid exponential decay of the associated fields [42]. According to [98], microwaves travel through circular waveguides in transverse electric (TE) and transverse magnetic (TM) modes. The TE_{11} mode has the lowest cutoff frequency of all modes in a circular waveguide. The respective cutoff frequency is calculated as $f_{co} = \frac{1.841c}{2\pi r}$ with $c = 299\,792\,458\,\mathrm{m\,s^{-1}}$ being the speed of light and r the radius of the circular waveguide. Setting f_{co} to 2500 MHz, the maximum employed frequency in the system, yields r = 0.035 m. Consequently, all openings with a diameter below 0.070 m can be shielded using circular metallic stubs that act as cutoff waveguides.

These openings include the stubs for sensor connections and the inlet valve for air. The remaining larger openings are shielded using metal gauze with a mesh width of 0.8 mm, allowing gases to pass through while reflecting microwaves. The gauze is installed in a way that keeps the walls of the process chamber as flat as possible to minimize interactions with the microwaves.

2.2.2 FD equipment

The integration of the process chamber into the laboratory-scale FD system is schematically shown in Figure 2.4. For CFD, a custom-built heat exchanger, shown in Figure 2.5, is installed in the chamber as a product support. A thermostat AC200 (Thermo Fisher Scientific, Henningsdorf, Germany) is connected to the heat exchanger. The thermostat can regulate the temperature of the heat transfer medium within a range of -5 °C to 70 °C. In MFD experiments, a plate made of polyether ether ketone (PEEK) with a base area of 200 mm × 200 mm serves as the product support. Two PEEK cylinders connect this plate to a load cell through the two openings in the bottom wall.

The process chamber is connected through a butterfly valve on the back wall to a custom-made cold trap (UCCT, Vienna, Austria) and a NEO D 65 vacuum pump (Leybold, Cologne, Germany), which are connected in series. The cold trap acts as a condenser and includes a cooling coil for the resublimation of vapor. It is set to a default temperature of -60 °C. A diaphragm valve connecting the cold trap to the vacuum pump can be electrically controlled to regulate the chamber pressure, opening only when the pressure exceeds the set value. An SSG HY2020 (TRUMPF, Freiburg, Germany) is connected to the waveguide at the top of the process chamber via a coaxial cable. For this work, the side wall waveguide opening is sealed by a metal plate since only one SSG is used. The SSG can generate microwaves with power up to 600 W and frequencies from 2400 MHz to 2500 MHz, adjustable in 0.01 MHz increments.

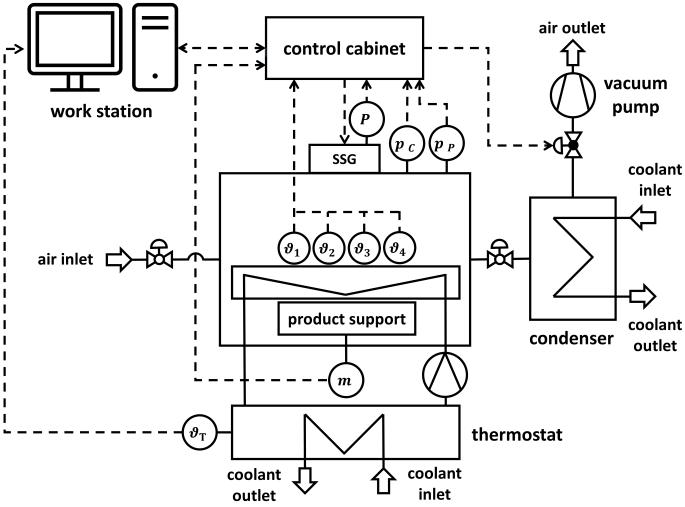

Figure 2.4: Schematic diagram of the laboratory-scale plant setup for CFD and MFD. m - load cell, P - microwave power sensor, p_C - capacitive pressure sensor, p_P - Pirani vacuum gauge, ϑ_{i} - fiber optic temperature sensors, ϑ_T - thermostat temperature sensor.

2.2.3 Sensor network

The sensor setup in the laboratory-scale system is designed to ensure precise monitoring and control of the process parameters. The stainless steel process chamber is equipped with pressure sensors, temperature sensors, a load cell, and microwave sensors. The sensor setup is schematically shown in Figure 2.4. The depicted setup enables real-time data acquisition, laying the basis for process control.

A CMR363 capacitive pressure sensor (Pfeiffer, Asslar, Germany) measures the chamber pressure. A VCP63 Pirani vacuum gauge (Thyracont Vacuum Instruments, Passau, Germany) is the secondary device for measuring chamber pressure. The capacitive pressure sensor is used for process control, as the signal from the Pirani vacuum gauge depends on the composition of the gaseous phase [99], which can change during drying, as described in Section 2.1. The capacitive

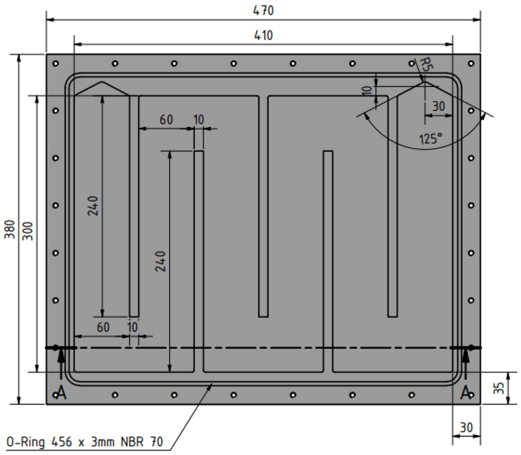

Figure 2.5: Sectional view of the heat exchanger for CFD from above with the channels for the flow of the heat transfer medium. The dimensions are given in millimeters.

sensor was purchased in a calibrated state during plant construction. The Pirani gauge has been calibrated to the signal of the capacitive sensor at 0.5 mbar. This calibration is sufficient for the commissioning experiments since the pressure was set to 0.5 mbar in all experiments. However, for future work, the sensor should be calibrated to multiple pressures in the relevant range for FD below 6.12 mbar. These calibrations were not performed as part of this thesis.

Temperature monitoring is realized with four FOS-TG fiber optic temperature sensors (Rugged Monitoring, Quebec, Canada). In addition, an internal temperature sensor is installed in the bath of the AC200 thermostat to measure the temperature of the heat transfer medium in CFD. These sensors were calibrated using a Pt-25 platinum resistance thermometer MKT25 (Rosemount, Shakopee, USA) through a three-point calibration process to ensure accurate measurements. The calibration curves for the three sensors used in the commissioning experiments are shown in Figure A.1 in the Appendix.

The weight of the product is measured using a PW4MC3/2kg load cell (Hottinger Brüel & Kjaer, Darmstadt, Germany), connected to the product support and used

exclusively for MFD. The load cell is not usable in CFD experiments because the material to be dried must be placed on the heat exchanger, which cannot be connected to the load cell. The load cell was calibrated with calibration weights covering product weights up to 300 g in the vacuumed process chamber. Figure A.2 in the Appendix shows the calibration curve for the load cell.

Internal sensors in the HY2020 SSG monitor forward and reflected microwave power. The SSG was acquired with calibrated sensors during the construction of the system.

Measurement signals from pressure and product temperature sensors are converted from analog voltage signals to digital signals using a Mega 2560 microcontroller (Arduino, Chiasso, Switzerland) within a custom-built control cabinet. The Mega 2560 handles voltage signals ranging from 0 V to 5 V. Higher voltages from 0 V to 10 V are reduced to the required range using a custom-made voltage divider. The load cell signal is an exception, as it provides a digital signal to the Mega 2560. The Mega 2560 is connected to a central work station for signal monitoring and process control, which is programmed in Matlab 2020b (Mathworks, Natick, USA) with two separate instances, as described in Section 2.2.4. The work station is connected to the AC200 thermostat via USB for temperature monitoring and to the HY2020 SSG via Ethernet for process control and monitoring.

The control cabinet also supplies power to the sensors using two power supply units at 5 V and 24 V. Only the fiber optic temperature sensors, the microwave power sensors, and the temperature sensor integrated into the thermostat are supplied via external power supply units. An electric connection from the Mega 2560 to the electrical valve between the condenser and the vacuum pump enables electrical switching of the valve to control the chamber pressure.

For security purposes, particularly regarding the use of microwaves, an emergency stop is mounted on the control cabinet to manually cut the power supply to the plant in case of malfunctions. Further security measures include limit switches installed on the top right and top left of the process chamber door. Figure 2.4 shows the limit switches (H). The power supply to the SSG is only enabled when the two limit switches are activated to ensure that the process chamber door is

closed. Additional restrictions on the power supply to the SSG are implemented in the process control algorithms, as described in Section 2.2.4.

2.2.4 Software

Two separate instances in Matlab 2020b are integrated for process monitoring and control. The first instance is used to monitor and control FD parameters. This instance must always be activated since its functions are crucial for MFD and CFD. The second instance is employed to monitor and control the microwave parameters. Therefore, it is only required for MFD.

2.2.4.1 Instance 1 – FD parameters

The first instance provides a graphical user interface (GUI) for monitoring FD parameters. Slightly different scripts are used for CFD and MFD due to the different parameters recorded in each process. The CFD version of this instance monitors all relevant parameters for CFD, including sample temperature, chamber pressure measured by the capacitive sensor and Pirani gauge, and thermostat temperature. The MFD version additionally measures the weight of the product, omitting the measurement of thermostat temperature.

Data monitoring intervals are set to two seconds. All parameters are plotted live for online process evaluation. Various parameters, which can be used as process termination criteria, are continuously calculated and displayed. These parameters include the difference in chamber pressure recorded with the capacitive sensor and the Pirani vacuum gauge, smoothed as averages of 100 measurements, and the change in sample weight over the last hour for MFD. The data recorded from the experiments are stored in Matlab files. A backup text file is created at every recording interval to ensure data preservation in the event of problems during the process termination, which would lead to an error in the Matlab file creation.

The instance also controls the chamber pressure by switching the valve to the vacuum pump based on capacitive sensor readings in accordance with a predetermined value in the algorithm. The valve only opens when the detected pressure exceeds the set value, thereby regulating the pressure to the specified level. The precision of pressure control decreases when the chamber pressure is increased. The reason for this is the constant interval of two seconds between pressure readings, which is the basis for pressure control. At higher pressures, more molecules are removed from the process chamber during the set time due to the higher density of the gaseous phase. This leads to a higher decrease in chamber pressure at high pressure levels. Therefore, the averaged chamber pressure is always lower than the set value, with a more pronounced tendency at higher pressure values. The pressure control has been successfully tested up to a set value of 1.0 mbar. This range is sufficient for the investigation of FD but does not cover the theoretical maximum pressure in FD of 6.12 mbar, the pressure at the triple point of water.

The activation of the HY2020 SSG, required in the second instance, depends on the initialization of the process monitoring program as a safety measure. If the first instance is inactive, the SSG will not be supplied with power, rendering the second instance useless.

2.2.4.2 Instance 2 – microwave parameters

The second instance is used to control and monitor the microwave parameters. Figure 2.6 shows the GUI of instance 2. The SSG must be connected to activate the connection before each use and disconnected after each experiment as a safety measure via the 'Connect' and 'Disconnect' buttons. The 'Frequency sweep' button starts a frequency sweep for process characterization with the default settings covering a range of 2400 MHz to 2500 MHz in intervals of 0.1 MHz. After each frequency sweep, data on forward power, reflected power, energy efficiency, frequency, and SSG temperature are stored.

The GUI also enables the microwave power application with defined, time-independent microwave properties through the 'Power application' button. The

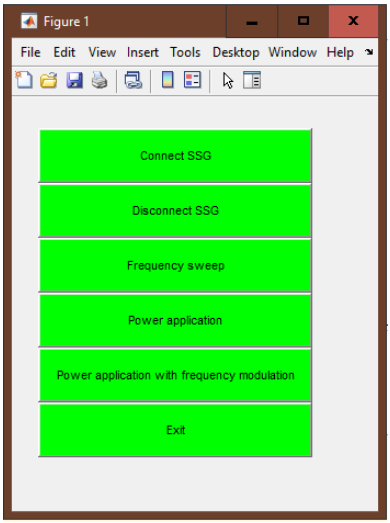

Figure 2.6: GUI of instance 2 for microwave control and monitoring.

microwave parameters power, applied frequencies, and activation ratio must be specified in a menu before each power application. The entered frequencies are applied sequentially from the lowest to the highest for 10 s each before the next cycle begins. The activation ratio describes the time the SSG is active during each 10 s frequency application. Once all the required parameters have been entered, a power application button will appear, allowing the microwaves to be activated and deactivated at specific times.

The 'Power application with frequency modulation' button is used to apply control algorithms in Matlab with a targeted adjustment of microwave parameters beyond the methods described here. The respective more sophisticated algorithms for automatic frequency adjustment in real time are described in detail in Chapter 5.

2.3 Experimental setup

2.3.1 Model product

The model product used for the experiments was tylose gel with ascorbic acid as a tracer substance. The tylose gel comprised 76.23 wt% demineralized water, 22.77 wt% Tylose MH1000 (Kremer Pigmente, Aichstetten, Germany), and 1.00 wt% ascorbic acid (Carl Roth, Karlsruhe, Germany). The preparation process involved heating demineralized water to 65 °C at 200 rpm using a heatable magnetic stirrer (C-MAG HS 7, IKA Werke, Staufen im Breisgau, Germany). The ascorbic acid was dissolved in the heated water and kneaded with the tylose powder to form a homogeneous mass. Each sample was weighed at 12.50 $\pm$ 0.05 g, formed into cuboids of approximately 25 mm $\times$ 25 mm $\times$ 20 mm, and frozen at -30 °C for at least 14 h. The product was packed airtight before freezing to prevent water loss prior to FD.

2.3.2 Process characterization

Characterizing the process via reflected microwave power as a function of frequency is essential for targeted frequency application in MFD. For each characterization in a frequency sweep, 24 frozen tylose gel cuboids were taken from the freezer and placed centrally on the product support in a 6 $\times$ 4 arrangement with 5 mm spacing in between. Figure 2.7 shows the arrangement of the samples with a numbering system to facilitate the identification of the samples. Three FOS-TG temperature sensors were inserted into drilled holes in samples 4, 6, and 10. This choice contains one sample at the edge, one at the corner, and one in the center of the arrangement.

A chamber pressure of 0.5 mbar was set in the process chamber and a vacuum was applied for 10 min. Then a frequency sweep was performed in the range of 2400 MHz to 2500 MHz at intervals of 0.01 MHz with a set forward power of

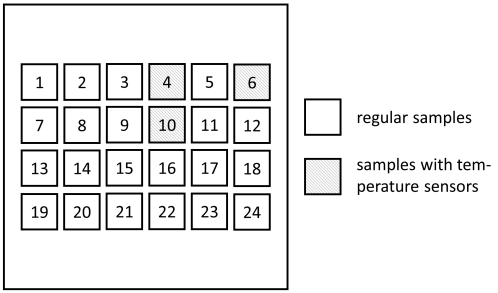

Figure 2.7: Schematic depiction of the tylose gel samples on the product support. Samples are numbered for easy identification. The bottom row is adjacent to the door of the process chamber.

50 W. The dissipated power P_d in the experiments was calculated according to Equation 2.1 and the energy efficiency η was calculated according to Equation 2.2.

With this procedure, frequency sweeps were performed for an empty process chamber and tylose gel samples at the drying states of 0%, 50%, and 100%. These drying states correspond to the approximate weight ratio between the water removed during MFD and the water initially contained. Frequency sweeps for the drying states 50% and 100% were performed directly after MFD, as described below, without terminating the vacuum. Additionally, a setup connecting the SSG to the process chamber through a coaxial cable, which was inserted between the WR340 waveguide couplings at the SSG and on top of the process chamber, was compared with a setup with a direct connection through a WR340 waveguide. All setups were characterized in triplicate.

2.3.3 Drying experiments

For MFD, the setup and sample placement were identical to those for the process characterization. Microwaves were applied after 10 min of vacuum application with a set forward power of 50 W and an activation ratio of 0.5. The microwave application marked the start of the process time. In the commissioning experiments, six constant frequencies from 2400 MHz to 2500 MHz in 20 MHz intervals were

applied in all experiments. MFD was terminated when the drying rate calculated over 1 h fell below 0.25 g/h, which indicated that drying was complete since only small amounts of water were removed from the material.

For CFD, samples were placed centrally on the heat exchanger in positions analogous to the MFD setup. The thermostat was initially set to -5 °C to prevent the samples from melting in contact with the shelf and then increased to 30 °C after the vacuum was applied for 10 min in analogy to the start of the power application in MFD, marking the start of the process time. The process duration was extended by 20% when all temperature sensors showed a temperature difference of less than 2 K/h over 20 min. The low rate of temperature change signaled that all monitored samples reached a temperature plateau, which indicated the completion of drying. The extension of 20% was applied based on the literature, which recommends a time surcharge of 10% to 30% to account for differences in the drying behavior of samples [96]. All drying experiments were performed once, as they were only intended to provide proof of concept for the plant design.

2.4 Results and discussion

2.4.1 Process characterization

Figure 2.8 shows the energy efficiency in the frequency range of 2400 MHz to 2500 MHz for investigated setups regarding the comparison of an empty process chamber with a process chamber containing tylose gel samples at a drying state of 0% and the two transmission line setups with and without a coaxial cable. The energy efficiency is derived from the reflected microwave power, as described in Section 2.1.

In all setups, the maxima of energy efficiency show a smooth profile, while more signal noise can be observed around the minima. The frequencies of these local maxima are referred to as RFs. A more detailed definition of RFs is given in Section 1.3.3.

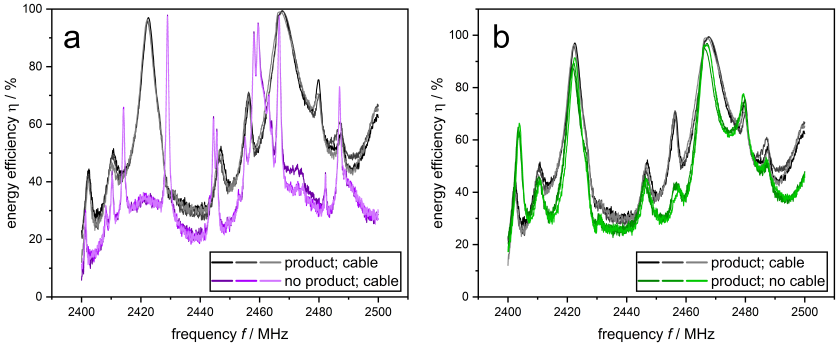

Figure 2.8: Process characterization as the energy efficiency of microwaves depending on the frequency for (a) varying material inside the process chamber and (b) varying connections to the SSG. Product means tylose gel samples (drying state 0%) inside the process chamber and cable means using a coaxial cable in the transmission line from the SSG to the process chamber. Experiments were carried out in triplicate.

In Figure 2.8 (a), the empty process chamber is characterized by a higher number of local maxima in energy efficiency compared to the process chamber with tylose gel samples, indicating a higher number of distinct RFs. The observation of an apparently higher number of RFs with a more narrow peak width when material is excluded from the process chamber is in line with theoretical considerations [46]. The explanation in the literature is that the introduction of a workload leads to a higher density of modes and broader widths of the energy efficiency peaks around RFs, which leads to no clear differentiation between RFs due to their overlapping peaks. Therefore, more RFs in the frequency range 2400 MHz to 2500 MHz should be present in experiments with tylose gel in the process chamber. However, these RFs presumably cannot be detected in the frequency sweep because of their superposition.

When microwaves are applied to an empty process chamber, the question arises as to where the electromagnetic energy dissipates. The electromagnetic energy must dissipate somewhere, otherwise the energy efficiency would be 100% independent of frequency. Wall losses, see Section 1.3.3, and leakage from the process chamber are two possible modes of electromagnetic energy dissipation. With RFs, however, the applied microwave energy should amplify the electromagnetic

field inside the process chamber by constructive interference, see Section 1.3.3. In a lossless process chamber, the electromagnetic field would increase indefinitely. However, applicators are not lossless due to the limited conductivity of the materials surrounding the cavity and wall losses increase with the electromagnetic field strength [46]. Moreover, above a critical power, dielectric breakdown may also occur, leading to a consumption of electromagnetic energy, as described in Section 1.4. Therefore, the electromagnetic field cannot be increased indefinitely in practice, and electromagnetic energy is dissipated even in an empty cavity that contains no dielectric.

The inclusion of a coaxial cable represents a change in the transmission line from the SSG to the process chamber. Wave reflection in a transmission line occurs due to a mismatch between the line and the load [100]. Therefore, variations in the transmission line are expected to lead to differences in microwave reflections. Figure 2.8 (b) shows that excluding the coaxial cable results in a curve pattern similar to its inclusion. The count of RFs remains unchanged and their frequencies are comparable. However, the inclusion of a coaxial cable lead to an increased average energy efficiency in the frequency range 2400 MHz to 2500 MHz of 53.5% compared to 46.6% without a coaxial cable, indicating increased impedance matching. The inclusion of a coaxial cable seems to increase the average energy efficiency at the initial stage of MFD. In contrast to this general trend, using a coaxial cable decreases energy efficiency at the RFs around 2403 MHz and 2480 MHz from 64.1% to 42.2% and from 76.0% to 72.1%, respectively. The lower energy efficiency at these RFs shows the frequency-dependent behavior of microwave reflections in dependence on the transmission line. In summary, the choice of the transmission line influences microwave reflections. In order to compare the energy efficiency between processes, the transmission line setup has to be kept constant. In the further course of this work, the setup with a coaxial cable is used.

Figure 2.9 shows the frequency-dependent energy efficiency for tylose gel at drying states of 0%, 50%, and 100% obtained from MFD experiments. The average energy efficiency decreases with the drying state. For the respective drying states of 0%, 50%, and 100%, it amounts to 53.5%, 48.4%, and 40.0%.

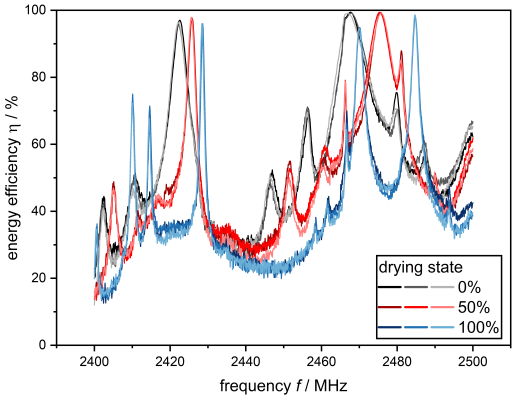

Figure 2.9: Process characterization as the energy efficiency of microwaves in dependence on frequency for the drying states 0%, 50%, and 100%. The drying state indicates the amount of water removed from the product in MFD. Experiments were performed in triplicate.

The curve patterns of energy efficiency among the drying states are similar. However, there are notable differences, such as an increase in the apparent number of RFs with an advancing drying state. At the drying state 0%, nine distinct RFs are observed, while at 50% and 100%, eleven distinct RFs are evident. Energy efficiencies of above 90% can be achieved at several RFs for all drying states. The peaks associated with the RFs get narrower as the drying state progresses, particularly noticeable between 2420 MHz and 2430 MHz. A shift in RFs to higher frequencies can be observed as the drying state advances, particularly visible in the frequency bands 2420 MHz to 2430 MHz and 2485 MHz to 2495 MHz. However, the overlapping of multiple peaks associated with individual RFs complicates the evaluation of frequency shifts in the entire spectrum.

Increases in the drying state correspond to decreases in the DPs of the material to be dried as a result of water removal, similar to the observations made when comparing an empty process chamber with a process chamber containing material. Consequently, an increase in the identifiable number of distinct RFs and a narrowing of associated peak widths are anticipated [46], alongside their shift to higher frequencies [42] and the decrease in average energy efficiency, as less electromagnetic energy is dissipated as heat in materials with a lower dielectric loss

factor [54]. The results highlight the necessity to adapt the frequency in real time during MFD to continuously apply highly energy-efficient RFs, which are present throughout MFD. The search for RFs in narrow frequency bands around previously utilized RFs appears promising, as RFs gradually shift to higher frequencies with advancing drying state.

2.4.2 Commissioning CFD

Figure 2.10 shows the parameters monitored in the CFD commissioning experiment over the process time. The thermostat temperature was initially set from -5 °C to 30 °C, marking the start of the process time. The measured thermostat temperature confirms that the set temperature of 30 °C has been reached in the thermostat bath.

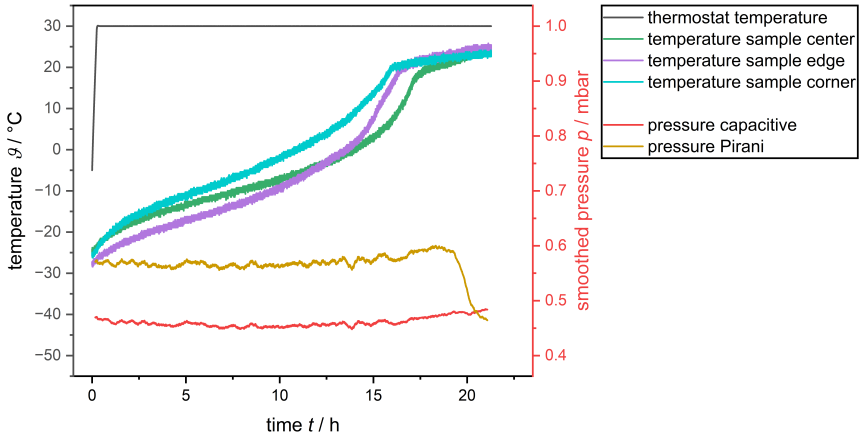

Figure 2.10: Process parameters recorded during the CFD commissioning experiment. The following assignments apply to the samples for temperature: Green – sample center (position 10), violet – sample edge (position 4), light blue – sample corner (position 6).

The temperatures of the monitored samples increase continuously during CFD. The increase in thermostat temperature causes the initial rise in sample temperature. Subsequently, the temperature increases only gradually, reflecting an

approximate balance between heat input through the shelf and heat consumption to supply the latent sublimation enthalpy. As the process progresses and the sublimation rate decreases, the rate of temperature change increases because less energy is consumed by sublimation. The dry samples then reach an equilibrium temperature, where the heat input from the shelf approximately equals heat losses to the environment by thermal radiation and conduction.

Towards the end of drying, the sample temperature gradually approaches an equilibrium temperature of 23 °C to 25 °C, affirming expectations from the literature [35, 97]. The sample temperature is expected to be lower than the thermostat temperature due to heat losses from the samples and the shelf, as reflected by the final sample temperatures below 30 °C. Sample 6 in the corner of the arrangement reaches the approximate equilibrium temperature first, followed by sample 4 at the edge and sample 10 in the center. The rapid increase in the sample temperature at the corner of the arrangement can be attributed to the large surface available for energy input by thermal radiation, as observed in CFD [101].

The measured sample temperature is at all stages higher than the sublimation temperature of ice of -27.3 °C at 0.5 mbar [102]. This difference is presumably due to the formation of a dry layer between the temperature sensor and the sublimation front, compare Figure 1.2.

The chamber pressure, as recorded by the capacitive sensor, remains slightly below 0.5 mbar throughout CFD. The Pirani sensor records a higher pressure of about 0.6 mbar until approximately 19 h into the process, after which it drops to around 0.5 mbar. The Pirani vacuum gauge was calibrated to the capacitive sensor at 0.5 mbar with no material present inside the process chamber. Therefore, it was calibrated to the gaseous composition of ambient air. The differences recorded by pressure sensors are probably caused by the differing principles on which these sensors operate, as outlined in Section 2.1. The higher pressure measured with the Pirani gauge during the drying section, where mainly water vapor is present, is in line with the literature [14, 95]. The marked decrease in pressure indicated by the Pirani gauge at about 19 h indicates a shift in gas composition from predominantly water vapor to mainly nitrogen in the process atmosphere,

signaling that sublimation is complete [96]. This finding confirms the suitability of the selected termination criterion based on the change in the sample temperature.

In conclusion, the parameters associated with FD were qualitatively as predicted. The experiment indicates that the constructed setup can effectively carry out and monitor CFD experiments.

2.4.3 Commissioning MFD

Figure 2.11 displays the process parameters monitored during the MFD commissioning experiment that are not directly associated with microwaves. Compared to Figure 2.10, the thermostat temperature is substituted with the sample mass.

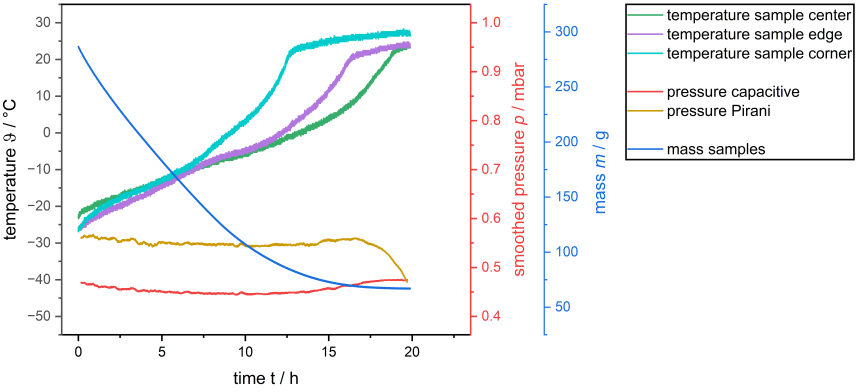

Figure 2.11: Process parameters associated with freeze-drying recorded during the MFD commissioning experiment. The following assignments apply to the samples for temperature: Green – sample center (position 10), violet – sample edge (position 4), light blue – sample corner (position 6).

The sample temperature curves in MFD are quantitatively comparable to those observed in CFD in terms of their general shape. The similarity of the temperature curves suggests analogous process characteristics and interpretations. The sequence in which the samples reach their approximate final temperatures in dependence on the sample position in MFD mirrors that of CFD. This order

suggests that thermal radiation from the chamber walls accelerates the drying of outer samples, analogous to CFD. The spread of final temperatures is higher for MFD with about 20 °C to 28 °C. This broader range is probably caused by the varied dissipation of microwave energy among the samples towards the end of the drying process.

The convergence of chamber pressures, as indicated by the Pirani gauge and the capacitive sensor, marks the completion of drying, analogous to CFD.

The sample mass continuously decreases from 286.6 g to 67.2 g with a gradually decreasing slope. Therefore, the sample mass confirms the completion of drying detected by the comparative pressure measurement, as the final weight approximates the estimated dry mass of the samples of 71.3 g. The process logging does not start at 300 g since a vacuum application of 10 min precedes the start of MFD. During this period, the samples begin to dry. The enthalpy of sublimation is provided by conduction, thermal radiation, and the energy stored in the heat capacity of the samples. The trend of decreasing sample mass during drying is qualitatively in agreement with the literature on MFD [11, 92].

The process parameters during MFD were as expected. Therefore, MFD experiments can be effectively performed within the laboratory-scale plant.

Figure 2.12 displays the microwave parameters forward power and reflected power recorded during the MFD commissioning experiment. Dissipated power and energy efficiency, which are also shown, are calculated from these parameters. All parameters are averaged across the six applied frequencies.

Within the initial 0.5 h, there is a rapid decline in forward power from 88 W to 77 W. Afterward, the forward power maintains an average of approximately 75 W, though a slight overall decrease is observed. In contrast, the reflected power increases from 33 W to 50 W after an initial decline. Three distinct plateaus of reflected power are observable, starting at approximately 3 h, 11 h, and 16 h. The increase in reflected power after the first 0.5 h by about 17 W surpasses the decrease in forward power of around 4 W in the same period. Consequently, the dissipated power and energy efficiency decrease during MFD since they are

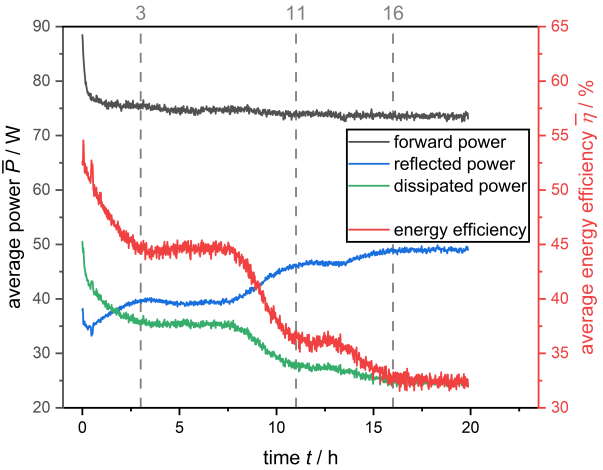

Figure 2.12: Microwave parameters recorded during the MFD commissioning experiment. All parameters are averaged over one cycle of the six applied frequencies.

calculated from forward and reflected power, as described in Section 2.3.2. These parameters derived also reflect the plateaus observed in the forward power.

The observed decrease in dissipated power and energy efficiency throughout MFD aligns with expectations. As drying progresses, the DPs of the tylose gel decrease as a result of the removal of water, which is susceptible to microwave dissipation. Consequently, less power is dissipated in the samples as the proportion of dried material increases.

Figure 2.13 shows the forward power at the individual frequencies applied. The average forward power during MFD of about 80 W is about 60% higher than the set forward power of 50 W. The difference highlights the issue of deviating output power from the SSG at low power levels.

A broad spectrum of forward power ranges from 40 W to 110 W among the applied frequencies. A notable decrease in power during the first 0.5 h of MFD for all frequencies suggests a specific start-up behavior of the HY2020 SSG, presumably caused by temperature stabilization within the SSG. After this initial period, the forward power at individual frequencies stabilizes. The power levels vary

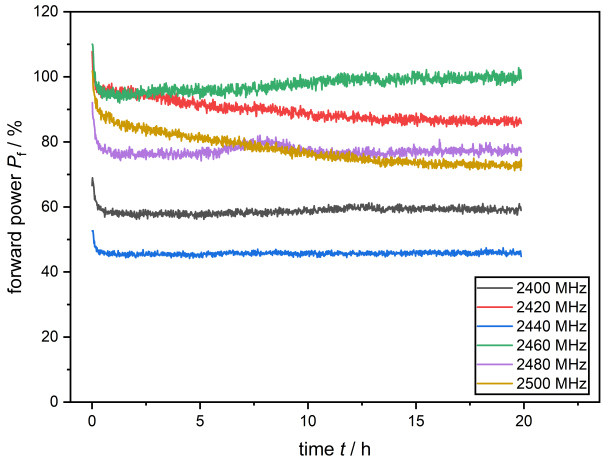

Figure 2.13: Forward power in the MFD commissioning experiment resolved for the six frequencies applied.

considerably with averages of 45.7 W at 2440 MHz up to 97.7 W at 2460 MHz, showing a highly frequency-dependent behavior of the SSG.

The observed variability results in frequencies being weighted differently during the process. For example, more than twice the power is applied on average at 2460 MHz compared to 2440 MHz. However, including energy efficiency as a metric allows one to evaluate the efficiency of converting electromagnetic energy into heat at each frequency. For future work, it would be advantageous to maintain a constant forward power across all frequencies independent of process time to standardize the power application and increase the predictability of the applied forward power.

Figure 2.14 displays the energy efficiency among the applied frequencies as a function of process time. The energy efficiency varies among individual frequencies, ranging from 12.8% at 2400 MHz to 99.0% at 2480 MHz. Throughout the drying process, the energy efficiency at each frequency continuously changes. There is no consistent trend over time that applies to all frequencies. For example, the energy efficiency at 2420 MHz drops from 83.5% to 30.8%. At 2440 MHz, it

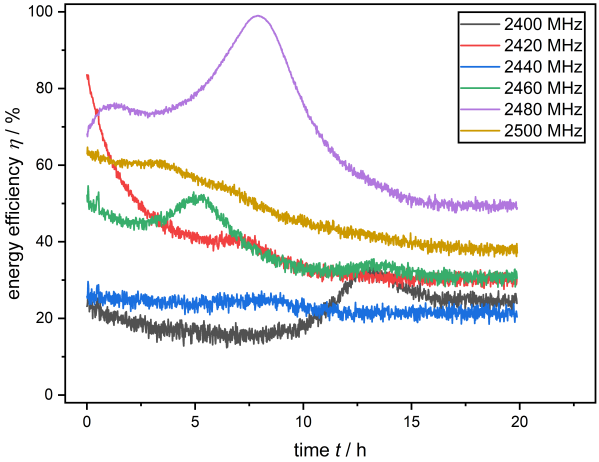

Figure 2.14: Energy efficiency in the MFD commissioning experiment resolved for the frequencies applied.

decreases only from 25.7% to 20.4%. Most frequencies exhibit one or two peaks in energy efficiency, with maximum values often deviating tremendously from the average, most notably at 2480 MHz.

The frequency-dependent differences in energy efficiency suggest the presence of various modes within the multimodal cavity in the frequency range of 2400 MHz to 2500 MHz. Multiple modes lead to varying electromagnetic field distributions and, consequently, different dissipation patterns of electromagnetic energy in the material [23]. The observed maxima in energy efficiency at individual constant frequencies can be explained by the shift of RFs to higher frequencies during drying observed in the process characterization of different drying states, see Figure 2.9. For example, at least two RFs pass by 2480 MHz during MFD. Thus, the results of the process characterization and MFD commissioning run agree.

The three plateaus observed in the averaged microwave parameters in Figure 2.12 result from overlapping microwave parameters of individual frequencies. The plateaus are determined mainly by the dominant peak in energy efficiency of the 2480 MHz frequency.

Figure 2.14 illustrates that using constant frequencies throughout MFD does not result in the highest energy efficiency. The application of RFs during MFD emerges as particularly promising due to their high energy efficiency and distinct associated modes with individual heating patterns. A key challenge is the shift of the RFs during MFD. These shifts necessitate advanced process control to exploit their benefits entirely. Overcoming this challenge could enable an energy-efficient, rapid, and product-friendly MFD process.

2.5 Conclusions

A laboratory-scale plant was designed and constructed to investigate FD. The modular plant setup enables MFD and CFD experiments within the same process chamber. The plant dimensions were chosen to realize a multimodal resonator on a scale particularly suitable for laboratory-scale experiments. The chamber is equipped with peripheral devices to enable FD and control the process conditions. An SSG was installed as part of the system to generate microwaves. The SSG enables flexible electrical control of the microwave parameters. An array of sensors provides the basis for a comprehensive data acquisition system, including fiberoptic temperature sensors, a load cell to monitor product weight, pressure sensors, and microwave power sensors. The control system utilizes two instances of Matlab software for real-time process monitoring and process control for nuanced adjustment of process parameters. Safety measures, such as emergency stops and shielding against microwave leakage, ensure safe operation. In addition, options for future expansion of the system were included, e.g., to connect additional sensors or SSGs.

The process characterization of frequency-dependent microwave reflections showed a higher average energy efficiency when using a coaxial cable as an additional part of the transmission line. This shows the dependency of microwave reflections on the transmission line used. In contrast to the general trend, decreased energy efficiency with the coaxial cable at 2404 MHz and 2480 MHz indicates the frequency-dependent behavior of microwave reflections in the transmission

line. An advancing drying state of the product led to a lower average energy efficiency in accordance with the literature. A general trend of RFs shifting to higher frequencies was observed during MFD, although the overlap of the peaks associated with RFs complicates the observation of this trend.

Commissioning experiments for CFD and MFD demonstrated the capability to perform these processes reliably with the designed setup. CFD experiments adhered to the expected product temperature curves, pressure curves, and drying kinetics. Similarly, MFD experiments not only reiterated the operational efficacy but also highlighted the advanced capability of the setup to handle the complexities of microwave integration. The sample mass during MFD also followed the expected trends. A detailed analysis of the microwave parameters revealed an uneven distribution of forward power among the applied frequencies. This behavior must be taken into account when investigating the process. However, considering the energy efficiency enables an analysis of the process that is not affected by forward power. As expected, the average energy efficiency decreased during MFD. However, the energy efficiency of the individual frequencies during drying followed different trends, including local maxima at varying process times. These findings agree with the results from the process characterization of the microwave reflections. Furthermore, the results suggest the application of energy-efficient RFs in MFD as a promising approach to process control. Their shift in frequency poses a challenge. However, due to the predictable nature of the shifts to higher frequencies, RFs can potentially be continuously applied in future frequency-based control concepts.

The successful MFD and CFD experiments allow for the investigation of MFD within the scope of this thesis. In addition, the flexible modular design of the system and the inclusion of SSGs opens the possibility of further research on MFD beyond the scope of this thesis. The system design could be modified or refined in future studies to allow further research in various directions.

3 Microwave-assisted freeze-drying with frequency-based control concepts via solid-state generators: A simulative and experimental study

This chapter was published as:

Sickert, T.; Kalinke, I.; Christoph, J.; Gaukel, V. Microwave-Assisted Freeze-Drying with Frequency-Based Control Concepts via Solid-State Generators: A Simulative and Experimental Study. Processes 2023, 11(2), 327, doi:10.3390/pr11020327.

Variables, figures, and abbreviations were adapted for consistency.

3.1 Abstract

Freeze-drying (FD) is a common process to extend the shelf life of food and bioactive substances. Its main drawback is the long drying time and associated high production costs. Microwaves can be applied to significantly shorten the process. This study investigates the effects of modulating the electromagnetic field in microwave-assisted freeze-drying (MFD). Control concepts based on microwave frequency are evaluated using electromagnetic simulations. The concepts are then applied to the first part of primary drying in a laboratory-scale system with solid-state generators. Targeted frequency modulation in the electromagnetic simulations enabled an increase in energy efficiency or heating homogeneity throughout MFD while having negligible effects on the power dissipation ratio between frozen and dried product areas. The simulations predicted the qualitative effects observed in the experimental proof of concept regarding energy efficiency and drying homogeneity. Additionally, shortened drying times were observed in the experiments with a targeted application of energy-efficient frequencies. However, differences occurred in the quantitative validation of the electromagnetic models for energy efficiency in dependence on frequency. Nevertheless, the models can be used for a time-efficient investigation of the qualitative effects of the control concepts. In summary, frequency-based control of MFD represents a promising approach for process control and intensification.

3.2 Introduction

Conventional freeze-drying (CFD) is an essential unit operation in many process chains of the food and pharmaceutical industries. The reason for the widespread use of CFD is the preservation of valuable quality characteristics, such as the high retention of valuable ingredients [103–105], advantageous rehydration properties [103], and high volume retention [2]. The product-preserving characteristic of

CFD is associated with the exclusion of liquid water and prevailing low temperatures [1], as well as the exclusion of oxygen from the process [2]. The FD process is generally composed of three stages, which may overlap in time [37]:

- Freezing of the product,
- Primary drying, in which frozen water is removed by sublimation, and
- Secondary drying, in which the remaining water is removed from the product.

Drying times for food and pharmaceuticals range from hours to days. When using CFD for drying pharmaceuticals, primary drying is usually the most expensive and time-consuming step [106]. In the drying of food, secondary drying is often skipped for economic reasons. Therefore, there is great potential in optimizing the lengthy primary drying stage for foods and pharmaceuticals.

In CFD, the enthalpy of sublimation is usually supplied by the mechanisms of thermal conduction and thermal radiation, originating from the temperature-controlled shelves or the walls of the process chamber. In contrast, microwave-assisted freeze-drying (MFD) applies electromagnetic waves to provide the enthalpy of sublimation. Through interactions of microwaves with the product, electromagnetic energy is converted into heat directly in the product [41]. Thus, limitations from heat transfer resistance to the sublimation front can be circumvented. This makes MFD especially suitable for products in which heat transfer limits the drying rate, e.g., materials with high porosity, such as foams, or materials with low thermal conductivity. Several papers in the literature have shown a significant reduction in drying time for MFD in comparison to CFD [8, 68, 107]. This could potentially offset the economic disadvantages resulting from the need for additional process equipment and the use of electrical energy to supply the enthalpy of sublimation. Moreover, no temperature gradient from the product surface to the sublimation front is necessary for heat transfer in MFD. While in CFD, the energy input may be restricted due to temperature limits at the product surface, this does not apply to MFD.

Ma and Peltre [108, 109] investigated the MFD of beef in a two-part study with a theoretical and experimental part as early as 1975. Since then, a large number of studies on MFD have been conducted with various materials. Examples include experimental studies on the drying of foods [8, 12, 110, 111], starter cultures [11], pharmaceuticals [69], and model products [112]. Furthermore, MFD has been studied in simplified one-dimensional thermodynamic models [71, 113] as well as in more complex electromagnetic models coupled with thermodynamic models [112].

However, microwave-assisted processing using conventional magnetrons as microwave generators is subject to limitations. Luan et al. [58] demonstrated fluctuations in the frequency spectrum of identical household microwave ovens depending on various factors. This makes reproducible process control difficult to impossible. Moreover, corona discharges may occur during the application of microwaves, especially at pressures common for FD [8] and high peaks of microwave power. The latter is typical when using magnetrons due to common on-off control. These discharges threaten product quality and lead to unnecessary power consumption. Limitations of the magnetron pose a constraint on the controllability of microwave-assisted processes. This is especially true for microwave-assisted drying, in which the non-uniform energy input into the product is a particular problem [114].

One possible approach to overcome these challenges is the deployment of the so-called solid-state generator (SSG) for the generation of microwaves, which is based on semiconductor technology. In contrast to magnetrons, the SSG enables the targeted electrical control of frequency, power, and phase shift. In combination with the possibility of measuring the forward and reflected powers as feedback parameters, SSGs enable the development of so-called “smart” systems for microwave-assisted processing, capable of detecting the state of the product and influencing the relevant parameters of the electromagnetic field [17]. The influence of power splitting between multiple microwave sources and phase shift on microwave heating, as enabled by SSGs, has already been investigated by Bianchi [115]. Their study showed that it is possible to achieve desired energy efficiencies or heating homogeneities via modulation of the electromagnetic field. Varying

the frequency during microwave-assisted processes in experiments enabled more homogeneous temperature profiles compared to operation at single frequencies [19, 21, 116]. Yang et al. [21] also demonstrated that energy efficiency could be increased by the selective application of multiple frequencies, chosen based on heating uniformity and heating rate. However, a higher heating rate, associated with high energy efficiency, resulted in less heating homogeneity in comparison to a process only optimized for heating homogeneity. Yakovlev [23] detected a higher heating homogeneity in electromagnetic simulations compared to single frequencies by applying multiple frequencies. The observation was valid for equidistant as well as resonant frequencies (RFs). In addition, higher energy efficiency was found when energy-efficient RFs were used compared to an alternative control approach using equidistant frequencies. The above results show the potential of selectively controlling the electromagnetic field to increase both energy efficiency and heating homogeneity in microwave-assisted processing. However, there appears to be a trade-off between the two parameters in which pure maximization of one comes at the expense of the other. To the best of our knowledge, no studies have been published on the modulation of the electromagnetic field during drying. In contrast to heating processes, the dielectric properties (DPs) of the product change considerably throughout drying due to the removal of water. The change in material properties, in turn, affects the electromagnetic field within the process chamber [42]. This results in a complex coupling of electromagnetic and thermodynamic processes. Whereas there are numerous studies dealing with the modeling of CFD, e.g., [106, 117, 118], there are only a few works on modeling MFD, e.g., [71, 112, 113]. In some of the latter, the assumption of a spatially homogeneous microwave field was made [71, 113] to solve a thermodynamic model. In the work of Wang et al. [112], a thermodynamic model was coupled with an electromagnetic model, but drying was only simulated at a constant frequency of 2450 MHz. Similarly, MFD with SSGs has only been carried out experimentally at a constant frequency of 2450 MHz [69]. Thus, the investigation of a targeted modulation of the electromagnetic field during MFD emerges as a gap in knowledge that provides an opportunity for further research.

The present work, therefore, aims to investigate the effects of modulating the frequency of the electromagnetic field during MFD. For this purpose, electromagnetic models are developed to represent the MFD of chunky tylose gel, which is used as a model food product. By simulating multiple discrete drying states, the models are decoupled from the thermodynamics of the process. The DPs of the product, which are required for the models, are determined experimentally. The verified models are then used to investigate the effects of different frequency-based control concepts on energy efficiency and heating homogeneity in MFD. Subsequently, the control concepts are applied in a laboratory-scale MFD system to provide proof of concept for the first part of primary drying, which ended with the removal of 20 wt% of the water contained at the start of MFD. In the experiments, the effects of frequency modulation on drying time, energy efficiency, and homogeneity of drying are investigated in the context of qualitative comparability.

3.3 Materials and methods

3.3.1 Electromagnetic model

3.3.1.1 Governing equations and assumptions

Maxwell's equations [59] are the fundamental equations forming the basis for the electromagnetic models representing MFD. Maxwell's equations in their differential form [119] are given as

$$\nabla \cdot \vec{D} = \rho \tag{3.1}$$

$$\nabla \cdot \vec{B} = 0 \tag{3.2}$$

$$\nabla \times \vec{E} = -\frac{\partial \vec{B}}{\partial t} \tag{3.3}$$

$$\nabla \times \vec{H} = \frac{\partial \vec{B}}{\partial t} + \vec{I} \tag{3.4}$$

In Equations 3.1 to 3.4, $\vec{E}$ is the electric field intensity and $\vec{D}$ the electric flux density. Respectively, $\vec{H}$ represents the magnetic field intensity and $\vec{B}$ the magnetic flux density. ρ is the electric charge density, $\vec{I}$ is the electric current density, and t denotes the time. Perfect electrical conduction is set as a boundary condition at the walls of the process chamber and the waveguide.

The electromagnetic waves interact with the materials in the process chamber and convert electromagnetic energy into heat in lossy dielectrics. The complex relative permittivity ε_r, defined as

$$\varepsilon_r = \varepsilon_r' - i\varepsilon_r'' \tag{3.5}$$

is used to characterize these interactions. ε_r' is the relative dielectric constant and ε_r'' the relative dielectric loss factor. Dielectric losses through all mechanisms are lumped in ε_r''. The DPs depend on a variety of factors, including temperature, frequency of electromagnetic waves, aggregate state, and composition of the dielectric, see, e.g., the work by Llave et al. [53]. In the simulations of the present work, the DPs are only differentiated between the dried and the frozen regions of the product. The influences of temperature and frequency are neglected.

The average volume-specific power absorption P_A is calculated in the electromagnetic simulations in analogy to

$$P_A = 2\pi f \varepsilon_0 \varepsilon_r'' |E_{rms}|^2 \tag{3.6}$$

as defined by Metaxas and Meredith [46]. In Equation 3.6, f represents the frequency of the electromagnetic field, ε_0 the vacuum permittivity, and E_{rms} the root mean square of the electric field strength.

In the present work, there is no coupling of the electromagnetic models with thermodynamic equation systems to simulate mass and heat transfer. The influence of the drying progress on the electromagnetic field is represented by the simulation of several discrete drying states of primary drying in MFD. The drying state z

characterizes the proportion of the dried volume divided by the volume of the entire product. Thus, $z = 0\%$ corresponds to a completely frozen product, while $z = 100\%$ corresponds to a completely dried product. The drying states from 0% to 100% are simulated in an interval of 10% via separate electromagnetic models, which are solved numerically. The progress of drying in these simulations is represented by a uniform retraction of the frozen volume from all sides into the sample interior, leaving a dried outer layer. The total volume of the products is assumed to be constant throughout drying.

3.3.1.2 Model specifications

Figure 3.1 shows the process chamber and the arrangement of the materials utilized in the electromagnetic models. These resemble the experimental arrangements in the process chamber for MFD. The process chamber is a cuboid cavity with dimensions of 612 mm $\times$ 400 mm $\times$ 300 mm, as described in the work of Yakovlev [23]. A WR340 waveguide is placed in the center of the top of the cavity. Centrally on the bottom of the cavity, a plate made of polyether ether ketone (PEEK) with a base area of 200 mm $\times$ 200 mm is located as product support. The support is connected to the bottom of the cavity by two cylinders made of PEEK. A set of 24 tylose gel samples (25 mm $\times$ 25 mm $\times$ 20 mm) is centrally located on the product support in a 6 $\times$ 4 arrangement, each 5 mm apart. The dried and frozen regions of the product were assigned the DPs of the dried and frozen tylose gel, respectively. The remaining space inside the cavity was set to the DPs of a perfect vacuum. The DPs of the materials are listed in Table 3.1. The properties of tylose gel were determined experimentally in the present work and are displayed in Section 3.4.1 as a function of temperature.

3.3.1.3 Simulation procedure

For the electromagnetic simulations, the Frequency Domain Solver in the software CST Studio Suite 2020 (Dassault Systèmes, Vélizy-Villacoublay, France)

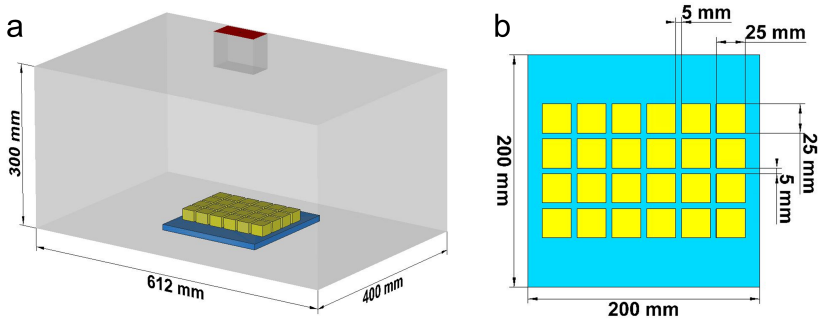

Figure 3.1: (a) Geometry of the process chamber in the electromagnetic simulations; (b) Geometry of the individual product samples and the product support in the electromagnetic simulations. Yellow — tylose gel; blue — product support made of PEEK; red—inlet waveguide.

Table 3.1: Dielectric properties of the materials in the electromagnetic simulations.

Material	Relative dielectric constant ε_r'/-	Relative dielectric loss factor ε_r''/-	Source
PEEK	3.142	0.0085	[120]
tylose gel, dried	1.264	0.0473	present study
tylose gel, frozen	3.649	0.5807	present study
vacuum	1.000	0.0000	per definition

was used. The simulations were performed on the parallel computer system bwUniCluster 2.0 + GFB-HPC, a state service within the framework of the Baden-Württemberg Implementation Concept for High-Performance Computing. Core count and memory were varied according to the requirements of the simulations up to a maximum of 32 cores and 150 GB RAM. First, a grid study was performed to verify the simulations at the drying states 0%, 10%, and 100%. Afterward, the models of the 11 drying states were solved numerically in the frequency range of 2400 MHz to 2500 MHz. In the first simulation runs, the frequencies used were set. The results of the subsequent runs were evaluated in post-processing.

3.3.1.4 Post-processing

CST-Studio provides the scattering parameter S_{11} in the investigated frequency range of 2400 MHz to 2500 MHz as an output. The energy efficiency was calculated from the simulation results for a single port system with

$$\eta = 1 - |S_{11}|^2 \tag{3.7}$$

according to Więckowski [64]. Therefore, only the conversion of electromagnetic energy into heat was considered in the calculation of energy efficiency. The efficiency of microwave generation was excluded. This allowed for comparison with experimental results, as the SSG provided a record of a comparable data set.

The effects of the following frequency-based control concepts were investigated in post-processing for every drying state:

- Single Minimum Frequency (1MF) — single frequency with the global minimum of energy efficiency;
- Single Resonant Frequency (1RF) — single frequency with the global maximum of energy efficiency;
- Six Equidistant Frequencies (6EF) — six frequencies from 2400 MHz to 2500 MHz in the interval 20 MHz;
- Six Resonant Frequencies (6RF) — six frequencies with the highest local maxima of energy efficiency.

For every simulated drying state, the average energy efficiency $\bar{\eta}$ was calculated for the control concepts according to

$$\bar{\eta} = \frac{\sum_{i=1}^{n} \eta_{\mathrm{i}}}{n} \tag{3.8}$$

as the arithmetic mean of the energy efficiencies η_{i} at the n frequencies applied.

Monitors of the volume-specific power absorption were set for all frequencies utilized. Additionally, the integral dissipated power in the frozen and dried volumes of the individual samples was calculated. Therefore, the spatially resolved power dissipation patterns between and inside the individual samples could be investigated.

The heating homogeneity factor ζ was determined as

$$\zeta = \frac{\bar{P}_{d,smp}}{P_{d,smp,max}} \tag{3.9}$$

and thus defined as the ratio of the average dissipated integral power in all samples $\bar{P}_{d,smp}$ to the maximum integral dissipated power $P_{d,smp,max}$ in a single sample. Hence, ζ is a measure of the average dissipated power in a single sample standardized to the maximum dissipated power in a sample. When multiple frequencies were applied in a control concept, the homogeneity factor was calculated from an equally weighted superposition of all the power dissipation patterns involved.

3.3.2 Experiments

3.3.2.1 Model product

Derivatives of methyl cellulose, known by the trade name tylose, have already been used as a model food product both to study microwave-assisted heating [53, 121] and to study freezing [122, 123]. Thus, the material is ideally suited for an investigation of MFD. In this work, a tylose gel based on a powder of methyl 2-hydroxyethyl cellulose was used as a model product. The tylose gel is composed of 76.23 wt% demineralized water, 22.77 wt% Tylose MH1000 (Kremer Pigmente, Aichstetten, Germany), and 1.00 wt% L-(+)-ascorbic acid (Carl Roth, Karlsruhe, Germany). Demineralized water was heated to 65 °C at 200 rpm using a heatable magnetic stirrer C-MAG HS 7 (IKA Werke, Staufen im Breisgau, Germany). The appropriate amount of L-(+)-ascorbic acid was dissolved in water and the solution was kneaded with the tylose powder to form a homogeneous mass. The tylose gel

was weighed at 12.50 g for each sample, formed into cuboids of approximately 25 mm × 25 mm × 20 mm, and frozen at -30 °C for at least 14 h. To avoid water loss in the frozen state, the product was packed airtight before freezing.

3.3.2.2 Dielectric properties

The DPs of the fresh and freeze-dried samples were measured with a μWave-Analyser (Püschner, Schwanewede, Germany) in a temperature range of -20 °C to 45 °C. The sample was tempered to -20 °C before measurement. The temperature of the measuring head was set to -20 °C with a connected external cooling system (Unistat 161 W, Huber, Offenburg, Germany). The pre-tempered sample was inserted into the μWaveAnalyser and equilibrated for 1 h. Subsequently, the temperature was continuously increased at 0.1 K/min to 45 °C. Dielectric property measurements were performed at a frequency of 2450 ± 50 MHz and recorded every 30 s using μWaveAnalyser 3.2.0 software (Püschner, Schwanewede, Germany). Measurement of an empty vial served as a reference. The temperature was recorded using the software SpyControl 2.0 (Huber, Offenburg, Germany) and a temperature sensor (PT100, Huber, Offenburg, Germany), which was inserted into the measuring head.

All measurements were conducted in duplicate. Time-dependent dielectric measurement data and time-related temperature data were processed in Matlab R2019a (MathWorks, Natick, MA, USA)

3.3.2.3 MFD system

Figure 3.2 depicts the schematic setup of the laboratory-scale MFD system. The process chamber with dimensions of 612 mm × 400 mm × 300 mm is manufactured from stainless steel. A P 65 D vacuum pump (SASKIA, Ilmenau, Germany) is connected to the process chamber. Between the vacuum pump and the process chamber is a cold trap (UCCT, Vienna, Austria) set to a temperature of -60 °C. A WR340 waveguide is centrally embedded in the top of the process chamber.

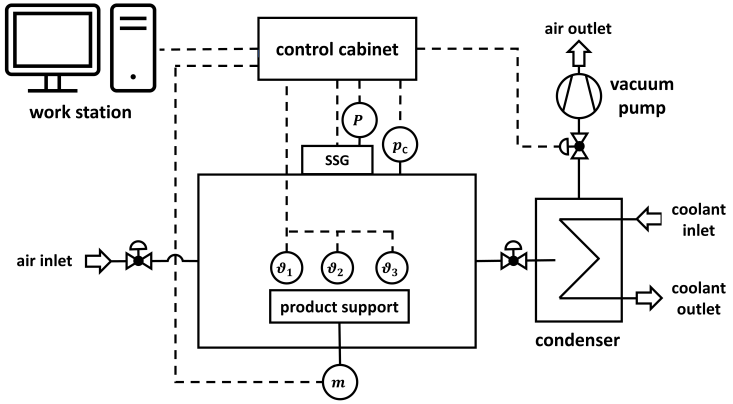

Figure 3.2: Schematic layout of the laboratory-scale MFD system. Information streams are shown as dotted lines. P — forward and reflected microwave power SSG; p_c — pressure capacitive sensor; m — mass load cell.

An HY2020 SSG (TRUMPF, Freiburg, Germany) is connected to the waveguide at the cavity via a coaxial cable. The generator has a maximum output power of 600 W and can be tuned in the frequency range of 2400 MHz to 2500 MHz with an accuracy of 0.01 MHz. In addition to the reflected and forward microwave power as well as the respective frequencies, the weight of the product and the pressure in the process chamber are recorded online via Matlab R2020b (MathWorks, Natick, MA, USA). The sensors used are a CMR363 capacitive pressure sensor (Pfeiffer, Aßlar, Germany), a PW4MC3/2kg load cell (Hottinger Brüel & Kjaer, Darmstadt, Germany), and the internal sensors of the HY2020 SSG. The pressure in the process chamber as well as the frequency and power of the microwave field can be adjusted via the self-made process control system. In the present work, the pressure in the system was set to 0.5 mbar.

3.3.2.4 Process characterization & drying procedure

The 24 frozen tylose gel samples were placed centrally on the product support in the process chamber in a 6 $\times$ 4 arrangement with a spacing of 5 mm in

accordance with the electromagnetic models (see Figure 3.1). Ten minutes after the vacuum was applied in the process chamber, the SSG was switched on and process characterization or drying was started.

For the process characterization, a frequency sweep in the range of 2400 MHz to 2500 MHz was performed at an interval of 0.1 MHz with the minimally possible forward power of 50 W. The forward power P_f and reflected power P_r were recorded at each frequency. By inserting the respective values in the equation

$$\eta = 1 - \frac{P_r}{P_f} \tag{3.10}$$

the energy efficiency η of the conversion of electromagnetic energy into heat could be calculated for each frequency in the experiments. This enabled the detection of RFs, which are defined as local maxima of energy efficiency.

For drying via MFD, the control concepts 1MF, 1RF, 6EF, and 6RF were applied in accordance with the simulations. The forward power of the SSG was set to 50 W. Since preliminary tests had shown product damage with this setting, the output power of the generator was applied for 2.5 s at each frequency and then paused for 7.5 s, corresponding to a ratio $r_{on} = 0.25$ of time for active microwave generation to total time. When multiple frequencies were utilized, the frequency loop was run from the lowest to the highest frequency and then the next loop was started at the lowest frequency. The selected frequencies of the individual control concepts were kept constant during the process runs. The average energy efficiency $\bar{\eta}$ in the experiments was calculated in analogy to Equation 3.8 as the arithmetic mean of the values of all frequencies for each loop if several frequencies were applied. Otherwise, $\bar{\eta}$ corresponds to the value of the respective individual frequency. A loss of 20 wt% of the water mass was used as a termination criterion. The results of the first phase of primary drying are sufficient to provide a proof of concept and are simple in their implementation since no frequency adjustment is required. In addition, incomplete primary drying allows detailed observation of drying homogeneity since the differences in sample weights are more pronounced

than in complete drying. Figure 3.3 depicts a schematic overview of the process steps during MFD.

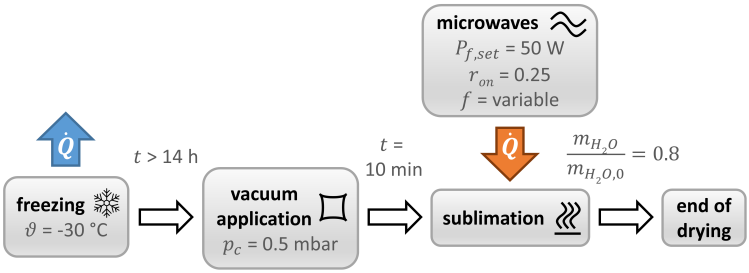

Figure 3.3: Schematic overview of the process steps and corresponding parameters for MFD.

The process characterization and drying runs were conducted in triplicate. Before and after each experiment, the samples were weighed on a Type 1518 balance (Sartorius, Göttingen, Germany). The samples were then cut in half and visually inspected for macroscopic product damage. This was followed by gravimetric determination of residual moisture for each sample to evaluate the homogeneity of drying. For this purpose, the freeze-dried samples were dried in a drying oven T 6060 (Heraeus, Hanau, Germany) at 105 °C for at least 24 h. Subsequently, the weight of the samples was determined using a precision balance LS 220A SCS (Precisa, Dietikon, Switzerland) and used to determine the drying homogeneity between the samples.

3.4 Results and discussion

3.4.1 Dielectric properties

The DPs of fresh tylose gel, shown in Figure 3.4 (a), vary considerably in the temperature range studied. This temperature-dependent behavior of DPs ε_r' and ε_r'' of fresh tylose gel is in line with the literature [53]. The largest increase is

detected in the range of -10 °C to 2 °C. This phenomenon can be explained by the melting of frozen water. As the DPs of water at microwave frequencies [124] are much higher than those of ice [125], partial melting of frozen water from approximately -5 °C leads to a significant increase in DPs. The slight increase at lower temperatures, namely -20 °C to -5 °C, is probably caused by an increasing fraction of liquid water in the tylose gel with increasing product temperature, as elucidated in previous studies based on differential scanning calorimetry of tylose gel [126]. The higher ε_r'' value of the tylose gel in the present study containing ascorbic acid compared to published data on tylose gel [53] is presumably due to the compositional differences in the tested material. It has been demonstrated that the addition of compounds to tylose gel can lead to changes in DPs, e.g., for sodium chloride [53, 127] and sucrose [127]. At about -5 °C to 0 °C, inconsistencies in dielectric property measurement are attributed to measurement errors caused by partial melting of frozen water in this temperature range. The measurement procedure is not feasible for this temperature range of phase transition. Since the DPs at the aforementioned temperatures are not relevant for the remainder of the present work, a detailed discussion is omitted.

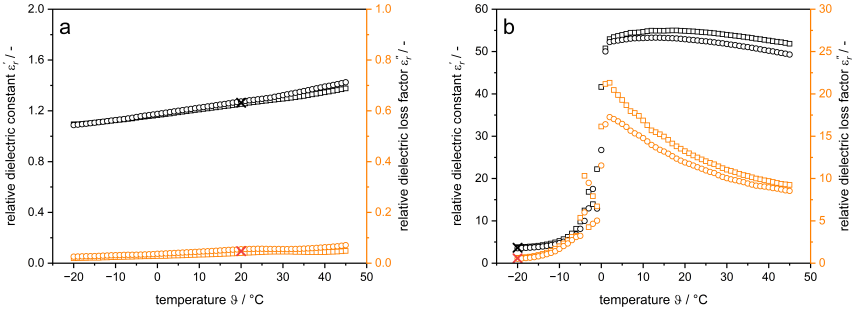

Figure 3.4: (a) Dielectric properties of fresh tylose gel; (b) Dielectric properties of freeze-dried tylose gel. The results were obtained in duplicate. The arithmetic means of the dielectric properties utilized in the simulations are marked with an x.

The DPs of the freeze-dried tylose gel are much lower than those of the fresh gel, as depicted in Figure 3.4 (b). The DPs increase slightly with temperature, probably due to the increasing mobility of the molecules interacting with the

electromagnetic field. Because of the lack of phase transitions inside the material, no significant shift in the DPs occurs. In ice, microwave energy dissipates only to a small extent due to the low DPs [125]. Combined with the low DPs of the freeze-dried tylose gel, this suggests that the microwave energy is dissipated in the frozen product by the interaction of microwaves with bound water, which is contained in the frozen but not in the dried product. This idea is consistent with the literature [71].

Due to the unknown and time-dependent temperature distribution during MFD, no variable DPs were assigned to the product in the simulations. The DPs of the fresh gel at -20 °C were set for the frozen product and the DPs of the dried gel at 20 °C were set for the dried product. The temperature of the frozen product was chosen since the temperature of -20 °C for the frozen product is closest to the ice vapor pressure at the present total pressure of 0.5 mbar, as stated in the literature [128]. The temperature of the dried product is set to room temperature since the differences in the temperature range investigated are relatively minor. The DPs at the respective temperatures are calculated as the arithmetic mean of the duplicate runs and are marked in Figure 3.4. The exact values of the DPs used in the electromagnetic models are given in Table 3.1.

3.4.1.1 Model verification

The normalized power absorption NPA is used in electromagnetic simulations as a parameter to verify the electromagnetic model as a function of the number of cells or time steps in transient simulations [129, 130]. In the present work, the NPA for the simulations is defined with

$$NPA = \frac{P_{d,total}}{P_f} \tag{3.11}$$

as the ratio of the dissipated power in all materials $P_{d,total}$ to the forward power of the SSG P_f at 2450 MHz.

Figure 3.5 shows the NPA as a function of the number of cells for the drying states 0%, 10%, and 100%. These represent the start and end of drying as well as a drying state in which the dried product layer is comparably thin, posing a challenge for discretization. The grids with the lowest number of cells of the individual drying states were generated with the same settings of the program for mesh generation. The same applies to the settings for the subsequent higher numbers of cells. The numbers of cells differ for the drying states because the internal mesh generation of the software depends on the composition of the DPs of the materials. For the 100% drying state, only simulations with four instead of five meshes were performed since the computational requirements for the fifth mesh exceeded the available memory space. From the mesh with the third lowest number of cells, there are only minor changes in the NPA. The absolute deviation from the mesh with the highest cell count is only 0.207%, 0.153%, and 0.002% for the drying states 0%, 10%, and 100%, respectively. Therefore, based on these solver settings, a mesh-independent convergent solution can be expected. The settings for this mesh generation are transferred to the models of all drying states.

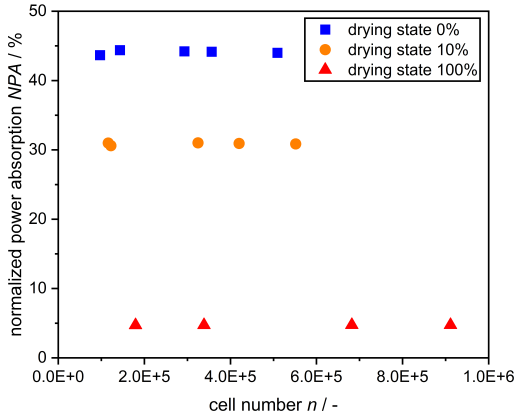

Figure 3.5: NPA at 2450 MHz displayed as a function of the number of mesh cells in the electromagnetic simulations for various drying stages.

3.4.1.2 Model validation

Figure 3.6 depicts the energy efficiency in dependence on the frequency in the range of 2400 MHz to 2500 MHz. The data were obtained from an experimental frequency sweep using the SSG and the post-processing of the electromagnetic simulation of the drying state 0%. The simulative results show clearly defined peaks at RFs, while the results from the experiments at the beginning of drying show both clearly defined peaks and broader peaks with fluctuations in energy efficiency. Presumably, these fluctuations are caused by several RFs that are closely spaced. Except for the general existence of maxima and minima in a comparable magnitude, no detailed agreement can be observed between the energy efficiency from the simulation and the experimental frequency sweeps. The experimental data, on the other hand, are well reproducible.

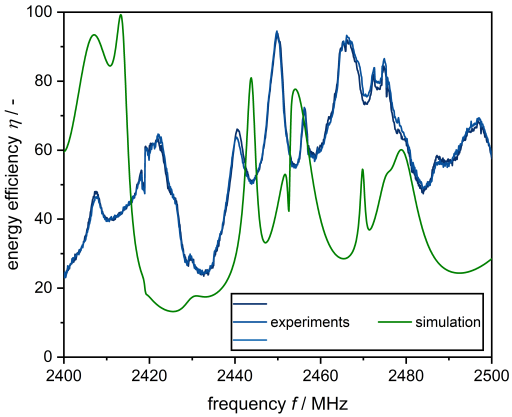

Figure 3.6: Energy efficiency in the frequency range of 2400 MHz to 2500 MHz obtained from the electromagnetic simulations at a drying state of 0% (green) and experimentally in the laboratory-scale plant in triplicate at 0.5 mbar (blue). The energy efficiency was calculated for the simulation according to Equation 3.7 and for the experiments according to Equation 3.10.

Obviously, the electromagnetic model does not provide an exact reproduction of the electromagnetic field in dependence on the frequency. The electromagnetic

model would require further revision and validation for an accurate representation of the microwave field. Nevertheless, as long as minima and maxima occur in comparable numbers and magnitudes in both cases, the electromagnetic models can be used to develop frequency-based control concepts in dependence on the energy efficiency of the frequencies to be applied. The models can be regarded as a tool for the time-efficient investigation of the qualitative impact of control concepts throughout drying. Electromagnetic simulations have already been used in the literature to find specific combinations of energy efficiency and heating homogeneity for microwave-assisted heating [115], which can be done with the developed model for MFD. However, the respective model was not validated for the process chamber investigated. Other models of microwave-assisted processes were validated with analytical results in an empty cavity [23], temperatures measured with fiberoptic sensors [71, 131], or spatial distributions of heating patterns [132, 133]. These methods do not necessarily indicate an accurate representation of the electromagnetic field in the entire frequency range of 2400 MHz to 2500 MHz. Therefore, it remains unclear whether the simulated results in the literature are of practical relevance when varying the frequency throughout MFD. The present study aims to overcome this gap via an experimental proof of concept.

3.4.1.3 Effects of drying state on energy efficiency

Figure 3.7 shows the energy efficiency calculated in the electromagnetic simulations as a function of frequency and drying state. The energy efficiency varies considerably in the frequency range of 2400 MHz to 2500 MHz, ranging from 13.2% to 99.3% for the 0% drying state to 3.0% to 99.7% for the 100% drying state. With progressive drying, the average energy efficiency decreases continuously from 42.4% to 19.9% (data not shown). This is consistent with the expected trend due to the increasing proportion of dried tylose gel with relatively low DPs (see Table 3.1), which leads to lower effective DPs in the cavity. Analogously, a reduction of effective DPs due to a lower product mass results in lower average energy efficiency. This has been demonstrated, for example, in simulations of microwave-assisted heating [134]. Multiple peaks in energy efficiency above

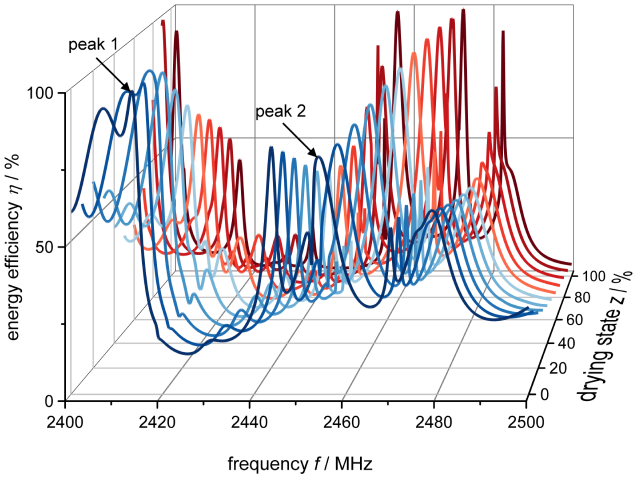

Figure 3.7: Energy efficiency in the frequency range of 2400 MHz to 2500 MHz obtained from the electromagnetic models of all drying states in the range of 0% to 100%. Peak 1 and peak 2 mark two prominent energy-efficient peaks throughout drying.

80% for all drying states indicate the potential benefits of a targeted excitation of specific frequencies over the whole course of drying to increase energy efficiency. On the other hand, the disadvantage of non-targeted excitation of microwaves, especially towards the end of drying, becomes apparent.

The frequency-dependent energy efficiencies for adjacent drying states in Figure 3.7 follow similar curves. The energy-efficient peaks, which indicate the presence of so-called resonant modes, shift to slightly higher frequencies with an increase in the drying state. The observed shift is consistent with theoretical considerations that calculate a shift of resonant modes to higher frequencies for a decrease in effective DPs in a cavity [42]. The result suggests that similar resonant modes and associated heating patterns appear in the process chamber throughout multiple drying states.

To investigate the frequency shifts of the peaks further, the frequencies of the representative energy-efficient peaks 1 and 2 over the drying state are depicted in Figure 3.8. The peaks were chosen since one or the other has the highest energy

efficiency during all drying states, making them easy to spot and relevant for the control concepts 1RF and 6RF. The shift to higher frequencies during the drying progress is more pronounced for peak 2 than for peak 1. Therefore, the curve of energy efficiency over frequency is a result of the overlapping of multiple resonant modes in different compositions throughout drying. The cause is presumably the superposition of multiple modes displaying different magnitudes in frequency shift with an increase in the drying state. It is not obvious from the appearance of a peak whether only one mode occurs or a superposition of several modes is present. The lower frequency of peak 1 for the drying states 20% and 30% compared to the previous drying state in Figure 3.8 contradicts the trend of a shift to higher frequencies. The superposition of the peaks of two resonant modes may be the explanation for this observation. A previously separated resonant mode shifts into the mode at peak 1 from a lower frequency. The superposition results in one local maximum, which is shifted to a lower frequency as the resonant mode from a previously lower frequency is still at a frequency slightly below that of the mode associated with peak 1 in preceding drying states.

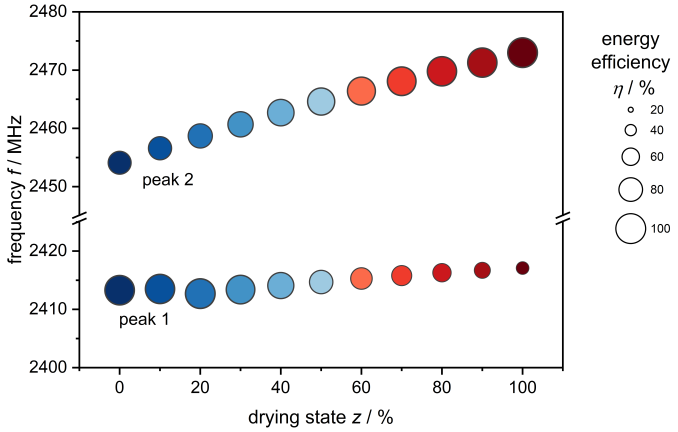

Figure 3.8: Frequency of peaks 1 and 2 plotted over the drying state, obtained from electromagnetic simulations. The size of the bubbles indicates the energy efficiency of the respective peaks.

The energy efficiency of the peaks in Figure 3.8 shifts upwards for peak 2 and downwards for peak 1 with an increasing drying state. The occurrence of spatial maxima of the electromagnetic field at locations with lossy dielectrics determines the energy efficiency of the peaks. Since the pattern of the electromagnetic field is not known in advance, no predictions can be made about the energy efficiency of different frequencies throughout drying.

3.4.1.4 Effects of control concepts

3.4.1.4.1 Energy efficiency Figure 3.9 illustrates the average energy efficiency over the drying progress as a function of the applied frequency-based control concepts. A detailed overview of the applied frequencies in the control concepts and their respective energy efficiency is given in Section A2 in Tables A.1 to A.4. The energy efficiency for 1RF and 6RF, in which RFs are applied, is significantly higher than for 6EF and 1MF throughout the entire drying process.

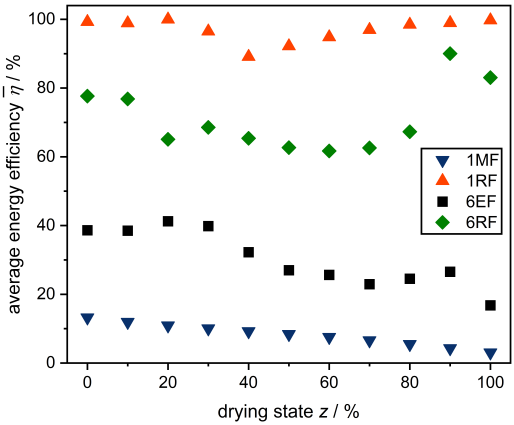

Figure 3.9: Average energy efficiency of the respective control concepts plotted over the drying state, calculated from the electromagnetic simulations.

The control concepts 1MF and 6EF show a tendency of decreasing energy efficiency with increasing drying state. These results are consistent with the observations of the decreasing average energy efficiency in the frequency range of 2400 MHz to 2500 MHz (see Figure 3.7). In contrast, the energy efficiencies of 1RF and 6RF decrease at intermediate drying states and return to high energy efficiencies towards the end of drying. This is due to the behavior of the RFs throughout drying. The energy efficiency of 1RF during MFD is caused by the initial decreasing energy efficiency of peak 1 and, in the later drying stages, the increasing energy efficiency of peak 2 (compare to Figure 3.8). The decrease in energy efficiency for 6RF up to about the drying state of 70% is consistent with the overall decreasing energy efficiency in the relevant frequency range. The increasing energy efficiency towards the end of drying can at least partially be attributed to a new RF entering the frequency range of 2400 MHz to 2500 MHz due to the shift of resonant modes to higher frequencies (compare Tables A.1 to A.4 in Section A2). Electromagnetic simulations in the literature also showed high values of dissipated energy by the application of RFs, which were chosen based on scattering parameters [18].

In summary, relatively high energy efficiency can be achieved over the entire course of drying when RFs are applied with 1RF or 6RF. In contrast, the energy efficiency of the remaining control concepts decreases during drying, which leads to inefficient energy input, especially towards the end of drying. This finding highlights the need for a continuous, targeted frequency adjustment throughout drying.

3.4.1.4.2 Heating homogeneity Figure 3.10 displays the heating homogeneity factor over the drying state for the different control concepts, which enables the evaluation of the homogeneity between the samples. When using multiple frequencies in 6EF and 6RF, there is a higher homogeneity factor compared to single frequencies at almost all drying states. This trend is consistent with more homogeneous microwave-assisted heating in electromagnetic models for the application of multiple frequencies [23, 132]. The highest homogeneity with 6EF is presumably due to less dominant individual heating patterns. On

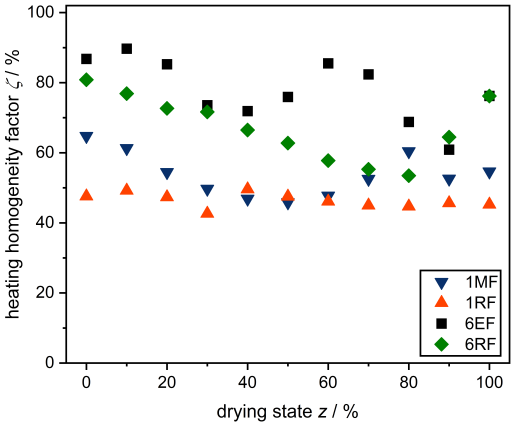

Figure 3.10: Heating homogeneity factor for the investigated control concepts as a function of the drying state, determined from the electromagnetic simulations.

the other hand, a few highly energy-efficient heating patterns with similar heating patterns might lower the homogeneity with 6RF.

Therefore, the application of several frequencies weighted according to power or time while specifying the desired energy efficiency represents an approach to achieve high heating homogeneity in MFD in future work. The targeted application of multiple frequencies has already been simulated for microwave-assisted processes with different optimization criteria, including heating homogeneity and energy efficiency [23, 63, 115, 132]. However, the heating homogeneity was only evaluated inside a single product, which is only of limited significance for the drying of multiple chunky products.

To evaluate the heating homogeneity inside the samples, Table 3.2 shows the heating patterns for 1MF, 1RF, 6EF, and 6RF in an exemplary product sample at half height. The dependence of the heating pattern on the drying state and control concept is evident. 1RF and 6RF show the highest power densities, especially in the frozen center towards the end of drying. For all control concepts, there is always a higher power density in the frozen core of the product than in the

Table 3.2: Patterns of the volume-specific power absorption from the electromagnetic simulations in an exemplary cuboid of tylose gel (top left in Figure 3.1 (b)) in dependence on drying state and control concept at half height of the cuboid. At the drying states 20%, 40%, 60%, and 80% the sample consists of a frozen core and a dried outer layer, while the drying state 0% is a completely frozen cuboid and the drying state 100% respectively fully dried.

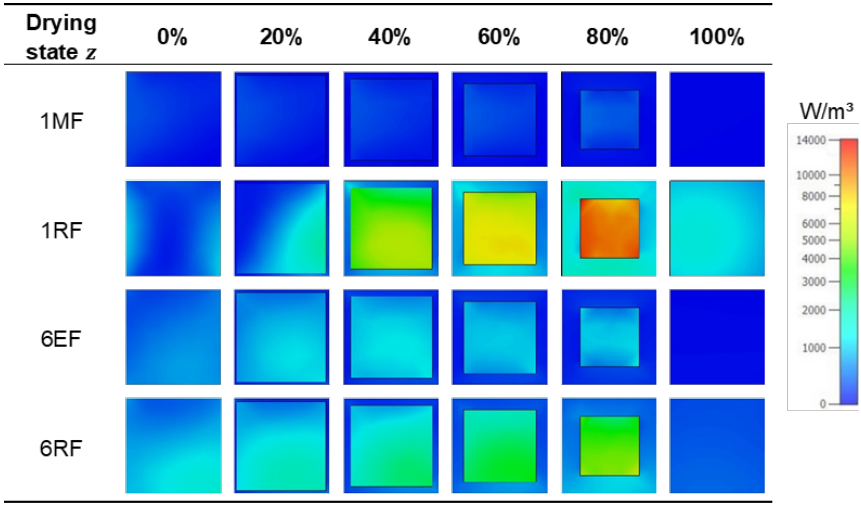

dried layer. This can be explained by the higher DPs in the frozen area (compare Table 3.1).

Figure 3.11 shows the proportion y_{frozen} of dissipated power in the frozen layer divided by the total dissipated power in the same exemplary sample. It can be seen that the distribution of the power in the product depends significantly on the drying state. In comparison, the control concept used has only a minor effect. This result illustrates the selective character of microwave-assisted processing, which is known in the literature [41]. This is particularly advantageous in MFD since the energy is introduced directly into the frozen core where the energy is required for sublimation. Towards the end of drying, there is a high power input in a relatively small frozen volume. If constant power density is desired in frozen areas, power should be reduced toward the end of the process.

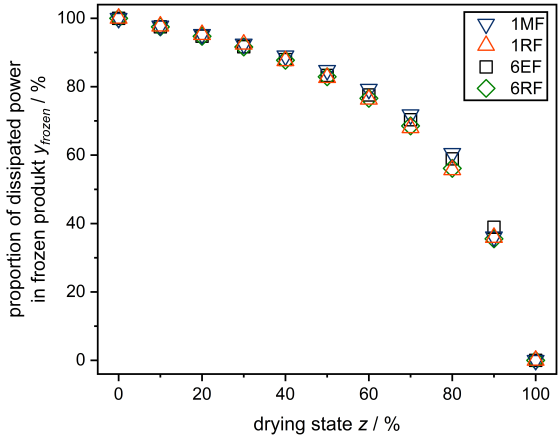

Figure 3.11: The proportion of power dissipation in an exemplary cuboid made of tylose gel (top left in Figure 3.1 (b)) in the frozen region relative to the total power dissipation in the respective cuboid as a function of the drying state for the investigated control concepts, obtained from the electromagnetic simulations.

3.4.1.5 Experimental proof of concept

3.4.1.5.1 Energy Efficiency Figure 3.12 depicts the average energy efficiency plotted over the process time as a function of the applied control concepts for the removal of 20 wt% water without an adaption of the initial frequencies. The applied frequencies are listed in Table A.5 in Section A2. During this part of the drying process, the energy efficiency ranks $\eta_{1RF} > \eta_{6RF} > \eta_{6EF} > \eta_{1MF}$. This order is consistent with the results from the electromagnetic simulations (see Figure 3.9). Experimental results from the literature also show high energy efficiency when selected energy-efficient frequencies are applied in microwave-assisted heating [21, 135]. Therefore, the proof of concept of the electromagnetic simulations was successful in terms of energy efficiency. In the experiments, high energy efficiency generally correlates with short drying times. A targeted selection of frequencies in MFD can thus be used in a process intensification to accelerate the time-intensive primary drying without increasing power consumption.

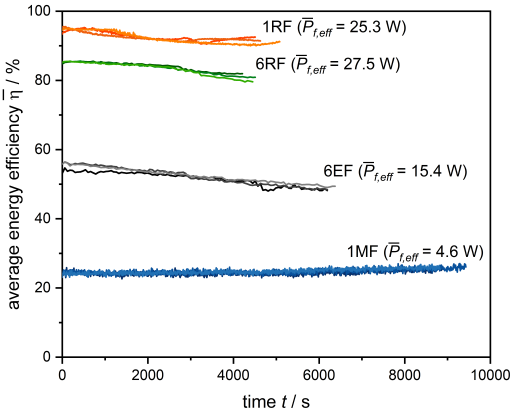

Figure 3.12: Average energy efficiency from MFD experiments plotted over drying time for different control concepts. Experiments were conducted in triplicate. $\bar{P}_{f,eff}$ denotes the effective forward power averaged across the respective repetitions.

Despite a higher energy efficiency, the process time using the 1RF control concept is longer than using the 6RF control concept (see Figure 3.12). This can be explained by a non-constant forward power by the SSG used, as the power output of the SSG is slightly dependent on the frequency. This is likely due to inaccuracies in the calibration of the power output of the SSG, which unfortunately could not be fully resolved during these investigations. Taking into account the effective power applied in the individual experiments, the experiments with the highest effective power have the lowest drying time. This is shown in Figure 3.12, which displays the average effective forward power $\bar{P}_{f,eff}$ of the experiments in triplicate for each control concept. $\bar{P}_{f,eff}$ is calculated for each experiment with

$$\bar{P}_{f,eff} = \frac{\sum_{i=1}^{n} \eta_\mathrm{i} P_{f,\mathrm{i}} t_\mathrm{i}}{t_{total}} \tag{3.12}$$

as the sum of the product of the energy-efficiency η_i with the forward power $P_{f,\mathrm{i}}$ and the time t_i at all applied frequencies, divided by the process time t_{total}. The tendency regarding the shortened drying time with increasing effective power is

consistent with thermodynamic considerations and observations from the literature in experiments [8, 11, 12, 111] and simulations [71].

3.4.1.5.2 Drying homogeneity In the present work, the homogeneity of drying is used as an indirect indicator of homogeneity of power input instead of infrared imaging because endothermal sublimation occurs in MFD. The basic assumption is a lower residual moisture content with higher energy input. Figure 3.13 displays the residual moisture distribution of the individual samples for the applied control concepts.

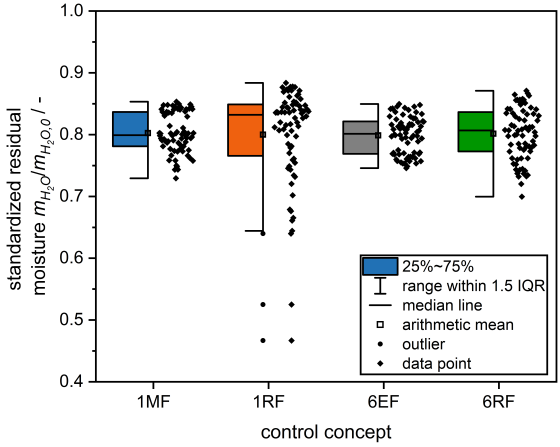

Figure 3.13: Distribution of residual moisture after MFD for the different control concepts standardized to the water mass in the samples before drying. The data sets consist of experiments in triplicate for each control concept with 24 samples each. The colors match the control concepts in analogy to the previous figures. IQR–interquartile range.

The range of residual moisture is largest for 1RF and smallest for 6EF. This result is consistent with the predictions from the electromagnetic simulations shown in Figure 3.10. There is a clear correlation of frequency number with drying homogeneity in the results for similar effective microwave power. For 6EF, a smaller spread is found in comparison with 1MF. The same tendency can be seen when comparing 6RF with 1RF. Additionally, a smaller difference between the

median and mean is found for 6RF than for 1RF. The results are qualitatively in line with the expectations from the simulations, which predict more homogeneous heating for the application of multiple frequencies. In the literature, the tendency of a more uniform energy input with multiple frequencies is also shown for microwave-assisted processes [19, 116]. Due to the obtained results, the validity of this statement can now be extended to the first part of primary drying in MFD.

In contrast to the expectations from the simulation results, a higher range of residual moisture is found for 6RF compared to 1MF, although several frequencies were applied with 6RF. One possible explanation is the occurrence of thermal radiation in the experiments, which is not accounted for in the electromagnetic models. The longer process time and lower effective power when utilizing 1MF probably lead to a higher proportion of power input by thermal radiation from the uncooled surfaces of the process chamber. Moreover, more time is given to thermal equalization processes. These effects could lead to more homogeneous drying with 1MF, even though the power dissipation of microwaves should be less homogeneous. Therefore, the supplementation of MFD with power sources based on additional heat transfer mechanisms, e.g., thermal radiation or conduction, in hybrid processes remains an interesting focus for future work. Park et al. [71] already simulated shortened process times when combining MFD with CFD.

The partly high ranges of residual moisture and outliers, as can be seen with 1RF, are caused by the rapid drying of individual samples. Presumably, this occurs in samples with the highest power input. In extreme cases, high power absorption leads to the melting of the frozen product area and subsequent product damage due to puffing. Visible puffing occurred in two drying experiments applying 1RF in one sample each. The puffed samples can be seen in Figure 3.13 as outliers with a residual moisture $m_{H_2O}/m_{H_2O,0} < 0.6$. These low residual moisture contents are probably caused by the high power input into the molten samples in combination with the reduced mass transfer resistance due to the large pores formed. The product damage due to puffing can be avoided by applying multiple RFs with 6RF, even though a higher effective power is coupled in. This underlines the advantage of more homogeneous power input by applying multiple frequencies in MFD.

3.4.1.6 Limitations and future work

Though a useful tool for gaining qualitative insights into the MFD process, the results from the electromagnetic simulations do not depict the actual distribution of the microwave field in MFD. Possible reasons for partial mismatches between the results from simulations and experiments in validation and proof of concept are:

- Simplification of the geometries of cavity and samples, as well as possible deviations in positions and dimensions;
- Temperature- and frequency-dependency of the dielectric properties are not taken into account;
- Exclusive simulation of the electromagnetic field at discrete times of drying, leading to no consideration of thermodynamic effects;
- Simplifying assumptions throughout drying, including a uniform retreat of the sublimation front in all samples and no shrinkage.

Further fine-tuning of the models is possible but cumbersome. It is questionable if the efforts can lead to improvements, which enable further insights. Utilization of the developed electromagnetic model and the discovered advantageous features of frequency modulation in future work is a promising possibility to explore the high potential of using SSGs in MFD in a time-efficient manner. Additional parameters to be investigated are, e.g., the phase shift or power distribution between multiple SSGs.

The effect of different frequency-based control concepts has been successfully investigated in experiments during the first part of primary drying. However, the frequencies of the control concepts were not adjusted at a drying state of 10% as in the electromagnetic simulations. The complete drying with a variation of the controlled frequencies throughout MFD remains an application-relevant topic for future research. The MFD process should then be compared to the established CFD by classifying product and process parameters.

3.5 Conclusions

A model of MFD for drying a chunky model product of tylose gel in a laboratory-scale system was successfully developed and verified to investigate the effects of modulating the electromagnetic field throughout drying. The purely electromagnetic model has been decoupled from thermodynamic equations by solving for several discrete drying states. The DPs of fresh and freeze-dried tylose gel were acquired experimentally and utilized in the simulations. The properties indicate dissipation of the electromagnetic power in frozen tylose gel mainly by interactions with bound water. Validation of the simulations via experimentally determined energy efficiency in the frequency range of 2400 MHz to 2500 MHz at the beginning of drying did not show quantitative agreement. Nevertheless, a comparability of the curves in terms of the number and magnitude of the detected maxima was observed. Therefore, electromagnetic simulations can be employed as a time-efficient tool to predict the qualitative effects of frequency modulation in MFD. Due to the limitations of the model, experimental proof of concept is always required.

In post-processing of the simulations, the following generally valid correlations were found by applying different frequency-based control concepts in MFD:

1. Higher energy efficiency over the whole course of drying when applying energy-efficient RFs;
2. More uniform heating homogeneity between products when targeting multiple frequencies;
3. Insignificant effect on power distribution between frozen and dried regions in individual products. The distribution is mainly determined by the higher DPs of the frozen region.

In the experimental proof of concept, qualitative agreement with predictions from simulation results was demonstrated regarding energy efficiency and drying homogeneity for the first part of primary drying. Moreover, the higher energy

efficiency with a targeted frequency modulation was associated with shortened process times without an increase in power consumption.

4 A time-saving approach to parameter studies in microwave-assisted freeze-drying

This chapter was published as:

Sickert, T.; Bergmann, R.; Christoph, J.; Gaukel, V. A Time-Saving Approach to Parameter Studies in Microwave-Assisted Freeze Drying. Processes 2023, 11(10), 2886, doi:10.3390/pr11102886.

Variables, figures, and abbreviations were adapted for consistency.

4.1 Abstract

Microwave-assisted freeze-drying (MFD) is particularly suited for drying heat-sensitive materials. However, optimizing process parameters is time-consuming due to lengthy individual experiments. This study investigates the feasibility of partial MFD for parameter studies, with the process being terminated after removing 20 wt% of the water contained. The proposed approach reduces the time required for parameter evaluation by 92.0% compared to complete MFD. It also enables the evaluation of the samples' drying homogeneity. A subsequent parameter study based on partial MFD was then conducted to evaluate the effects of chamber pressure, microwave power, and microwave frequencies on the drying kinetics and drying homogeneity. Lowering the average chamber pressure from 0.87 mbar to 0.19 mbar reduced the process duration by 18.8%. An increase in the dissipated specific microwave power from 0.048 W/g to 0.143 W/g reduced the duration by 46.7%. The targeted application of frequencies increased the average energy efficiency to as high as 92.4%, contributing to a shortened process duration of up to 51.2%. Only the application of multiple frequencies caused a notable increase in drying homogeneity. In summary, this study demonstrates the feasibility and time-saving benefits of partial drying for parameter studies in MFD and potentially different types of drying processes

4.2 Introduction

Freeze-drying (FD) is an established method in process engineering, yielding products of a particularly high quality [1]. Recent work on FD covered microwave-assisted freeze-drying (MFD) as an approach to process intensification [8, 11–13, 67–69, 136, 137]. In conventional freeze-drying (CFD), energy is supplied through the mechanisms of thermal radiation, conduction, and convection [37]. In MFD, by contrast, electromagnetic energy dissipates into heat directly inside the product by interactions of the microwaves with the product as a dielectric [54]. During MFD, the absorption of microwave energy by interactions with bound

water accounts for a major part of energy input, whereas frozen water absorbs energy to a minor extent only [137]. Microwave application offers a variety of advantages for drying, such as avoiding heat transfer resistances through the product surface [48], selective generation of heat in product areas containing large amounts of water [138], as well as short process durations and cost savings [41]. Comparing MFD to CFD, the drying time was reduced by about 40% for chunky products, such as sea cucumber [8] and barley grass [67]. Reductions as high as 70% to 80% were reported for viscous products, such as monoclonal antibody formulations [68], lactic acid bacteria cell concentrate [11], and foamed raspberry puree [12]. The quality of the final product obtained was similar or superior to products processed with CFD.

Conventionally, microwaves are generated with magnetrons [17], which are high-power vacuum tubes. While magnetrons are relatively cheap and readily available to supply high microwave power, they offer only limited control of the microwaves generated. Power regulation, for instance, is usually implemented by a simple on–off control. A more advanced control of the magnetron is technically complex, as can be seen, for example, in the study by Yang et al. [139]. In contrast to this, the generation of microwaves by a solid-state microwave generator (SSG) enables the precise and rapid modulation of microwave properties and provides feedback on the reflected and forward power as a function of the product state. For instance, SSGs produce a stable and narrow frequency bandwidth compared to magnetrons [140]. When using several SSGs, the power, frequency, and phase shift of every generator can be controlled individually. In the context of MFD, this enables additional degrees of freedom for process control, as the microwave field can be controlled specifically throughout drying to intensify the process. In comparison, process control in CFD is limited to the regulation of chamber pressure and shelf temperature [5, 35, 37]. The following sections provide a brief overview of the expected effects of the process parameters of chamber pressure, microwave power, and microwave frequency on MFD.

In theory, a higher chamber pressure should result in lower sublimation rates for CFD due to decreased pressure gradients from the sublimation front to the process chamber [5]. However, this correlation is only valid if the temperature at

the sublimation front and, thus, the vapor pressure remain constant. Assegehegn et al. [35] experimentally investigated the impact of chamber pressure on CFD for pharmaceutical model formulations. Increasing the chamber pressure in the range of 0.05 mbar to 0.20 mbar led to higher sublimation rates at a constant shelf temperature. The result can presumably be attributed to the higher product temperature caused by the elevated chamber pressure. The increased product temperature results in a higher pressure gradient through the dried layer where the pressure increase at the sublimation front exceeds that on the product surface, i.e., of the chamber. In line with this, a decrease in the sublimation rate was observed with a higher chamber pressure when regulating the product temperature to a constant value via the shelf temperature. For MFD, Wang et al. [89] observed no significant effect of chamber pressures of 0.15 mbar and 0.65 mbar on the drying duration. In contrast to this, Ambros et al. [11] noted higher drying rates for increases in chamber pressure in the range of 0.6 mbar to 2.0 mbar in MFD. As in CFD, faster drying correlated with higher product temperature. Regarding product quality, Ambros et al. [11] detected a decrease in survival rate and membrane integrity with increasing chamber pressure for the lactic acid bacteria *B. lactis* and no effect on these parameters for *L. paracasei* during MFD. Krokida et al. [141] observed decreasing porosity of agricultural products in CFD with increasing pressure. The proposed cause was an increase in product temperature above the glass transition temperature. In summary, chamber pressure influences mass transfer through the product via the pressure on the product surface and the vapor pressure at the sublimation front. The latter also influences heat transfer by affecting the sublimation temperature. Therefore, the effect of chamber pressure on the drying rate in MFD is not obvious and may vary depending on the product and the process conditions. Care must be taken to ensure that the product quality is not affected by exceeding product-specific temperature limits, e.g., the glass transition temperature. Measuring product temperature, hence, is a useful benchmark for evaluating the stress on the product.

Increases in microwave power in MFD are associated with decreases in process duration for various experimental setups [8, 11, 12, 67, 89–92]. Presumably, this correlation is caused by the increase in product temperature with higher

microwave power, as observed in the literature for MFD of sea cucumber [8] and barley grass [67]. The higher temperature increases the vapor pressure at the sublimation front, thereby elevating the gradient, which drives the mass transfer. However, a higher product temperature is generally associated with a deterioration in product quality. Examples presented in the literature include the darker color of banana chips [92], as well as decreases in sensory evaluation scores in a hedonic assessment of instant vegetable soup [90], and reduced microbial survival rates of *B. lactis* [11]. On the other hand, no effect of microwave power on the survival rate of *L. paracesei* was reported by Ambros et al. [11]. Jiang et al. [91] observed no clear trends in sensory evaluation results of banana chips with different sugar contents on a hedonic scale. Only above a critical power level of 2.2 W/g were the ratings consistently lower. Thus, it depends on the thermal stability of the product investigated and the range of power applied whether changes in the power level lead to any effect on the product at all. As for chamber pressure, power levels in MFD may be increased until a relevant deterioration of the product is reached by an exceedingly high temperature.

Regarding the influence of microwave frequency on MFD, there is only limited literature available. For microwave vacuum drying at frequencies of 915 MHz and 2450 MHz, Li et al. [25] conducted measurements of the dielectric properties (DPs) and moisture content of Chinese yam. Both frequency and moisture correlated with differences in DPs, which in turn affect the power dissipation and, thus, the drying process. For CFD, Nakagawa and Kono [26] tracked the drying progress using an open-ended coaxial microwave resonator in the frequency range from 3 MHz to 3000 MHz. They observed a shift in peak resonant frequency to higher frequencies. According to theoretical calculations in the literature [42], this indicates a decrease in DPs during FD. These dependencies of DPs on drying progress and frequency pose a challenge for frequency control in MFD. In a previous study, however, Sickert et al. [137] developed frequency-based control concepts in electromagnetic simulations and applied them successfully to MFD in experiments with an SSG. More homogeneous power dissipation and drying at a similar dissipated microwave power were observed for the application of multiple frequencies. A targeted excitation of energy-efficient resonant frequencies (RFs)

led to the highest energy efficiencies. Higher dissipated power, associated with high energy efficiency, correlated with a shorter process duration. More extensive work covered the influence of frequency selection on microwave-assisted heating with SSGs. Targeted excitation of multiple frequencies was found to increase heating homogeneity in simulations [18, 23] as well as experiments [19, 21, 135]. Frequency modulation was also utilized to increase energy efficiency, as indicated by temperature measurements [18, 19, 21, 135]. These findings support the results of Sickert et al. [137], which revealed that frequency is an important process parameter in MFD.

The higher number of process parameters for MFD in comparison to CFD is associated with both opportunities and challenges. While advanced process optimization becomes possible, a non-optimized drying procedure could result in subpar drying performance. Therefore, parameter studies are crucial, but also time- and labor-intensive due to the long drying times of FD ranging from several hours to days. Partial MFD offers an opportunity for time savings, enabling higher experimental throughput in parameter studies. The current work aims to investigate the feasibility of conducting parameter studies with partial MFD, where only 20 wt% of the contained water is removed. This approach has not yet been specifically investigated for the parameter study of any drying process, as far as the authors are aware. The experiments are carried out in a laboratory-scale MFD system with a chunky model product, tylose gel. First, partial and complete MFD runs are compared regarding their drying kinetics and drying homogeneity. Particular emphasis is placed on the potential of partial drying for evaluating drying homogeneity. In partial MFD, differences in residual moisture should be more pronounced than in complete drying where the moisture content converges towards equilibrium. Additionally, the potential time savings achieved with partial drying are quantified. Subsequently, parameter studies on the chamber pressure, microwave power, and microwave frequency are carried out to quantify their influence on drying kinetics and drying homogeneity. Four frequency-based control concepts are investigated, including single frequencies with minimal and maximal energy efficiency as well as six frequencies that provide the maximal energy efficiency or are spaced equidistantly from 2400 MHz to 2500 MHz. To validate

the approach proposed for evaluating the effects of process parameters on MFD, the results from the parameter study using partial drying are compared with the literature data for complete drying processes. Based on the literature available, increasing the chamber pressure in the drying process should result in shorter drying times due to the higher product temperature. Similarly, higher microwave power and energy efficiency achieved via frequency control are expected to accelerate drying. For all parameters, it is crucial to keep the product temperature below a product-specific threshold to avoid product impairment. The application of multiple frequencies should lead to higher drying homogeneity. By exploring partial MFD for use in parameter studies and comparing its results with complete MFD, this research contributes to efficient process optimization, shortening the development time, and increasing the drying efficiency.

4.3 Materials and methods

4.3.1 Model product

Cuboids of tylose gel were used as a model product in this study. The samples were prepared as previously described [137]. Briefly, cuboids of 12.50 ± 0.05 g and approximately 25 mm $\times$ 25 mm $\times$ 20 mm in dimension were prepared in a composition of 76.23 wt% demineralized water, 23.77 wt% Tylose MH1000 (Kremer Pigmente, Aichstetten, Germany), and 1.00 wt% L-(+)-ascorbic acid (Carl Roth, Karlsruhe, Germany). Subsequently, the samples were frozen at -30 °C for at least 14 h.

4.3.2 MFD system

The setup of the laboratory-scale MFD system was identical to that used in a previous study [137]. The process chamber was made of stainless steel and had inner dimensions of 612 mm $\times$ 400 mm $\times$ 300 mm. Centrally, at the bottom of the process chamber, a plate made of polyether ether ketone with a base area

of 200 mm × 200 mm was installed as product support and connected to a PW4MC3/2 kg load cell (Hottinger Brüel & Kjaer, Darmstadt, Germany). A cold trap (UCCT, Vienna, Austria) was attached to the process chamber and set to a temperature of -60 °C in all experiments. A NEO D 65 vacuum pump (Leybold, Cologne, Germany) or a P 65 D vacuum pump (SASKIA, Ilmenau, Germany) was connected to the cold trap during the experiments. Chamber pressure was measured at the top of the process chamber with a CMR363 capacitive pressure sensor (Pfeiffer, Aßlar, Germany). A script in Matlab R2020b (MathWorks, Natick, MA, USA) was used to record the weight of the product as well as to record and control the chamber pressure. A WR340 waveguide was centrally embedded in the top of the process chamber and connected to an HY2020 SSG (TRUMPF, Freiburg im Breisgau, Germany) via a coaxial cable. The SSG could be set to frequencies between 2400 MHz and 2500 MHz with an accuracy of 0.01 MHz and had a maximum output power of 600 W. It was equipped with internal sensors to detect forward and reflected power. A second script in Matlab R2020b controlled forward power and frequency in addition to recording the microwave properties.

4.3.3 Process characterization

A total of 24 frozen tylose gel samples were placed centrally on the product support in a 6 × 4 arrangement at a 5 mm distance, as depicted in Figure A.3 in Section A3. A vacuum was applied to the process chamber 10 min before microwave application. The measurement of process time started when the SSG was activated. Process characterization was carried out to detect the frequency-dependent energy efficiency η in the range of 2400 MHz to 2500 MHz in an interval of 0.1 MHz. The forward power P_f ,set was set to the minimally feasible value of 50 W. With each measurement, the forward power P_f and the reflected power P_r were recorded. The energy efficiency η was calculated via

$$\eta = 1 - \frac{P_r}{P_f}. \tag{4.1}$$

This enabled the detection of RFs, which are defined as the frequencies of local maxima in energy efficiency. The dissipated power P_d was calculated using

$$P_d = P_f - P_r \tag{4.2}$$

as the difference between the respective powers. The calculations in Equations 4.1 and 4.2 are based on the assumption that all power not reflected to the SSG must dissipate inside the process chamber. The power reflected by the coupling of the coaxial cable with waveguides or dissipated by heat losses in the coaxial cable is not considered. All process characterizations were conducted in triplicate and the arithmetic mean of the RFs was applied in the subsequent drying experiments.

4.3.4 Drying procedure

The placement of the samples and the starting procedure of the process were chosen as in the process characterization. Before the start of each experiment, process parameters were set according to the specifications of the respective experiment in the parameter study (see Section 4.3.5). These were the set chamber pressure $p_{c,set}$ as well as the microwave properties of set forward power $P_{f,set}$, control concept for the frequency, and activation ratio r_{on}. The parameter r_{on} describes the ratio of the active time of the SSG ton to the total time of drying t_{total}, according to

$$r_{on} = \frac{t_{on}}{t_{total}} = \frac{t_{on}}{t_{on} + t_{pause}}, \tag{4.3}$$

where t_{pause} is the total inactive time of the generator. While $P_{f,set}$ was kept constant during all experiments, the value of r_{on} was adjusted to achieve specific time-averaged power levels. This allowed for the application of a lower time-averaged power level than determined by the minimally feasible value of $P_{f,set}$ and potential nonlinearities that may occur when $P_{f,set}$ is changed directly were avoided. Each frequency utilized was applied for 10 s with the respective

r_{on} governing the period during which the microwave generator emitted power. When using multiple frequencies, the microwave application started at the lowest frequency and worked its way up to the highest frequency before starting the next frequency loop. The sequence of a frequency loop is shown in Figure 4.1 as an example of an arbitrary control concept with six frequencies.

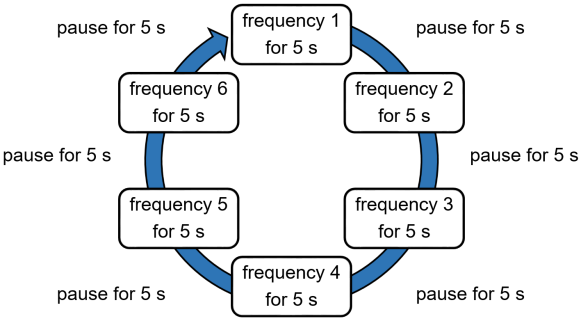

Figure 4.1: Exemplary sequence for a frequency loop of an arbitrary control concept with six frequencies and $r_{on} = 0.5$. Frequencies 1 to 6 are sorted in the order of ascending frequency.

Partial MFD was terminated when 20 wt% of the initially contained water mass was removed. The initial water mass was calculated from the composition and weight of the samples before drying. Complete MFD, conducted as a benchmark process, was terminated when the drying rate $\dot{m}$ was less than 0.25 g/h, calculated over a period of 1 h.

The average specific dissipated power $\bar{P}_{d,s}$ for each experiment was calculated using

$$\bar{P}_{d,s} = \frac{r_{on} \sum_{i=1}^{n} \frac{P_{d,\mathrm{i}}}{n}}{\sum_{j=1}^{24} m_{MFD,\mathrm{j}}} \tag{4.4}$$

as the product of r_{on} with the arithmetic mean of the dissipated power $P_{d,\mathrm{i}}$ of n applied frequencies throughout the whole process divided by the sum of the weights of the 24 individual samples $m_{MFD,\mathrm{j}}$. The average specific forward

power $\bar{P}_{f,s}$ was calculated in analogy to Equation 4.4, while the average chamber pressure $\bar{p}_c$ was calculated as the arithmetic mean of all recorded values of chamber pressure. The average drying rate $\dot{m}_{av}$ was determined using

$$\dot{m}_{av} = \frac{\Delta m_{pow}}{t_{total}} \tag{4.5}$$

as the weight difference during power application Δm_{pow} divided by process duration t_{total}. Experiments in the parameter studies on frequency and pressure were conducted in triplicate. The experiments in the parameter study on power are single experiments since the power variations among experiments are taken into account when evaluating the results.

4.3.5 Process parameters

Table 4.1 provides an overview of the specifications set in the experiments comparing the termination points between partial and complete drying as well as the experiments of the parameter studies. Set chamber pressure $p_{c,set}$ was varied from 0.2 mbar to 1.0 mbar in the respective parameter study. The default value in all other experiments was 0.5 mbar. The set forward power $P_{f,set}$ of the microwaves was 50 W for all experiments. The power applied in the parameter study on microwave power was varied by modifying the activation ratio r_{on} between 0.25 and 1, while 0.25 was the default value in the remaining experiments. Microwave frequency was varied by applying different frequency-based control concepts. The required RFs had been identified in advance by process characterization. The frequency-based control concepts used were:

- Single Minimum Frequency (1MF) - frequency displaying the global minimum of energy efficiency;
- Single Resonant Frequency (1RF) - frequency displaying the global maximum of energy efficiency;

- Six Equidistant Frequencies (6EF) - frequencies from 2400 MHz to 2500 MHz at an interval of 20 MHz;
- Six Resonant Frequencies (6RF) - frequencies with the highest local maxima of energy efficiency

Table 4.1: Specifications of set chamber pressure, set forward power, activation ratio, and frequency-based control concepts in the experiments to compare termination points and parameter studies.

	Comparison	**Parameter Study**		
	Termination	**Pressure**	**Power**	**Frequency**
Set chamber pressure $p_{c,set}$ / mbar	0.5	0.2; 0.5; 1.0	0.5	0.5
Set forward power $P_{f,set}$ / W	50	50	50	50
Activation ratio r_{on} / -	0.25	0.25	0.25; 0.50; 0.75; 1.00	0.25
Frequency-based control concept	6EF	6RF	6RF	1MF; 1RF; 6EF; 6RF

The experiments in the parameter studies on pressure and power were carried out with 6RF, whereas the experiments to compare the termination points took place with 6EF. In all drying experiments, the frequencies of the various control concepts were set at the beginning of the process and kept constant throughout drying. The set values for chamber pressure $p_{c,set}$ and forward power $P_{f,set}$ deviated from the averaged measured values due to process control. The measured values are shown in Tables A.6 to A.9 in Section A3. The frequencies applied and identified in process characterization are shown in Tables A.10 and A.11 in Section A3.

4.3.6 Sample analysis

The individual samples were weighed on a Type 1518 balance (Sartorius, Göttingen, Germany) to determine the masses before MFD $m_{MFD,0}$ and after MFD m_{MFD}. After cutting the samples in half, they were examined for signs of macroscopic product impairment. To assess the uniformity of drying, the residual moisture of each sample was determined gravimetrically. For this purpose, the freeze-dried samples were dried in a drying oven T6060 (Heraeus, Hanau, Germany) for at least 24 h at 105 °C. The weight of the samples was then determined using a precision balance LS 220A SCS (Precisa, Dietikon, Switzerland) and taken as the dry mass m_{dry} for the calculation of the standardized residual moisture $m_{H_2O}/m_{H_2O,0}$, according to

$$\frac{m_{H_2O}}{m_{H_2O,0}} = \frac{m_{MFD} - m_{dry}}{m_{MFD,0} - m_{dry}}. \tag{4.6}$$

4.3.7 Statistical analysis

A one-way analysis of variance (ANOVA) was used to inspect the experimental results for statistically significant differences. First, a Shapiro–Wilk test was used to check whether the population was distributed normally. Levene's test was used to test for equal variances, while Tukey's test was used for the comparison of the means. All significance levels were set to 0.05. Significant differences in means are indicated by different grouping letters when all criteria for performing an ANOVA were met.

4.4 Results

4.4.1 Comparison termination MFD

The drying kinetics of partial and complete MFD are depicted in Figure 4.2. No systematic differences between partial and complete drying were observed. All experiments exhibit the highest drying rate in the initial stage of the process, followed by a gradual decrease as drying progresses. This tendency is consistent with the literature [11, 90]. A high reproducibility of drying kinetics is evident for partial MFD experiments. In the case studied, it took 7.0% longer for complete MFD to reach the termination criterion than for partial MFD. The discrepancy might be attributed to a recalibration of the SSG before complete MFD, leading to a slightly lower average specific forward power $\bar{P}_{f,s}$ of 0.072 W/g in comparison to an average of 0.098 W/g for partial MFD. In terms of drying kinetics, partial MFD can therefore be considered representative of the initial part of complete MFD, in line with the anticipated behavior.

Implementing the partial drying termination criterion to complete MFD yields a process duration of approximately 1.9 h, corresponding to a 92.0% reduction compared to the duration of 23.2 h for complete MFD. Therefore, partial drying in parameter studies enables significantly higher experimental throughput, which results in shorter development times or a more customized process due to a higher number of tested parameter combinations. However, it is uncertain whether the results obtained in this early stage of the drying process will be useful when conducting a parameter study

To assess drying homogeneity, Figure 4.3 shows the standardized residual moistures for complete MFD in comparison to partial MFD. For complete MFD, there were only small variations in residual moisture in the range of 0.004 to 0.005. In contrast to this, partial MFD resulted in residual moistures of the individual samples ranging from 0.753 to 0.848, indicating differences in drying kinetics among the individual samples. The narrow range for complete MFD was presumably caused by a convergence of residual moisture towards equilibrium at the end

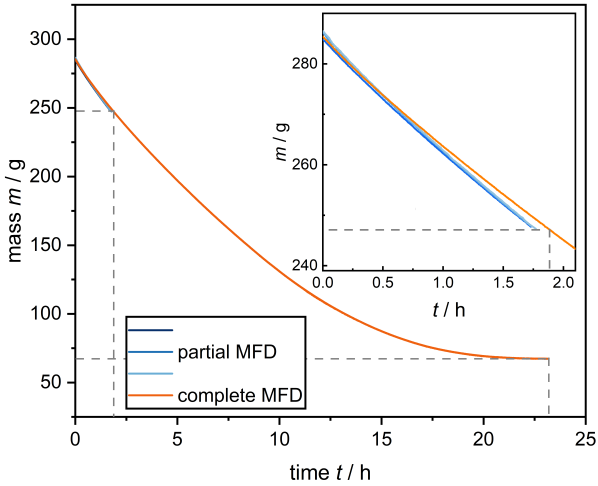

Figure 4.2: Drying kinetics of partial MFD in comparison to complete MFD. The inset plot provides an enlarged view of the initial two hours of MFD. The dashed lines mark the time and mass at which complete MFD reaches the termination criteria $m_{H_2O}/m_{H_2O,0} = 0.80$ and $\dot{m} < 0.25\ g/h$.

of drying. Samples that reach residual moisture near equilibrium first have the slowest drying rate at the end of the process, since only small amounts of water remain to be removed. The resulting narrow distribution of residual moisture is not suited for determining the drying homogeneity of the samples. In contrast to this, partial MFD allowed drying homogeneity to be evaluated due to a broader range of residual moisture. This is particularly relevant to evaluating the homogeneity of dissipated microwave power in MFD. A similar approach was used by Assegehegn et al. [35] to determine the drying homogeneity in CFD. Drying was terminated when the primary drying of vials with the highest drying rates was completed. On this basis, the average drying rates for all vials were calculated and the drying homogeneities for different process conditions could be compared. These results support the suitability of partial drying for parameter studies, as its drying kinetics are representative. Partial drying is particularly suitable for studying drying homogeneity.

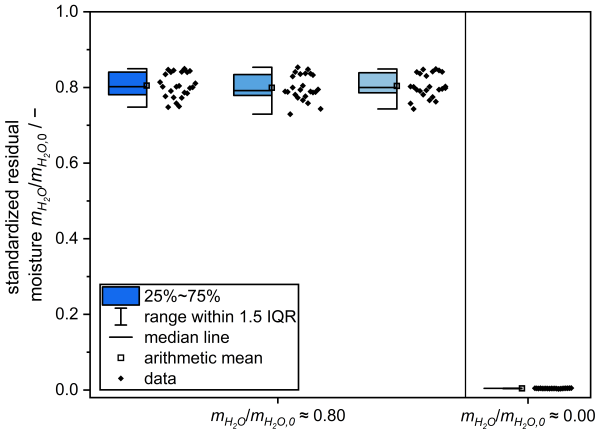

Figure 4.3: Comparison of standardized residual moistures for partial and complete MFD.

4.4.2 Parameter study

4.4.2.1 Chamber pressure

The process duration of partial MFD is plotted in Figure 4.4 for the chamber pressures investigated and the corresponding specific dissipated power. Figure A.4 in Section A3 provides the drying kinetics in detail. The decrease in average chamber pressure from 0.87 mbar to 0.19 mbar reduced the process duration by 18.8%, indicating a correlation between a lower chamber pressure and a shorter process duration. The differences in the arithmetic means of process duration are statistically significant, as shown in Table 4.2. In addition to chamber pressure, dissipated power must be taken into account. This is because the chamber pressure influences the frequency and energy efficiency of the applied RF, which leads to differences in power dissipation. Furthermore, specific dissipated powers varied at distinct chamber pressure levels due to differences in forward power among experiments, caused by limitations of the SSG setup used. These constraints are discussed extensively in Section 4.4.3. In the experiments of the parameter study, higher specific dissipated power should lead to a shorter process duration [8, 11, 12, 67, 89–92]. Accordingly, a trend to shorter process durations with higher

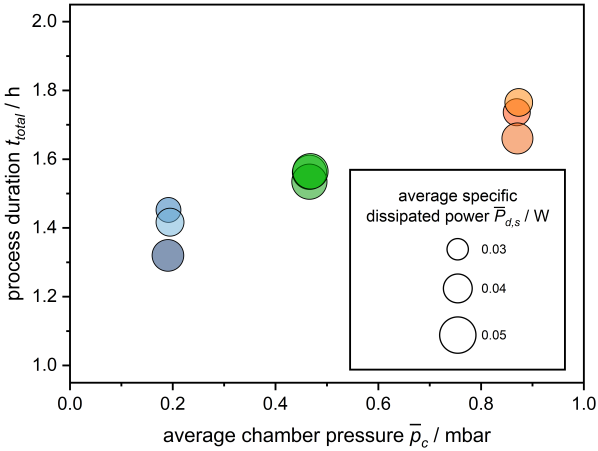

Figure 4.4: Process durations of MFD as a function of average chamber pressure. Bubble size indicates the average specific dissipated power of each experiment.

dissipated power at the individual chamber pressure levels indicates the suspected influence of the dissipated power. This is particularly visible at 0.19 mbar and 0.87 mbar in Figure 4.4. However, the correlation of chamber pressure with process duration cannot be explained solely by differences in dissipated power since the shortest process durations did not occur at the highest levels of dissipated power (see Table 4.2).

Shorter process durations with lower chamber pressures contradict the literature results for MFD. According to those results, decreases in chamber pressure led to longer drying durations in combination with a lower product temperature [11] or a negligible effect on drying time [89]. To investigate the causes of these contradictions in detail, a one-way ANOVA of several relevant process parameters was conducted. The corresponding results are shown in Table 4.2. The removed water mass was almost constant at 45.1 g for all chamber pressures. In contrast to this, the water mass removed during the 10 min of creating the vacuum before the application of microwaves was significantly lower for the average chamber pressure of 0.19 mbar than for the remaining pressure levels (compare Figure A.4 in Section A3). Consequently, less water had to be removed during microwave

application, which resulted in a shorter process duration. The lower sublimation temperature at a lower vapor pressure of ice [102] could be the cause of the difference in removed water mass before microwave application. Since the samples were frozen outside the process chamber and heated up during handling before MFD, their temperature presumably dropped to the temperature of sublimation when the vacuum was applied. The temperature of sublimation can be approximated by using the chamber pressure for the vapor pressure of ice when assuming that the atmosphere solely consists of water vapor and that mass transport resistance is negligible at the initial stage of drying. For the average chamber pressures of 0.19 mbar, 0.47 mbar, and 0.87 mbar, the sublimation temperatures are about -36.5 °C, -27.9 °C, and -21.8 °C, respectively [102]. Some of the energy released by cooling the samples may have provided the enthalpy of sublimation, resulting in a loss of ice from the samples. In addition, the lower temperatures of the samples at the lower chamber pressure presumably led to a higher energy input by thermal radiation. Therefore, the result of a higher mass of water removed prior to the application of microwaves with lower chamber pressure is consistent with theoretical considerations.

Moreover, the arithmetic means of the drying rate during power application at the average chamber pressures of 0.19 mbar and 0.47 mbar were significantly higher than for the experiments at 0.87 mbar. This suggests higher drying rates with a lower chamber pressure, contradicting the aforementioned literature [11, 89]. However, the relative differences in average drying rates at 0.47 mbar and 0.87 mbar in comparison to 0.19 mbar are relatively small, less than 10%. The higher drying rate at 0.19 mbar compared to 0.87 mbar is particularly informative since the data were obtained at similar average specific dissipated powers. The comparable drying rates between 0.19 mbar and 0.47 mbar may be explained by a slightly higher specific forward power and energy efficiency at 0.47 mbar, leading to a higher specific dissipated power. The cause of the slight rise in drying rate with increasing chamber pressure, contrary to the expectations based on the literature, could be the relatively low applied power. Thus, the process might have been limited by the heat transfer. Mass transfer limitations determined by the chamber pressure might have played a negligible role only. In addition, the

Table 4.2: Process parameters for the MFD experiments in the parameter study on chamber pressure. The values indicate the arithmetic mean and the standard deviation of the experiments performed in triplicate. Different letters indicate significant differences between the arithmetic means.

Set chamber pressure $p_{c,set}$ / mbar	**0.2**	**0.5**	**1.0**
Process duration t_{total} / s	5029 ± 246^{C}	5595 ± 60^{B}	6196 ± 195^{A}
Average chamber pressure $\overline{p}_c$ / mbar	0.19 ± 0.00^{C}	0.47 ± 0.00^{B}	0.87 ± 0.00^{A}
Removed water total Δm / g	45.1 ± 0.3	45.1 ± 0.1	45.1 ± 0.0
Removed water before power application Δm_{pre} / g	13.4 ± 1.3^{A}	9.0 ± 0.2^{B}	8.9 ± 0.7^{B}
Average drying rate during power application $\dot{m}_{av}$ / g/h	22.71 ± 0.82^{A}	23.24 ± 0.09^{A}	21.03 ± 0.71^{B}
Average specific forward power $\overline{P}_{f,s}$ / W/g	0.051 ± 0.006^{A}	0.060 ± 0.001^{A}	0.051 ± 0.003^{A}
Average energy efficiency $\overline{\eta}$ / %	75.3 ± 0.5^{B}	78.6 ± 0.8^{A}	76.7 ± 0.3^{B}
Average specific dissipated power $\overline{P}_{d,s}$ / W/g	0.038 ± 0.004^{B}	0.047 ± 0.001^{A}	0.039 ± 0.003^{B}

relatively thin, porous layer during partial MFD might not be representative of the mass transfer limitations in complete MFD. The implications for the applicability of partial MFD are discussed comprehensively in Section 4.4.3.

To investigate the effects of chamber pressure on drying homogeneity, the residual moisture of each sample versus chamber pressure is shown in Figure 4.5 (a). The residual moistures are in a similar range for all chamber pressures with no outliers, the respective minimum and maximum values being 0.747 and 0.869. Optical observation showed no impairment of the macroscopic structure in any sample. Thus, chamber pressure in the range of 0.19 mbar to 0.87 mbar does not appear to have a significant effect on either drying homogeneity or the product

structure in partial MFD of tylose gel with the set microwave properties. For each chamber pressure, the data points accumulate around three residual moistures at 0.76, 0.80, and 0.85. This may be explained by the dependency of the residual moisture on the position of the samples, as depicted in Figure 4.5 (b). The drying state of the samples differs since the power dissipation in MFD is inhomogeneous [137]. In addition to the energy input by microwaves, thermal radiation could also occur from the uncooled walls of the process chamber. Samples at the edges and corners of the arrangement are likely to be more exposed to thermal radiation due to the larger exposed surface. Accordingly, samples in the center of the arrangement generally exhibit the highest residual moisture, followed by samples at the edges and the corners of the arrangement. This is consistent with the observed faster drying of edge vials in CFD, associated with additional energy input due to thermal radiation [142]. Deviations from the expected residual moistures are presumably caused by a difference in dissipated microwave power between samples, as reflected by samples 3 and 4, which have relatively low residual moistures. Nonetheless, the effects of thermal radiation seem to be predominant over the effects of the pattern of the electromagnetic field during the examined part of MFD.

4.4.2.2 Microwave power

In the present study, the average forward power was varied by the activation ratio. However, the activation ratio affected the power level of the generator, as will be outlined in Section 4.4.3. To account for this phenomenon, the effect of microwave power is evaluated via the average specific dissipated power, as the product of energy efficiency and average specific forward power. Note that the value of the average specific dissipated power does not correlate linearly with the activation ratio, i.e., the individual activation ratios do not occur sequentially with increasing average specific dissipated power. The exact values of the activation ratio and the specific forward power are given in Table A.5 in Section A3.

The influence of the average specific dissipated microwave power on process duration is obvious from Figure 4.6. The average specific dissipated power here

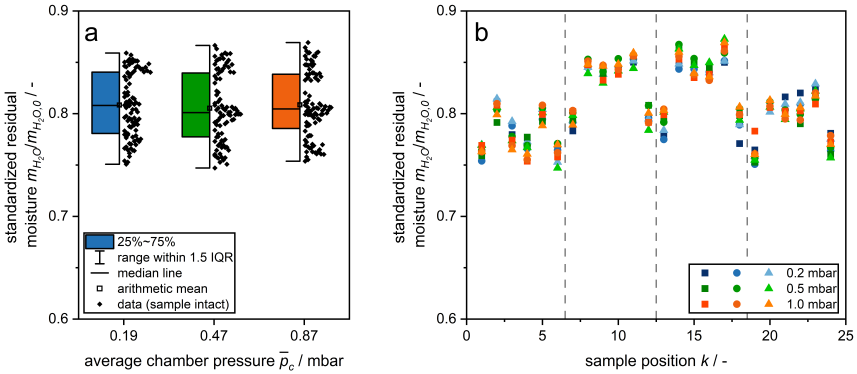

Figure 4.5: (a) Standardized residual moisture as a function of the average chamber pressure. Data sets consist of experiments in triplicate with 24 samples each. (b) Standardized residual moisture plotted over sample position for investigated average chamber pressures. The sample position k describes the placement of the samples, as depicted in Figure A.3 in Section A3. Different shapes mark individual experiments and dashed lines mark the transition between rows of samples.

correlates approximately linearly with the average forward power since the average energy efficiency was relatively constant at 77.7% to 80.3%. In Figure 4.6, the higher average specific dissipated power correlates with a shorter process duration. For instance, the process duration dropped by 46.7% when the average specific dissipated microwave power increased from 0.048 W/g to 0.143 W/g. The observed correlation between the higher microwave power and shorter process duration in partial MFD is in agreement with the literature on complete MFD [8, 11, 12, 67, 89–92]. Therefore, partial MFD seems to be suitable for qualitatively studying the effect of microwave power. The resulting drying kinetics at the investigated power levels are shown in detail in Figure A.4 in Section A3.

In Figure 4.6, isenthalpic lines are plotted next to the experimental data. The red line corresponds to the enthalpy of sublimation, while the blue line additionally accounts for the enthalpies for heating the dry product matrix and water vapor to ambient temperature. All data points should be located in the area colored gray between the isenthalpic lines when assuming that energy was supplied by microwaves only and all energy was utilized to supply the enthalpy of sublimation or to heat the product. These assumptions are not satisfied, since no data point

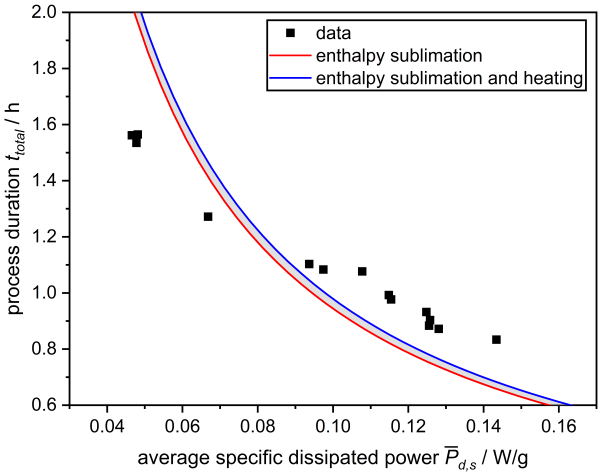

Figure 4.6: Process duration of MFD as a function of the average specific dissipated power. The red line indicates the time at which the average required enthalpy of sublimation is supplied by microwaves. The blue line additionally accounts for the average energy required for heating the dried product matrix and water vapor to room temperature, which is supplied by microwaves only.

is located within the gray area. At low power levels, less electromagnetic energy was dissipated in the process chamber than required for sublimation. At medium to high power, more energy was dissipated in the process chamber than required to heat the water vapor and dry product matrix in addition to providing the sublimation enthalpy. These observations suggest at least two mechanisms of energy transfer. The presence of some points below the curve of sublimation enthalpy indicates that there is another source of energy apart from microwaves contributing to the enthalpy of sublimation. One possible mechanism is thermal radiation from the uncooled walls of the process chamber. With low dissipated power, lower temperatures on the product surface might have contributed to an increased energy transfer by thermal radiation. At medium and high dissipated power, more energy dissipated in the process chamber than theoretically required for sublimation as well as for heating the samples and water vapor. This suggests that electromagnetic energy did not dissipate in the samples but elsewhere, e.g., in the product support or gaskets. In addition, it is known that microwave power

losses may occur in resonators due to induced currents in the walls of the process chamber [143]. Furthermore, it might be necessary to supply additional latent enthalpy to remove water from the samples, e.g., for the desorption of unfrozen water, which is known to be present in tylose gel [126].

To evaluate drying homogeneity, the standardized residual moistures of the dried samples are depicted as a function of the average specific dissipated power and as a function of sample position in Figure 4.7. The range of the residual moisture is approximately constant with average specific dissipated powers, ranging from 0.743 to 0.872 at <0.075 W to 0.741 to 0.875 at >0.125 W/g. These similar ranges can be explained by the same patterns of the electromagnetic field, which are not affected by microwave power. In contrast to frequency, microwave power only affects the amplitudes of the electromagnetic field. As with the parameter study on chamber pressure, the samples in the center of the arrangement in Figure 4.7 (b) have the highest residual moisture contents. Presumably, this is also due to the effect of thermal radiation. However, there are outliers in residual moisture at positions 1, 3, and 4 at a specific dissipated power >0.075 W/g. At >0.125 W/g, these outliers appear to be more frequent, although this statement is not conclusive due to the small number of outliers. Optical observations showed that these outliers were structurally impaired samples, as depicted in Figure A.6 in Section A3. The formation of relatively large pores inside the samples was presumably caused by the melting of the samples. Liquid water absorbs more microwave power than ice. The increased uptake of energy following melting probably led to the buildup of vapor pressure inside the samples. This impaired the macroscopic structure when the product matrix could no longer withstand the pressure gradient. This mechanism of product impairment is referred to as puffing. Puffing correlated with a relatively low residual moisture. This was probably caused by the relatively high amount of dissipated energy due to melting and the formation of large pores inside the samples.

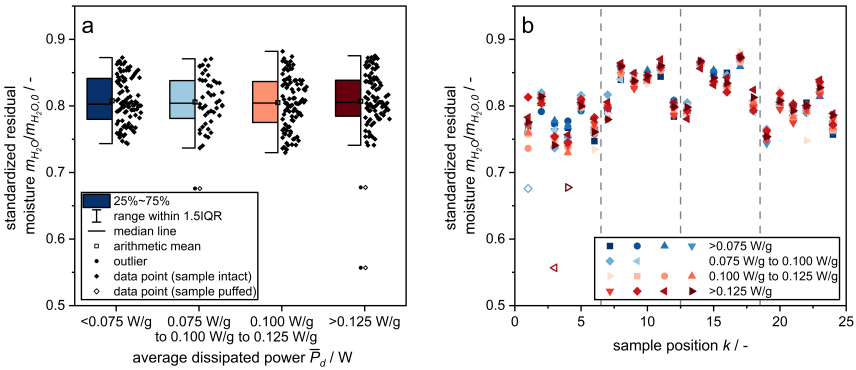

Figure 4.7: (a) Standardized residual moisture as a function of the average specific dissipated power for experiments in the parameter study on microwave power. (b) Standardized residual moisture plotted as a function of the position of the samples, grouped by the levels of average specific dissipated power. The sample position k indicates the placement of the sample in analogy to Figure 4.5 (b). Dashed lines mark the transition between rows of samples, while different shapes indicate individual experiments. Blank symbols mark samples with an impaired structure by puffing.

4.4.2.3 Microwave frequency

The results below complement already published data [137] to enable a comparison with the other parameters studied. To evaluate the effects of frequency on MFD, Figure 4.8 shows the process durations for the applied frequency-based control concepts with the bubble size reflecting the average specific dissipated power. In addition, Figure A.7 in Section A3 displays the drying kinetics in detail. The control concepts 1RF and 6RF have the shortest process durations in a comparable range, followed by 6EF and 1MF.

The results from a one-way ANOVA in Table 4.3 confirm significant differences in average drying duration between the control concepts 1MF, 6EF, and 6RF, while the difference between 6RF and 1RF is not significant. Compared to the most time-consuming control concept 1MF, the application of 6RF shortened the average process duration by 51.2%. In contrast to the parameter study on chamber pressure, both the total water mass removed and the water mass removed before microwave application remained relatively constant in all experiments. The

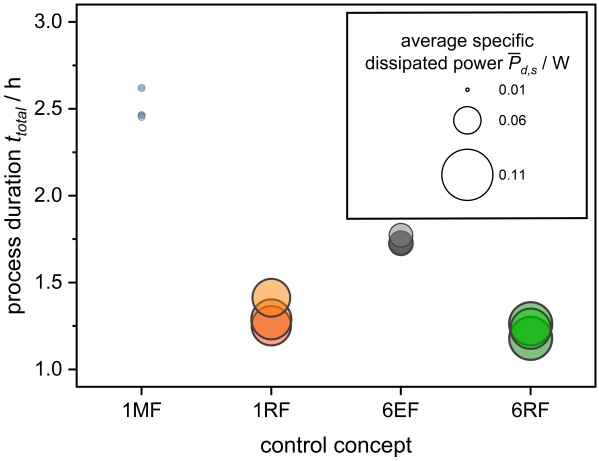

Figure 4.8: Process durations of MFD versus the applied frequency-based control concept. Bubble size reflects the average specific dissipated power of each experiment.

average chamber pressure was also constant, as expected. The average drying rates during power application differed visibly from 15.03 g/h for 1MF to 39.97 g/h for 6RF, although no statistical significance could be calculated since not all prerequisites for an ANOVA were fulfilled. Nevertheless, these results underline the tremendous influence of the applied frequencies on the drying rate.

The forward power of the SSG in the present study was dependent on frequency, leading to average specific forward powers of 0.063 W/g for 1MF up to 0.111 W/g for 6RF. These differences could not be fully resolved within the scope of this work. For instance, different forward powers may have been the cause of the slightly shorter process duration of 6RF compared to 1RF, despite the higher average energy efficiency of 1RF. Further details on the limitations of the experimental setup can be found in Section 4.4.3. Nevertheless, the statements made on the influence of frequency remain valid when the processes are evaluated in terms of energy efficiency or specific dissipated power. The differences in average energy efficiency are in the range of 24.6% for 1MF to 92.4% for 1RF. This large range of energy efficiency can be explained by the frequency dependence of modes, which are associated with specific patterns of the electromagnetic field

Table 4.3: Process parameters for the MFD experiments in the parameter study on frequency. The values indicate the arithmetic mean and the standard deviation of the experiments performed in triplicate. Different letters indicate significant differences between the arithmetic means.

Control concept	**1MF**	**1RF**	**6EF**	**6RF**
Process duration t_{total} / s	9044 ± 337^{A}	4744 ± 303^{C}	6275 ± 93^{B}	4413 ± 155^{C}
Average chamber pressure $\overline{p}_c$ / mbar	0.47 ± 0.00	0.46 ± 0.01	0.47 ± 0.00	0.47 ± 0.00
Removed water total Δm / g	45.6 ± 0.6	45.5 ± 0.3	46.3 ± 1.0	45.4 ± 0.2
Removed water before power application Δm_{pre} / g	7.9 ± 0.3^{A}	8.1 ± 1.0^{A}	8.2 ± 1.8^{A}	7.4 ± 0.8^{A}
Average drying rate during power application $\dot{m}_{av}$ / g/h	15.03 ± 0.18	28.44 ± 1.46	21.88 ± 0.41	30.97 ± 0.65
Average specific forward power $\overline{P}_{f,s}$ / W/g	0.063 ± 0.002^{C}	0.093 ± 0.002^{B}	0.098 ± 0.002^{B}	0.111 ± 0.004^{A}
Average energy efficiency $\overline{\eta}$ / %	24.6 ± 0.3^{D}	92.4 ± 0.3^{A}	52.1 ± 0.4^{C}	83.6 ± 0.4^{B}
Average specific dissipated power $\overline{P}_{d,s}$ / W/g	0.016 ± 0.000	0.086 ± 0.002	0.052 ± 0.001	0.093 ± 0.004

inside the process chamber. The different modes present with each control concept influence the interaction of the samples in the process chamber with the electromagnetic field, presumably causing differences in energy efficiency. The excitation of RFs in 1RF and 6RF was associated with a particularly high energy efficiency from 83.6% to 92.4%. The possibility of increasing energy efficiency with targeted frequency control has also been demonstrated in microwave-assisted heating [18, 19, 21, 135]. The energy efficiency, in turn, determines the specific dissipated power, which correlates with the drying rate. The same correlation of a higher drying rate with increasing dissipated power was observed in the parameter study on microwave power.

The application of frequency-based control concepts has significant effects on drying homogeneity in MFD. This is shown by previously published data [137], where a partial MFD was conducted using the experimental setup and control concepts of the present study. To complement the data already published, the residual moisture is plotted versus the sample position and the frequency-based control concept in Figure 4.9. Even though the typical patterns of residual moisture associated with thermal radiation are recognizable for all control concepts, differences can be found between the control concepts. The application of multiple frequencies instead of one frequency resulted in increased drying homogeneity at similar dissipated power, namely 1MF compared to 6EF and 1RF compared to 6RF. Puffing occurred in the experiments at 1RF exclusively, although the dissipated microwave power was lower than for 6RF. This indicates a more uniform average power dissipation over time when multiple frequencies are used. These results are consistent with the literature on microwave-assisted heating, which shows higher heating homogeneity for targeted excitation of multiple frequencies [19, 21, 135]. Frequency, hence, is the only parameter investigated that results in a substantially increased drying homogeneity.

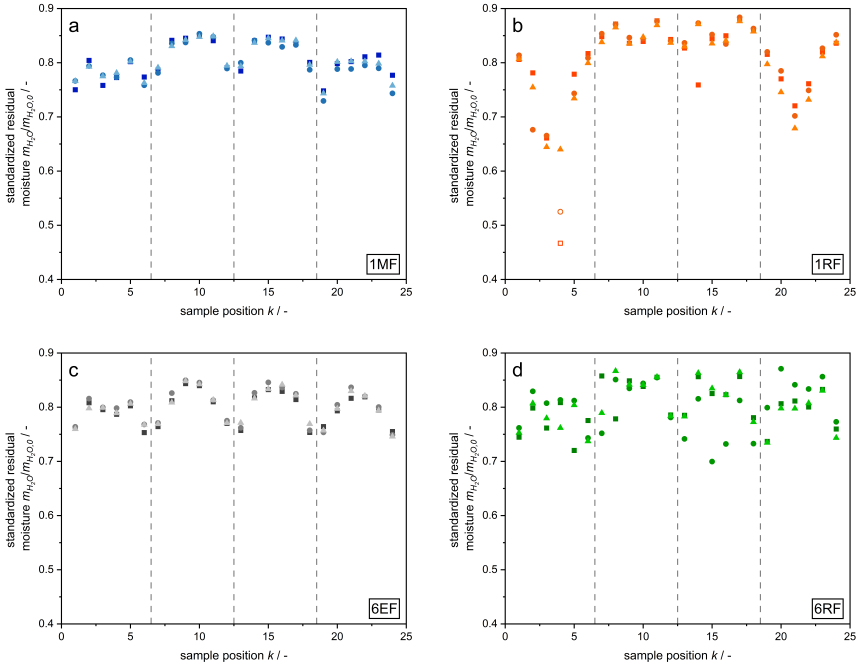

Figure 4.9: Standardized residual moisture plotted against the position of the samples for the control concepts (a) 1MF, (b) 1RF, (c) 6EF, and (d) 6RF. Blank symbols mark samples with an impaired macroscopic structure by puffing. The sample position k describes the placement of the sample in analogy to Figure 4.5 (b). Dashed lines mark the transition between rows of samples, while different shapes indicate individual experiments

4.4.3 Limitations and future work

The proposed approach of utilizing partial MFD in parameter studies enables tremendous time savings for the evaluation of process parameters like chamber pressure, microwave power, and microwave frequency regarding their influence on drying kinetics and drying homogeneity. While results from the parameter study on frequency and power are consistent with the expectations based on the literature, the results of the parameter studies on chamber pressure contradicted the expected results. Limitations of heat transfer due to low applied power or

the relatively thin dried layer that is not representative of a complete MFD are possible causes of the discrepancies, as discussed in Section 4.4.2.1.

Complete MFD would allow for the evaluation of the final product quality. This is inherently impossible for partial MFD since the samples are still partly moist. During MFD, however, the DPs of the product change significantly, causing shifts in the frequency-dependent energy efficiency and the frequency of resonant modes [137]. In the present study, modulation of frequencies during drying was omitted, since the shift of RFs during the initial part of primary drying was assumed to be negligible. During complete MFD, the applied frequencies would have to be adjusted throughout drying to ensure the excitation of desired frequencies over the whole course of drying.

Future work on partial MFD should focus on adjusting the termination criterion to investigate whether the expected results can be obtained for the influence of chamber pressure. Extending the process duration by applying a lower residual moisture content as a termination criterion, e.g., 60 wt% or 70 wt%, could be a solution. To test the universal suitability of partial MFD for parameter studies, its application to other products and parameter spaces should be investigated. In a broader context, partial drying could also be evaluated for other microwave-assisted drying processes. Additionally, complete MFD experiments with modulation of microwave frequency should be conducted to enable the evaluation of product quality. Various frequency-based control concepts should be compared since this study has shown that frequency is an influential parameter affecting drying kinetics, energy efficiency, and drying homogeneity. MFD should also be compared to CFD to ensure its competitiveness with the established process in terms of product quality and process duration.

In the present work, the forward microwave power varied considerably among experiments, as can be seen in Tables A.6 to A.9 in Section A3. A prominent example from the parameter study on microwave power is the decreasing forward power when the activation ratio increased. Presumably, this can be attributed to a temperature rise in the SSG with low pause times. This could not be prevented due to a lack of control based on the measurement of reflected power

and forward power. Recalibrations of the SSG between parameter studies are another possible cause of deviations. These inconsistencies in forward power may conceal the influence of chamber pressure and frequency in the respective parameter studies. To prevent these inconsistencies, the effects of fluctuations in average specific dissipated microwave power, which is directly linked to specific forward power, were taken into account in all experiments. For future studies, it would be desirable to achieve more equal forward power between experiments, e.g., through frequency-dependent calibration or adaptive power control. Lastly, future work should focus on using the developed framework for high-throughput experiments in MFD to optimize the process by varying multiple variables.

4.5 Conclusions

Partial MFD is suggested as an approach to a time-efficient process design by increasing the throughput of experiments in parameter studies. Experiments were terminated when 20 wt% of the initial water content was removed from the samples. This would lead to a 92.0% reduction in the process duration compared to complete MFD. As expected, partial MFD exhibited drying kinetics similar to the initial phase of complete MFD. Moreover, the early termination enabled an investigation of drying homogeneity, which could not be determined when drying the product completely. While the influence of process parameters on drying kinetics and drying homogeneity can be evaluated with the proposed approach, product quality cannot, as the samples are partly moist.

To verify the applicability of the proposed approach, parameter studies on chamber pressure, microwave power, and microwave frequency were carried out and compared to results from the literature. A reduction in process duration of 18.8% was observed with a decrease in average chamber pressure from 0.87 mbar to 0.19 mbar. The difference in process duration can be attributed to the removal of a higher mass of water before microwave application and higher drying rates during microwave application at a lower chamber pressure. The latter results are

not in line with the literature, where a decrease in drying time with chamber pressure due to a lower product temperature or no significant correlation was found. Moreover, higher microwave power up to the average specific dissipated power of 0.143 W/g led to a 46.7% shorter process duration in comparison to 0.048 W/g. A targeted adjustment of microwave frequency through control concepts had a significant influence on the process duration, reducing it by up to 51.2% in comparison to the longest process. One cause is the frequency-dependent energy efficiency, which influenced the specific dissipated power. The application of RFs exhibited the highest energy efficiencies ranging from 83.6% to 92.4%. These results for power and frequency are qualitatively consistent with the literature.

Generally, drying homogeneity was not influenced substantially by chamber pressure or microwave power, although outliers in residual moistures were observed in the parameter study on power for a specific dissipated power >0.075 W/g. The respective samples showed structural impairments presumably caused by the melting of the samples during MFD. However, drying homogeneity was increased when applying multiple frequencies at similar levels of specific dissipated power, as shown in a previous study [137].

Partial MFD produced the expected results regarding the influence of microwave properties. This underlines the general suitability of the approach proposed for investigating the influence of process parameters in a time-efficient manner. The expected influence of chamber pressure could not be observed, presumably due to low input power and limitations through mass transfer occurring during later stages of drying. Partial drying is not limited to MFD but may be applied to a wide range of drying processes. The achieved time savings could play an important role when investigating the simultaneous adaptation of multiple process parameters by using solid-state technology. Targeted adaptation of microwave frequency had the most pronounced effect on energy efficiency and could be utilized to increase drying homogeneity. For future work, selective adjustment of frequency during drying based on measurement of forward and reflected power seems to be a particularly promising approach.

5 Process intensification of microwave-assisted freeze-drying by frequency adjustment in real-time using solid-state technology

This chapter was published as:

Kaysan, T.; Zhou, X.; Gaukel, V. Process intensification of microwave-assisted freeze-drying by frequency adjustment in real-time using solid-state technology. J. Food Eng. 2024, 383, 112221, doi:10.1016/j.jfoodeng.2024.112221.

Variables, figures, and abbreviations were adapted for consistency.

5.1 Abstract

In microwave-assisted processes, solid-state microwave technology enables control of the electromagnetic field,which can be used for process intensification. This work investigates the impact of real-time frequency adjustment on microwave-assisted freeze-drying (MFD). Frequency-based control concepts were applied in experiments with tylose gel as a food model product in a laboratory-scale plant. By applying energy-efficient resonant frequencies based on feedback related to product state, the drying time was reduced by 24.2% compared to conventional freeze-drying (CFD) due to increases in energy efficiency. Comparable temperature profiles, residual moistures, and ascorbic acid retentions to CFD were achieved. However, structural degradation occurred with MFD in up to 10.4% of the samples. The degradation could be counteracted by more refined frequency and power application. In summary, this work demonstrates the high potential of frequency-based control for MFD process intensification.

5.2 Introduction

In process engineering, microwaves represent an alternative approach to energy supply, which can be used for process intensification. Contrary to convection, conduction, and thermal radiation in conventional thermal processing, the generation of heat via microwaves results from the interaction of the processed materials with an electromagnetic field [54]. The respective dielectric properties (DPs) characterize these interactions. Microwave application is associated with several advantages, such as selective heating, volumetric heating, and reduced process times [41]. In the context of food process engineering, the use of microwaves has been investigated for a variety of processes, such as freeze-drying (FD) [11, 137], vacuum drying [144, 145], heating [19, 21, 24], frying [146], and defrosting [20].

In recent years, solid-state generators (SSGs) have emerged in the context of process engineering. Literature reports their use for the generation of microwaves in various microwave-assisted processes [14, 18, 24, 27, 115, 140, 147–149].

Unlike conventionally used magnetrons, SSGs allow precise control of the electromagnetic field by modulating the microwave power, microwave frequency, and phase shift between SSGs [17]. The additional degrees of freedom in controlling the electromagnetic field can be used to optimize processes [150]. Adjusting the frequency proved to be particularly promising in this context. Applying frequency sweeps increased heating uniformity in microwave-assisted heating processes [132, 139]. More elaborate schemes of targeted frequency control, informed by preliminary experiments, resulted in increased energy efficiency [21, 24, 135] and temperature homogeneity [19, 21, 24, 135]. High energy efficiency was achieved by applying individually energy-efficient frequencies and the excitation of multiple frequencies increased temperature homogeneity. In some studies, the frequencies were intentionally selected based on the corresponding heating pattern so that hot and cold spots would compensate each other during processing [21, 135]. A trade-off between energy efficiency and temperature homogeneity was found when modulating the electromagnetic field [21, 115]. Only one of the two parameters could be maximized. Some authors suggest control concepts to achieve a high performance regarding both parameters [21, 24]. All of these control concepts for frequency are determined before the start of the experiment. Therefore, the applied frequencies are not affected by any real-time feedback related to the product state.

The mentioned control concepts are limited in their applicability to processes where the product state undergoes significant changes over time, arising from the substantial effort required to base control concepts for these processes solely on prior experiments. The changes in product state occur mandatorily in microwave-assisted processes where phase transitions are an explicit goal, such as drying, defrosting, or pyrolysis. In these processes, a shift of frequencies with a local maximum in energy efficiency, so-called resonant frequencies (RFs), over process time was observed in monomodal cavities [27, 148]. These shifts were associated with changes in product state, presumably correlated with changing DPs. Simulation-based preliminary work on microwave-assisted freeze-drying (MFD) in a multimodal cavity showed that multiple RFs shifted to higher frequencies [137]. It is considered possible to increase both energy efficiency and power

input homogeneity in MFD by applying multiple RFs, as it has been shown for microwave-assisted heating. The shifts in RFs, however, pose a challenge to their application throughout MFD, as frequency adjustment is required as a function of the product state. As far as the authors know, there has been no study of process control using frequency adjustment of RFs during the thermodynamically complex process of MFD based on real-time feedback related to product state. The approach would allow for targeted frequency adaption despite the substantial changes in product state. This extends the applicability of the approach to various processes and products without requiring excessive prior experiments.

This work investigates the effects of real-time frequency adjustment on the MFD process and selected product properties. The applied frequency-based control concepts are based on feedback related to the product state. The results are compared to conventional freeze-drying (CFD) as a benchmark. The experiments are conducted in a laboratory-scale dryer with tylose gel acting as a food model product. In MFD, microwave control is implemented using algorithms that adjust the microwave frequency based on product state. While focussing on control concepts with frequency adjustment during drying, control concepts with constant frequencies are also investigated as benchmarks. Targeted frequency adjustment is expected to increase energy efficiency throughout MFD, as shown for microwave-assisted heating. The resulting higher dissipated power may lead to an increase in product temperature and drying rate. Regarding product properties, there should be no discernible effect on residual moisture, provided that the termination criteria are selected appropriately for complete drying. Higher product temperature could lead to a decrease in thermally unstable compounds. Higher dissipated microwave power above a threshold is expected to cause more macroscopic impairment of the product, as observed in previous work for the initial stage of MFD [150].

5.3 Materials and methods

5.3.1 Model product

Tylose gel cuboids with ascorbic acid (AA) as a tracer substance served as a food model product. The sample preparation was identical to the procedure described in a previous paper [137]. In brief, tylose gel composed of 76.23 wt% demineralized water, 23.77 wt% tylose MH1000 (Kremer Pigmente, Aichstetten, Germany), and 1.00 wt% L-(+)-AA (Carl Roth, Karlsruhe, Germany) was produced. Then, cuboids of tylose gel were molded in dimensions of around 25 mm × 25 mm × 10 mm with a weight of 12.50 ± 0.05 g each and frozen at -30 °C for a minimum of 14 h.

5.3.2 Freeze-drying system

Figure 5.1 shows a schematic view of the laboratory-scale FD system and a depiction of the process chamber. The stainless steel process chamber had inner dimensions of 612 mm × 400 mm × 300 mm. A custom-made cold trap (UCCT, Vienna, Austria) and a NEO D 65 vacuum pump (Leybold, Cologne, Germany) were connected in series to the process chamber. The cold trap temperature and the chamber pressure were set to -60 °C and 0.5 mbar in all experiments. An HY2020 SSG (TRUMPF, Freiburg, Germany) was connected via a coaxial cable to a waveguide port centrally embedded in the top of the process chamber. The SSG could generate microwaves of up to 600 W in power and frequencies from 2400 MHz to 2500 MHz at intervals of 0.01 MHz. Based on qualitatively validated electromagnetic simulations, we inferred a relatively uniform distribution of the power associated with the dissipation of the electromagnetic field among the tylose samples, particularly when multiple frequencies are applied [137]. For CFD, a custom-built modular heat exchanger was placed in the process chamber as a product support. An AC200 thermostat (Thermo Fisher Scientific, Henningsdorf, Germany) could be set to -5 °C to 70 °C to regulate shelf temperature. The sensors used were a CMR363 capacitive pressure sensor (Pfeiffer, Aßlar, Germany), three

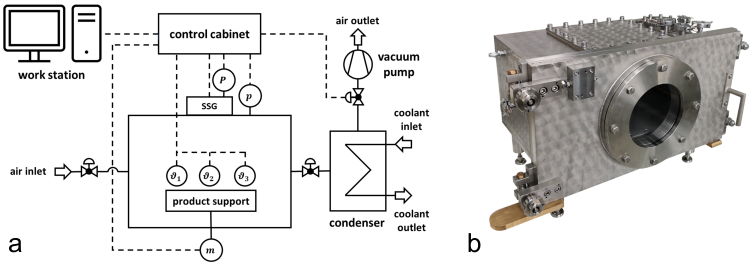

Figure 5.1: (a) Schematic representation of the laboratory-scale MFD setup. m – load cell, P – sensor microwave power, p_C – capacitive pressure sensor, ϑ_i – fiber optic temperature sensors. (b) Process chamber with no peripheral devices connected.

FOS-TG fiber optic temperature sensors (Rugged Monitoring, Quebec, Canada), and a PW4MC3/2 kg load cell (Hottinger Brüel & Kjaer, Darmstadt, Germany). Moreover, the internal sensors of the SSG for forward power and reflected power were used. The PW4MC3/2 kg load cell was connected to a product support made of polyether ether ketone, which was placed centrally at the bottom of the process chamber and could be used for MFD only. Scripts in Matlab 2020b (MathWorks, Natick, USA) were used to store the recorded process parameters and control the power and frequency of the microwaves throughout drying.

Calibration was performed for all sensors. FOS-TG sensors underwent three-point calibrations using a Pt-25 platinum resistance thermometer MKT25 (Rosemount, Shakopee, USA). The PW4MC3/2 kg load cell was calibrated using calibration weights, covering product weights up to 300 g. The SSG and the CMR363 pressure sensor were acquired in a calibrated state during the construction of the system.

5.3.3 Process characterization

Process characterization of MFD was conducted to determine the initial RFs. RFs are defined here as the frequencies with a local maximum in energy efficiency. Twenty-four frozen cuboids of tylose gel were placed centrally on the product support with a spacing of 5 mm, as depicted in Figure 5.2. Fiber optic temperature

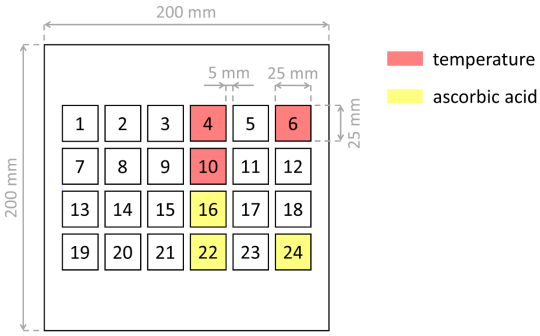

Figure 5.2: Placement of samples on product support for MFD. Samples equipped with fiber optic temperature sensors are marked in red and samples for determination of ascorbic acid content are marked in yellow. The samples in the bottom row are adjacent to the front door of the process chamber. The samples were placed centrally on the heat exchanger in the same arrangement for CFD.

sensors were positioned centrally in samples 4, 6, and 10, in which holes were drilled during sample preparation. Subsequently, the process chamber was sealed airtight and the valve to the vacuum pump was opened. The application of microwaves started 10 min after the vacuum application. A frequency sweep in the range of 2400 MHz to 2500 MHz was performed with an interval of 0.1 MHz and the minimally feasible set forward power of 50 W. From the reflected power Pr and forward power Pf monitored by the SSG, the energy efficiency η was calculated by $\eta = 1 - P_r/P_f$. The results of an exemplary frequency sweep are shown on the left in Figure 5.3. All process characterizations were repeated three times. The final RFs were calculated as the arithmetic means of the three RFs obtained.

5.3.4 Drying procedure

For MFD, the starting procedure and the placement of samples were identical to the process characterization described in Section 5.3.3. The application of microwaves marked the start of the process time. The process specifications set

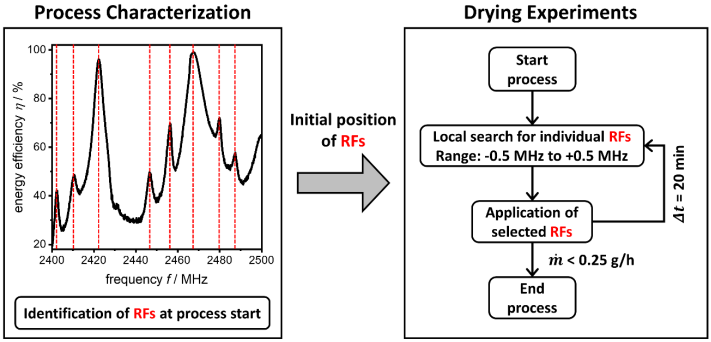

Figure 5.3: Flowchart of frequency adjustment during MFD experiments in the context of process characterization.

for all experiments were a forward power of 50 W and an activation ratio of 0.5. The latter describes the time ratio the SSG was active when applying each frequency for 10 s. When multiple frequencies were used, the frequencies were applied in a loop in ascending order. The following frequency-based control concepts were investigated.

- Single Constant Frequency (1CF) – constant frequency of 2420 MHz,
- Six Equidistant Frequencies (6EF) – six constant frequencies from 2400 MHz to 2500 MHz in an interval of 20 MHz,
- Six Minimum Resonant Frequencies ($6RF_{min}$) – six RFs displaying the lowest energy efficiencies, purposefully adjusted during MFD, and
- Six Maximum Resonant Frequencies ($6RF_{max}$) – six RFs displaying the highest energy efficiencies, purposefully adjusted during MFD.

The primary focus of the investigations was on the control concepts $6RF_{min}$ and $6RF_{max}$, which implemented real-time modulation of the microwave frequency

based on the product state. Previous electromagnetic simulations have demonstrated the potential benefits of similar control concepts based on applying multiple RFs [137]. The remaining control concepts, 1CF and 6EF, maintained constant frequencies throughout the drying process, allowing comparisons with benchmark processes. Specifically, 6EF was selected for its equivalence in the number of applied frequencies to $6RF_{min}$ and $6RF_{max}$, while 1CF represents the most straightforward application of microwave frequency. Furthermore, the substantial difference in energy efficiency between $6RF_{min}$ and $6RF_{max}$ enabled the assessment of the impact on energy efficiency or dissipated power within the control concepts employing real-time frequency modulation. MFD was terminated when the drying rate $\dot{m}$ was less than 0.25 g/h, calculated over 1 h.

The specifications for CFD were established in preliminary experiments using the criteria of complete and fast drying without compromising product quality. The thermostat temperature was initially set to -5 °C as the minimally viable temperature to prevent the melting of the samples due to contact with the hot shelf. The samples were placed centrally on the heat exchanger with the sample and temperature sensor positions shown in Figure 5.2. Following a vacuum application for 10 min, the thermostat was set to 70 °C, indicating the start of the process time. When all temperature sensors reached a temperature difference of less than 2 K/h over 20 min, the process was extended by 20% of the current process duration before termination. All drying experiments were conducted at least in duplicate.

5.3.5 Control algorithm frequency

The applied frequency-based control concepts can be subdivided into control concepts with constant frequencies, 1CF and 6EF, and concepts with frequency adjustment throughout drying, $6RF_{min}$ and $6RF_{max}$. An approach to real-time frequency adjustment was developed for $6RF_{min}$ and $6RF_{max}$ to enable the frequent update of RFs throughout drying in a time-saving manner. The concept is based on the shift of RFs to higher frequencies during MFD [137] and is depicted

schematically in Figure 5.3. The initial RFs, as determined in process characterization, were provided as inputs to the control algorithm. At the beginning of the process, the frequency range around all RFs was screened locally for maximum energy efficiency. The range was -0.5 MHz to +0.5 MHz around each RF at an interval of 0.1 MHz. The frequencies of maximum energy efficiency were stored as the new RFs. Subsequently, the most recent RFs were selected for the drying process. The six RFs with the lowest energy efficiency were applied for the control concept $6RF_{min}$, while the six RFs with the highest energy efficiency were used for $6RF_{max}$. Every 20 min, the screening and application of updated RFs were repeated analogously to the beginning of the process.

5.3.6 Sample analysis

5.3.6.1 Structure

An X-ray microscope Xradia 520 Versa (Carl Zeiss, Oberkochen, Germany) was employed to visualize the sample structure in μ-CT. Details on the microscope, the schematic experimental setup, and the principles of μ-CT can be found in the literature [151]. Exemplary specimens of intact and impaired samples were placed on the sample holder. For image capture, the imaging mode was set to tomography, the optical magnification to 0.4, the exposure time to 1 s, and the binning to 1. The source settings for voltage and power were 80 kV and 2 W, respectively.

5.3.6.2 Residual moisture

The weights of the samples after drying m_{FD} were determined using a balance type 1518 (Sartorius, Göttingen, Germany). Following FD, the samples were cut in half and examined for macroscopic structural impairment. Samples 16, 22, and 24 were set aside for later determination of AA retention. The remaining samples were placed in a T6060 drying oven (Heraeus, Hanau, Germany) at 105 °C for

at least 24 h. Subsequently, the samples were weighed using an LS 220A SCS precision balance (Precisa, Dietikon, Switzerland). The respective weight was used as the dry mass m_{dry} to calculate the dry basis residual moisture X_{res} with $X_{res} = (m_{MFD} - m_{dry})/m_{dry}$.

5.3.6.3 Ascorbic acid retention

Analysis of AA retention was performed according to [152]. For this purpose, samples 16, 22, and 24 were ground using a coffee grinder M 55 (Petra Deutschland, Ense, Germany) and then classified with a sieve into particles smaller than 1 mm. A Precisa LS 220A SCS precision balance was used to weigh a sample mass corresponding to 0.013 g AA in the undried state. The weighed sample was mixed with 50 mL of double-distilled water and stirred for 30 min at 200 rpm using a PC-420D magnetic stirrer (Corning, Corning, USA). The resulting suspension was homogenized with an ULTRA-TURRAX T 25 (IKA-Werke, Staufen im Breisgau, Germany) using an S 25 N - 18 G dispersing tool (IKA-Werke, Staufen im Breisgau, Germany) at 5000 rpm for 2 min. Subsequently, 2 mL of a 1 wt% starch solution (Carl Roth, Karlsruhe, Germany), 2 mL of a 2-M potassium iodide solution (Carl Roth, Karlsruhe, Germany), and 6 mL of 1-M sulfuric acid were added. The mixture was stirred at 280 rpm with a magnetic stirrer, while a 0.001-M potassium iodate solution (Carl Roth, Karlsruhe, Germany) was titrated dropwise until the equivalence point was reached. This was reflected by a color change of the liquid to red-violet. The titration volume was converted into the corresponding mass m_{AA} and retention $m_{AA}/m_{AA,0}$ of AA using the equation $m_{AA} = 3V_{IO_3^-} c_{IO_3^-} \tilde{M}_{AA}$. Here, $V_{IO_3^-}$ and $c_{IO_3^-}$ are the volume and molar concentration of the iodate solution, while $\tilde{M}_{AA}$ is the molar mass of AA. The initial mass of AA $m_{AA,0}$ was calculated from the mass of the weighed sample and the composition of the tylose gel. Since the potassium iodide solution is sensitive to light, it had to be prepared immediately before the experiment and then shielded from light. The determination was done in triplicate for each sample.

5.4 Results and discussion

5.4.1 Influence of frequency control on MFD

5.4.1.1 Energy

Targeted frequency application in microwave-assisted heating increased energy efficiency, resulting in a higher average product temperature [24]. For the initial stage of MFD, targeted frequency application was linked to increased energy efficiency [150]. Figure 5.4 (a) shows the energy efficiency as a function of time to evaluate the transferability of these results to complete MFD. In all experiments, energy efficiency tended to decrease during drying. Applying $6RF_{max}$ and $6RF_{min}$ yielded the highest energy efficiencies throughout drying, averaging 64.63% and 43.62%, respectively. The 6EF and 1CF control concepts followed in descending order with 40.12% and 37.49%, respectively. Targeted application of frequencies by real-time adjustment throughout MFD with $6RF_{max}$ led to an absolute increase in energy efficiency of 24.51% compared to 6EF. With 6EF, the same number of frequencies was applied but kept constant throughout drying.

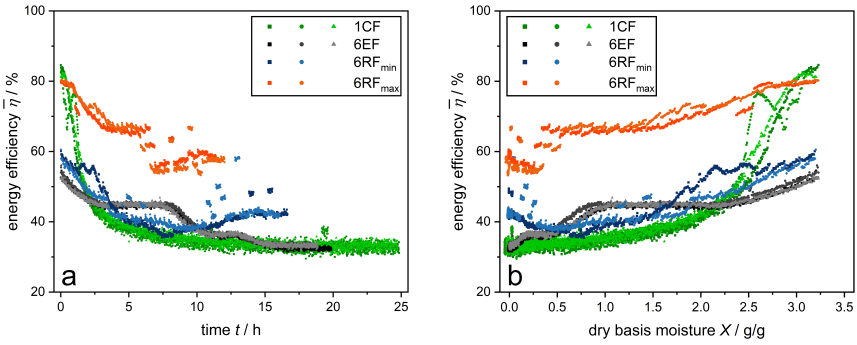

Figure 5.4: (a) Energy efficiency as a function of process time for the applied control concepts in MFD. (b) Energy efficiency as a function of dry basis moisture. The energy efficiency of the frequency loops in 6EF, $6RF_{min}$, and $6RF_{max}$ was calculated as the average of the individual frequencies.

Periodic jumps in energy efficiency occurred for the control concepts with frequency adjustment, $6RF_{min}$ and $6RF_{max}$. The jumps occurred at intervals of 20 min, immediately after the search for RFs. While relatively small jumps are probably caused by slight frequency adjustments, more pronounced jumps are related to applying a modified set of RFs. The latter occurred when local maxima in energy efficiency were lost or redetected around previously applied RFs. The replacement of previously applied RFs with different RFs of notably higher or lower energy efficiency presumably led to the more pronounced jumps in energy efficiency.

Figure 5.4 (b) shows the average energy efficiency as a function of dry basis moisture to emphasize the dependence of energy efficiency on product state. Using $6RF_{max}$ generally resulted in the highest energy efficiency throughout MFD, particularly at a moisture content of less than 2.5 g/g. On the other hand, the overall energy efficiency reached by $6RF_{min}$ was similar to those of control concepts without frequency adjustment.

A comparison of $6RF_{max}$ and $6RF_{min}$ shows that RF application can adjust the energy efficiency over a wide range throughout the drying process. This is particularly advantageous at low moisture content towards the end of drying. At this stage, energy efficiency is lowest when constant frequencies are used in 1CF and 6EF. The particularly low energy efficiency is probably due to the low DPs of the dried tylose gel compared to the frozen state [137]. The flexible solid-state technology may be used in further fine-tuning to adjust the energy efficiency between the values of $6RF_{min}$ and $6RF_{max}$ intentionally using different combinations of RFs. For example, using the highest possible number of RFs may result in a highly uniform drying process. Further increases in energy efficiency are also possible by higher weighting of highly energy-efficient RFs via a more prolonged activation of these frequencies.

Compared to the average energy efficiency of 43.6% of MFD with $6RF_{min}$, the process with 6EF reached a similar value of 40.1%. This corresponds to a relative deviation of 8.7%. Process duration varied between 16.32 h for the $6RF_{min}$ process and 18.97 h for the 6EF process, corresponding to a deviation

of 14.0% (see Section 5.4.1.3). This discrepancy can be explained partly by varying forward powers at different frequencies since multiplying forward power by energy efficiency gives the dissipated power. Literature shows the correlation of the dissipated power with the heating power in microwave-assisted heating [153] and with the drying kinetics in MFD [150]. Unfortunately, the SSG used delivered a frequency-dependent forward power, contributing to different power dissipation in the experiments. Figure 5.5 shows the dissipated power nominated to the sample weight at the start of MFD in dependence on process time. The differences in the relative positions among the experiments between Figures 5.5 and 5.4 (a) can be attributed to variations in forward power during the experiments. Aside from energy efficiency, forward power is the sole parameter influencing dissipated power (see Section 5.3.3).

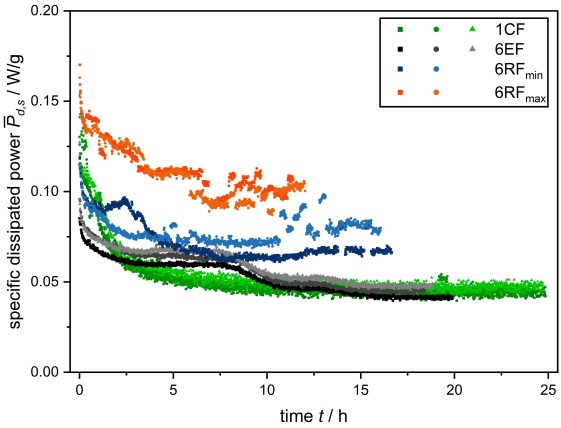

Figure 5.5: Dissipated power standardized to the sample mass at the start of MFD as a function of process time for the applied control concepts in MFD. The specific dissipated power of the frequency loops in 6EF, 6RF$_{min}$, and 6RF$_{max}$ was calculated as the average of the individual frequencies.

To further investigate the interactions among microwave parameters, Table 5.1 lists the average specific forward power, average energy efficiency, and average specific dissipated power for all experiments. Both specific dissipated power and energy efficiency vary for the control concepts. The specific forward power is comparable

Table 5.1: Average values of the microwave-related process parameters of all MFD experiments. The parameters were averaged over all frequencies and the entire process time.

Control Concept	**Average Specific Forward Power $P_{f,s,proc}$ / W/g**	**Average Energy Efficiency η_{proc} / %**	**Average Specific Dissipated Power $P_{f,s,proc}$ / W/g**
1CF	0.135; 0.137; 0.143	37.1; 37.6; 37.7	0.050; 0.052; 0.054
6EF	0.126; 0.133; 0.140	39.6; 40.8; 40.1	0.052; 0.057; 0.059
$6RF_{min}$	0.173; 0.188	43.3; 44.0	0.073; 0.079
$6RF_{max}$	0.181; 0.180	64.9; 64.3	0.112; 0.109

between 1CF and 6EF and between $6RF_{min}$ and $6RF_{max}$. Consequently, the difference in forward power must be considered when analyzing the impact on the process, especially when comparing the two groups of adjusted and non-adjusted control concepts. For instance, the different process durations of $6RF_{min}$ and 6EF at similar energy efficiency are caused by differences in the forward power. Despite these limitations, the apparent difference in energy efficiency between $6RF_{max}$ and the remaining control concepts reveals that microwave frequency influences the conversion of electromagnetic energy into heat, thereby affecting the drying process.

5.4.1.2 Sample temperature

Higher dissipated microwave power is expected to lead to increased temperatures of the samples. Figure 5.6 shows the temperature of sample 6 in the corner of the arrangement (see Figure 5.2) as a function of process time. Sample 6 was chosen, as this sample reached the highest temperature of samples 4, 6, and 10, as depicted in Figure A.8 in the Appendix. The presumable cause is thermal radiation from the walls of the process chamber, as was indicated in previous work [150]. Only one experiment of each process is shown for the sake of clarity. Figure A.9 in the Appendix shows the reproducibility of the temperature curves. The samples in CFD showed the most considerable deviations among

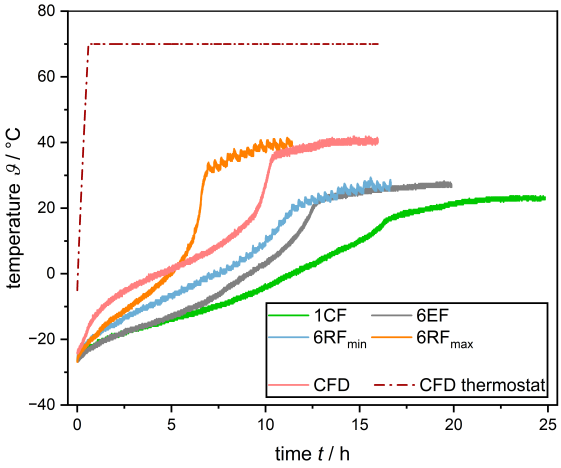

Figure 5.6: Temperature of sample 6 as a function of process time for MFD and CFD experiments. One experiment is shown for each process. The solid lines mark the temperatures measured inside the samples. The dash-dotted line marks the thermostat temperature in CFD.

experimental repetitions, presumably due to the varying contact area between the slightly uneven samples and the heat exchanger. The temperature curves are typical for MFD [11, 14]. The temperature initially increases relatively quickly as soon as microwave power is applied. A phase of slowly increasing temperature follows due to the energy required to supply the latent enthalpy of sublimation. After that, the rate of temperature change increases, as the decreasing sublimation requires less energy before the dry samples reach an equilibrium temperature. In this state, the dissipated microwave power and heat losses due to thermal radiation and conduction are approximately equivalent.

Periodic temperature jumps were observed when the frequencies were adjusted in 6RF$_{min}$ or 6RF$_{max}$, mirroring the observed jumps in energy efficiency. Therefore, the increase in energy efficiency led to a higher power loss inside the samples. The power was not just dissipated elsewhere, e.g., in the coaxial cable or as wall losses.

The dissipated power, standardized to the mass of the samples at the start of MFD and averaged over the respective experiments, increases in the order of 1CF,

6EF, $6RF_{min}$, and $6RF_{max}$ and amounts to 0.052 W/g, 0.056 W/g, 0.076 W/g, and 0.111 W/g, respectively. Following expectations, higher specific power dissipation correlated with higher product temperature throughout MFD, as shown in Figure 5.6. The maximum sample temperatures of all MFD experiments were 23.7 °C, 29.0 °C, 33.6 °C, and 43.8 °C for 1CF, 6EF, $6RF_{min}$, and $6RF_{max}$, respectively. Hence, maximum temperature is also correlated with specific dissipated power. However, the maximum temperature occurred in the final phase of MFD in all experiments. Therefore, it is expected only to be influenced by the power dissipation at this stage. The maximum temperature for CFD was 44.0 °C, slightly higher than the 43.8 °C for MFD with $6RF_{max}$. Thus, heat-sensitive products can be treated with both CFD and MFD due to a similar temperature stress. Final drying at lower temperatures becomes feasible when the specific dissipated power is reduced at this stage, as evidenced by the behavior observed with the other MFD control concepts.

5.4.1.3 Drying kinetics

An increase in power dissipation is expected to result in higher drying rates during MFD, as observed for its initial stage [150]. The assumption underlying this dependence is that the process is at least partly limited by heat transfer. Figure 5.7 illustrates the drying rate normalized to the dry mass of the samples over time. All kinetics show the highest drying rate in the initial stages, followed by a decline over process time. This drying kinetics behavior is qualitatively consistent with the MFD of banana slices [92] and lactic acid bacteria [11].

As expected, $6RF_{max}$ shows the highest drying rates, as it is the process with the highest average specific dissipated power (see Table 5.1). The dotted lines in Figure 5.7 indicate the process duration at which MFD and CFD termination criteria were met. Completion of CFD took 15.41 h on average. The only MFD process with a shorter duration was $6RF_{max}$ at 11.68 h. 1CF, 6EF, and $6RF_{min}$ resulted in longer durations of 24.47 h, 18.97 h, and 16.32 h, respectively. Consequently, $6RF_{max}$ reduced process time by 24.2% compared to CFD and 38.4% compared to 6EF, where the same number of frequencies was applied

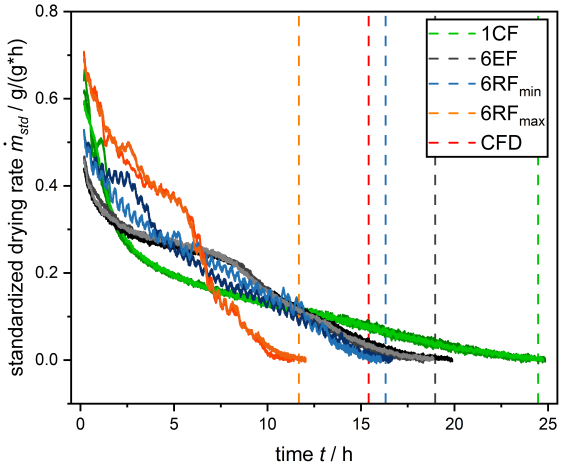

Figure 5.7: Drying rate standardized to the dry mass of the samples as a function of the process time of MFD for the applied frequency-based control concepts. Dashed lines mark the average duration of the drying process for MFD and CFD, while solid lines in the corresponding colors show the respective drying kinetics.

but kept constant throughout drying. Thus, MFD was successfully intensified via frequency modulation to reach drying times below the benchmark process of CFD.

The periodic jumps in drying rate for 6RF$_{max}$ and 6RF$_{min}$ indicate that the increased energy efficiency with each frequency adjustment directly translated into an increase in mass transfer. The relationship between energy efficiency, product temperature, and drying rate based on the reoccurring fluctuations of all three parameters with frequency adjustment every 20 min is apparent. In the literature, higher sample temperatures in MFD can also be associated with a higher drying rate [11].

5.4.2 Influence of frequency control on product properties

5.4.2.1 Structure

Previous work on partial MFD revealed structural impairments in some samples [150]. Complete MFD in this work led to the same effect in several samples. Figure 5.8 (a) shows tomographic images of exemplary samples with and without structural impairment. In the following, these are referred to as intact and puffed. The term puffed in this context refers to the inner structure of the samples. The sample volume is not influenced by puffing. The intact sample shows the typical lamellar structure of a freeze-dried product, as detected in carrots [154]. The same lamellar structure is visible in the outer layer of the puffed sample. In contrast, the interior of the puffed sample is characterized by relatively large pores with optically dense structures in between, typical of puffed products, e.g., puffed rice [155]. Figure 5.8 (b) displays a 3D segment of the puffed sample, illustrating the structural variances within the sample.

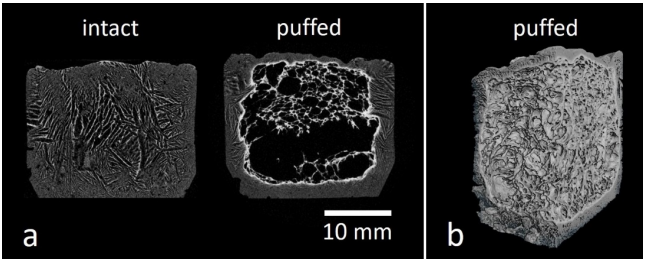

Figure 5.8: (a) Tomographic images of dried tylose gel samples in the intact and puffed state. (b) Segment from the 3D reconstruction of a puffed tylose gel sample.

The puffed structure is probably caused by the melting of frozen water in individual samples due to high dissipated microwave power during MFD. The emergence of liquid water leads to even higher dissipated power in the samples since it has relatively high DPs compared to ice. This effect is reflected by the jump in energy efficiency during one MFD experiment with 1CF at a moisture content of about

2.5 g/g, possibly due to a melted sample (see Figure 5.4 (b)). Accordingly, the drying rate in this experiment increased (see Figure 5.7) and puffing with 1CF occurred only in this experiment. The resulting increase in vapor pressure inside the sample probably caused the formation of the large pores. The same principle of sudden evaporation and expansion of water inside the material is used in explosion puffing drying, which results in a similar structure [156]. In the present work, the freeze-dried outer layer was too rigid to be affected by the pressure gradient. Consequently, the volume was not increased. Only the structure of the inner thawed layer was affected before the vapor could escape and drying progressed.

The ratios of puffed samples from CFD and MFD are shown in Table 5.2. There was no puffing in CFD, whereas puffing occurred in at least one MFD experiment for each control concept. Drying with $6RF_{max}$ resulted in the highest average puffed sample ratio of 10.4%, with puffing occurring in every experiment. The results are consistent with the proposed mechanism for puffing, as $6RF_{max}$ also exhibits the highest average dissipated specific power (see Table 5.1). The puffing of the samples was reduced when RFs with lower energy efficiency were applied in $6RF_{min}$. Puffing may also be reduced by varying the weights of individual frequencies applied or reducing the microwave power. However, these measures are likely to involve trade-offs regarding process performance.

Table 5.2: Ratio and average ratio of puffed samples of all FD experiments. One occurrence of puffing in 24 samples corresponds to a puffed sample ratio of approximately 4.2%.

Process	**CFD**	**MFD 1CF**	**MFD 6EF**	**MFD $6RF_{min}$**	**MFD $6RF_{max}$**
Puffed Sample Ratio y / %	0.0; 0.0; 0.0	0.0; 8.3; 0.0	0.0; 4.2; 0.0	8.3; 4.2	12.5; 8.3
Average Puffed Sample Ratio $\bar{y}$ / %	0.0	2.8	1.4	4.2	10.4

5.4.2.2 Residual moisture

If similar air humidity is assumed, all samples should have similar residual moisture content after drying. Figure 5.9 provides an overview of the dry basis residual moisture for the individual samples from all FD processes. The residual moisture of all samples is below 0.020 g/g except for one sample from 6EF, in which moisture is 0.029 g/g. The residual moisture ranges without statistical outliers are relatively similar for all processes, ranging from 0.005 g/g to 0.012 g/g with $6RF_{max}$ up to 0.004 g/g to 0.018 g/g with 1CF. The overlaps in the ranges of all processes indicate similar product stabilities for samples processed with CFD and MFD. The obtained values of residual moisture are comparable to those in the literature. These are dry basis residual moistures for CFD of strawberries of minimally 0.00 g/g to 0.01 g/g [3], around 0.05 g/g for MFD of apple chips [136], approximately 0.005 g/g to 0.025 g/g for MFD of various pharmaceutical model formulations [14], and the targeted value of 0.048 g/g for starter cultures [11].

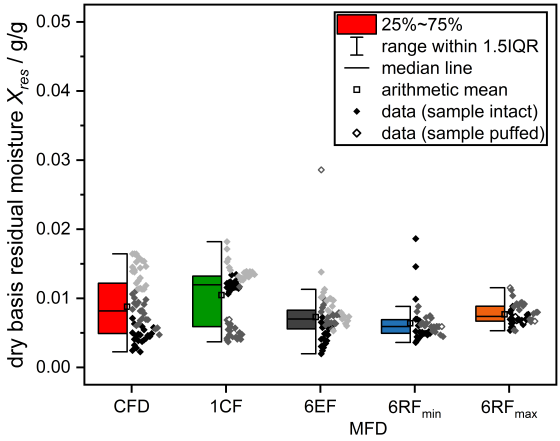

Figure 5.9: Dry basis residual moisture of samples from CFD and MFD with the applied control concepts. The samples of each experiment within the various processes are shown in a different shade of gray.

Even though there are no notable differences in residual moisture among the control concepts, there seem to be deviations between the experiments for individual control concepts. These deviations are particularly apparent for 1CF, where the residual moistures of two experiments are clustered around 0.013 g/g and the residual moistures of the third experiment are clustered around 0.005 g/g. The accumulations might be caused by air humidity fluctuations or puffing in the experiment with lower residual moisture. However, the residual moisture of puffed samples did not systematically deviate from the values of intact samples, as observed in the samples from $6RF_{max}$. Only one puffed sample at 6EF shows a much higher residual moisture than its intact counterparts.

5.4.2.3 Ascorbic acid retention

Higher product temperature could decrease AA content, as AA is a typical heat-sensitive nutrient [157]. Figure 5.10 depicts the AA retention in samples 16, 22, and 24 of all drying processes. All AA retentions of MFD are in the range of 86.4% to 99.3%, with most values lying above 90%. CFD shows an AA retention of 88.1% to 94.8%. The ranges of the MFD processes overlap with the CFD range. The only exception is the control concept 1CF, which shows a higher retention of 96.0% to 98.1%. Thus, all MFD processes exhibit high AA retention, comparable to or higher than the retention with CFD. The scattering of AA retention seems to be higher in the individual experimental setups of MFD and CFD than among them. The expected correlation of lower AA retention with higher product temperature was not observed. The detected AA retentions are in a range similar to the values in the literature. AA retentions of approximately 65% to 85% were observed for CFD and MFD of foamed raspberry puree with different formulations at microwave power levels from 1.0 W/g to 2.0 W/g at 0.1 mbar and 30 °C maximum product temperature [12]. Unblanched potato slices dried at 1.0 mbar showed AA retentions of about 92.5% for CFD at a shelf temperature of 55 °C and 94.4% for MFD with a microwave power of 1.6 W/g [107]. In contrast, CFD with a maximum product temperature of 55 °C had a notably higher AA retention of 80.3% than the 43.7% observed for MFD with

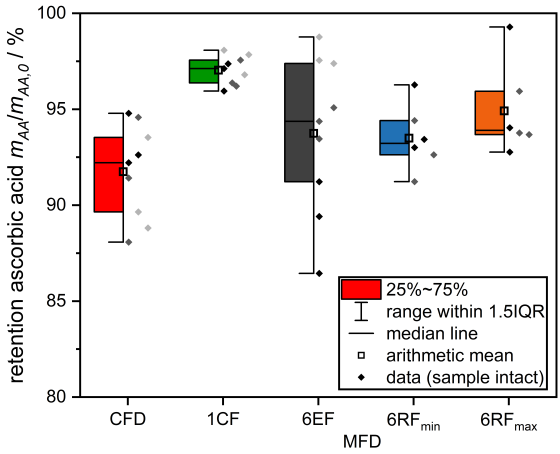

Figure 5.10: Ascorbic acid retention of samples 16, 22, and 24 from the conducted experiments in MFD and CFD. The samples of each experiment within the various processes are shown in a different shade of gray.

2 W/g, both at 1.0 mbar [158]. These results indicate local overheating during MFD, as observed for foamed raspberry puree at 2 W/g microwave power [12].

Regarding the degradation pathway, AA can react reversibly with oxygen to dehydroascorbic acid, which degrades irreversibly to 2,3-diketogulonic acid, followed by further degradation [159]. An investigation of the effect of oxygen concentration on the degradation kinetics of AA in malate buffer revealed no influence at temperatures of 50 °C and 60 °C [160]. At temperatures of 70 °C to 90 °C, however, higher degradation rates were detected with increasing oxygen concentration. These results underline the product-friendly nature of all FD processes investigated with a product temperature below 44.0 °C (compare Section 5.4.1.2) and the exclusion of oxygen at 0.5 mbar.

5.4.3 Limitations and future work

The forward power of the SSG was, unfortunately, frequency-dependent. As a result, the forward power could not be kept constant among the control concepts.

The variations in forward power were corrected by considering the dissipated power. In future experiments, the forward power should be controlled precisely via a feedback control based on the power emitted to enable direct comparison of all experiments. An additional limitation is the application of different termination criteria for MFD and CFD. While the termination criterion of MFD is based on the weight of the samples, CFD is terminated when all samples have reached their temperature plateau. The solution would be to apply the same termination criterion to both processes, e.g., by means of a comparative pressure measurement [96]. Note that the temperature measured inside the samples is not the sublimation temperature because a dried layer forms between the fiber optic temperature sensor and the sublimation front during MFD. To evaluate the temperature stresses in more detail, the literature suggests combining the use of marker substances with thermal imaging [72].

Regarding product analysis, it must be noted that handling the hygroscopic samples at varying humidity could have influenced the residual moisture. Additionally, the equivalence points for AA retention were detected by visual perception rather than by more precise automated methods and the experimental procedure lasted several hours, which may have caused degradation of AA during the measurements.

Process control strategies based on the control concepts investigated should be transferred to industry-relevant products in future work. The most promising control strategy seems to be the application of RFs with real-time adjustment. In preliminary MFD experiments with potatoes, puffing did not occur under process conditions similar to those in this work. These results suggest that tylose gel might be especially prone to puffing due to the rigid outer layer formed during MFD. Moreover, the investigated control concepts could be refined to shorten the process time or prevent puffing. This might be achieved by using more elaborate algorithms, such as genetic algorithms, or the combination with additional sensor data, like a frequency control based on the recorded product temperature or weight. Future work could also involve incorporating multiple SSGs in the MFD system, enabling the investigation of microwave application with a phase shift or simultaneous use of multiple frequencies. Scaling up MFD is another interesting line of work to investigate its competitiveness with CFD and

tackle a major challenge to its industrial application. Additionally, hybrid FD, where energy input from microwaves is combined with conventional heat transfer, could be explored experimentally. This combination could lead to synergistic effects between rapid microwave heating and compensatory thermal heat transfer that cools the samples when their temperature rises above the shelf temperature. Lastly, the underlying control strategies could be transferred to other microwave-assisted processes like heating or defrosting.

5.5 Conclusions

The present work demonstrates the advantages of frequency adjustment during drying for MFD based on feedback related to product state. The application of multiple energy-efficient RFs in the $6RF_{max}$ control concept resulted in an average energy efficiency of the conversion of electromagnetic energy into heat of 64.63%, which was an increase by an absolute value of 24.51% compared to the application of constant frequencies with 6EF. The highest temperature recorded among all MFD experiments, at 43.8 °C, was comparable to the maximum temperature of 44.0 °C in CFD. The specific forward power in the MFD experiments was frequency-dependent. Therefore, it varied among the control concepts. Nevertheless, the maximum energy efficiency for $6RF_{max}$ corresponded to the highest average specific dissipated power and, consequently, to the highest drying rate. These process conditions caused a process duration of 11.68 h for MFD with $6RF_{max}$, a reduction of 24.2% compared to CFD and 38.4% compared to MFD with 6EF. The effects of frequency adjustment on energy efficiency, product temperature, and drying rate were reflected by fluctuations of the parameters when RFs were adjusted every 20 min.

Similar residual moisture contents and AA retentions compared to CFD were obtained with all MFD control concepts. The product properties fell within the typical range observed for FD of food products, with dry basis residual moisture ranging from 0.002 g/g to 0.029 g/g and AA retention ranging from 86.4% to 99.3%. Structural impairment due to puffing was observed for MFD with all

control concepts and affected up to 10.4% of the samples. The number of puffed samples could be reduced by applying frequencies with lower energy efficiency or reducing microwave power. In contrast, no puffing occurred during CFD.

6 General discussion and outlook

This thesis aimed to investigate microwave-assisted freeze-drying (MFD), focusing on the targeted modulation of the electromagnetic field to increase energy efficiency, increase drying homogeneity, and shorten process duration. At the same time, the product quality of MFD should be comparable to that of conventional freeze-drying (CFD). The main findings of the thesis presented in this chapter follow the structure introduced in Section 1.5: (I) Process development, (II) Process understanding, and (III) Process intensification.

The foundation for the investigation of MFD was laid in part (I) Process development with the construction of a laboratory-scale drying system for MFD and CFD with subsequent commissioning experiments in Chapter 2. Promising control concepts for MFD were developed in Chapter 3. The control concepts utilize multiple resonant frequencies (RFs) and were developed based on the literature on microwave-assisted heating.

Subsequently, part (II) Process understanding provided a deeper insight into MFD. The effects of the frequency-based control concepts developed from the electromagnetic simulations were qualitatively validated in the experiments in Chapter 3, showing the opportunities and limitations in the applicability of the simulations. The partial drying approach was used in Chapter 4, terminating MFD before the completion of drying to facilitate parameter studies on microwave frequency, microwave power, and chamber pressure.

In part (III) Process intensification, control concepts based on real-time adjustment of microwave frequency were investigated in Chapter 2 and Chapter 5. A control concept based on the application of multiple RFs throughout MFD was compared to CFD and MFD with alternative control concepts. The processes were compared

in terms of process parameters, such as energy efficiency and process duration, as well as product properties, like compound retention and macroscopic structure.

6.1 Process development

Process development involved the construction of a laboratory-scale plant designed to enable MFD and CFD in a single experimental setup. The construction details and considerations that lead to the decisions in plant design are detailed in Chapter 2. The plant construction features a solid-state microwave generator (SSG), allowing for fast electrical control and measurement of the microwave parameters frequency and power. In addition, temperature sensors, pressure sensors, and a load cell are installed for detailed online monitoring of experiments. When designing the system, attention was paid to its expandability to enable flexible adaptations to future requirements.

The successful MFD and CFD commissioning experiments in the constructed drying plant demonstrated the progression of the process parameters sample temperature, chamber pressure, and sample weight in line with the literature. These results confirmed Hypothesis H2.1, which states that these process parameters are in accordance with expectations from the literature. The MFD commissioning experiment proved the suitability of the system for performing experiments with the application and monitoring of microwaves. One system limitation is the observed uneven distribution of forward power among the applied frequencies. Despite this limitation, calculating the energy efficiency as a normalized parameter enables an analysis of the process independent of the forward power. Energy efficiency in this work refers to the conversion of electromagnetic energy into heat.

Microwave reflections were characterized as a function of the drying state, the presence of the processed material, and the use of a coaxial cable. These factors influence the frequency-dependent microwave reflection, as seen in the number of RFs and their respective energy efficiency. The observed shift of RFs to higher frequencies with an increase in the drying state is consistent with the results from

the MFD commissioning experiments. The predictable shift of RFs can be used in frequency-based control concepts to apply energy-efficient RFs throughout MFD for an energy-efficient and homogeneous process.

The development of control concepts for MFD was achieved through electromagnetic simulations in Chapter 3. The simulations were decoupled from thermodynamics by performing eleven simulations representing different drying states. The highest energy efficiencies were achieved throughout MFD when RFs were applied, confirming the expectation of an increased energy efficiency by the excitation of RFs in comparison to a non-specific excitation during the entire MFD process postulated in Hypothesis H3.1. The energy efficiency of the control concepts that applied no RFs decreased during drying. This decrease leads to inefficient energy utilization, especially towards the end of drying. The targeted application of energy-efficient frequencies throughout the entire process is essential to achieve energy-efficient MFD. The results of the electromagnetic simulations reveal a more uniform power dissipation among samples throughout the entire process when six frequencies are applied, compared to a single frequency. This finding confirms Hypothesis H3.2, which postulated increased uniformity of dissipated energy with multiple frequencies. The control concepts had a negligible effect on the energy distribution between the frozen and dried regions in the individual samples. In summary, the application of several RFs is a promising approach to achieving high energy efficiency and drying homogeneity in MFD.

6.2 Process understanding

The electromagnetic simulations were validated in Chapter 3 based on experimental results of the energy efficiency in the range of 2400 MHz to 2500 MHz. Quantitative disagreements were found between the results of simulations and experiments. However, qualitative agreements were found for the comparison of the number of RFs and the respective magnitudes of energy efficiency. Therefore, Hypothesis H3.3, which stated that the results of the electromagnetic simulations can be validated, cannot be confirmed. The electromagnetic simulations do not

accurately represent the electromagnetic fields in experiments. Nevertheless, the simulations can serve as a tool for predicting the effects of frequency modulation in MFD due to qualitative similarities to the experiments. Experimental proof is always required due to the limitations of electromagnetic simulations.

Qualitative agreement with the simulation results for energy efficiency and drying homogeneity were found for the first part of MFD. The targeted application of constant frequencies, identified as RFs at the beginning of MFD, shortened the process duration without increasing electric power consumption.

Partial MFD was investigated in Chapter 4 as a promising approach to save time when performing time-consuming parameter studies, ending the process before complete drying. In this work, MFD was terminated after 20 wt% of the water initially contained in the product had been removed. Partial MFD showed a comparable decrease in sample mass to complete MFD and reduced the time required for an experiment by 92%. This reduction confirmed Hypothesis H4.1, which anticipated time savings with partial MFD of above 80%. Note that the termination criterion of 20 wt% water initially contained was set arbitrarily. Therefore, adjusting this criterion can lead to deviating time savings. A major advantage of partial MFD is the capability to analyze the drying homogeneity among the samples. The method reveals differences in the drying state among the individual samples. This result confirms Hypothesis H4.2, which states that partial drying enables an assessment of drying homogeneity due to a homogeneous drying equilibrium not being achieved. On the other hand, partial MFD does not allow an assessment of product quality because of incomplete drying.

Hypothesis H4.3 states that partial MFD is adequate to qualitatively examine the impact of microwave frequency, microwave power, and chamber pressure on the MFD process. Reducing the chamber pressure in partial MFD resulted in a shorter process duration, caused by the removal of more water prior to microwave application and higher drying rates. The latter contradicts the results in the literature. The application of energy-efficient RFs increased energy efficiency. Increasing the microwave power and the targeted application of RFs both resulted in a reduction in process duration, as was expected from the literature. The application of

several microwave frequencies led to an increase in drying homogeneity at similar levels of specific dissipated power. The chamber pressure and the microwave power did not influence the drying homogeneity. Outliers to low residual moisture at high microwave power were the only exceptions. The corresponding samples showed internal structural damage due to the formation of large pores, which was probably caused by the melting of the samples during MFD.

In summary, the investigation of partial MFD validated the proposed method for efficiently investigating the impact of microwave power and frequency, although the expected influence of chamber pressure was not observed. The latter is likely due to the fact that the initial drying phase is not representative of mass transfer limitations during later drying stages. Thus, Hypothesis H4.3 can only be confirmed for microwave frequency and power. However, partial MFD can be helpful in parameter studies, depending on which parameters are varied and which target parameters are relevant.

The investigations with partial MFD confirmed the results of the electromagnetic simulations described in Chapter 3. The use of multiple energy-efficient RFs was confirmed to increase both the energy efficiency and the homogeneity of drying in the initial phase of MFD.

6.3 Process optimization

Microwave frequency emerged as a key parameter for intensifying MFD based on the findings from Process development and Process understanding. Consequently, Process optimization focuses on investigating the impact of frequency modulation on MFD. The complete MFD process was examined, enabling analysis of product properties, like compound retention and macroscopic structure, which was possible due to the fully dried product. In addition, process parameters, such as sample temperature and chamber pressure, were monitored.

The use of multiple RFs had been shown to increase energy efficiency and drying homogeneity. Thus, a control concept applying multiple RFs was implemented

for MFD and evaluated against the benchmark processes of CFD and MFD with alternative control concepts. The necessity for real-time frequency control, established in Chapter 2, was addressed through an automated algorithm. The software continuously searches for new RFs within a narrow range around previously applied frequencies. This approach uses a feedback-driven process control that dynamically adapts to the changing product state.

Using multiple energy-efficient RFs resulted in an average energy efficiency higher than that of maintaining constant frequencies. The maximum sample temperature recorded among all MFD experiments was 43.8 °C, close to the 44.0 °C observed in CFD. The specific forward power in the MFD experiments varied with frequency, as detailed in Section 2.4.3. Thus, the forward power was not constant among the control concepts. Nevertheless, the application of the most energy-efficient RFs coincided with the highest average specific dissipated power, leading to the highest drying rate. These conditions resulted in a process duration of 11.7 h for MFD using multiple RFs, a decrease of 24.2% compared to CFD and 38.4% compared to MFD with the same number of constant frequencies. The frequency adjustments caused an increase in energy efficiency, sample temperature, and drying rates. This causation is evidenced by the fluctuations of the parameters each time the applied frequency set was modified. These results underscore the potential for increased energy efficiency and shorter drying duration of MFD by targeted application of energy-efficient RFs, which confirms Hypothesis H5.1.

Similar residual moisture content and ascorbic acid retention levels were achieved across all MFD control concepts, comparable to the results observed for CFD. These product properties corresponded to the typical ranges reported in the literature for freeze-drying (FD) of food products. However, structural damage as the formation of large pores was observed in up to 10.4% of the samples across all MFD control concepts, while no such impairment was observed for CFD. Hypothesis H5.2 states that the quality of the products obtained from MFD with the application of energy-efficient RFs is similar or superior to the products from CFD. This hypothesis is only partially confirmed concerning compound retention and residual moisture levels. The incidence of structurally impaired samples could be minimized through adapted frequency control or a reduction

in microwave power. In conclusion, MFD using RFs continues to show promise as a rapid and energy-efficient alternative to CFD as a fast and energy-efficient process.

6.4 Future outlook

This work explored opportunities for targeted microwave application during MFD on the basis of understanding the changes in the microwave field during the process. Particular emphasis was placed on investigating frequency control to increase energy efficiency, increase drying homogeneity, and shorten the process duration. The application of RFs with real-time adjustment based on the product state achieved all these criteria compared to other control concepts. Furthermore, the product quality achieved with MFD was comparable to that of CFD, apart from structural damage in some samples.

Future work could explore refinements in control concepts that apply RFs to achieve further reductions in process duration or increase drying homogeneity to minimize structural damage. The modification could involve using more advanced algorithms, such as genetic algorithms, or artificial intelligence to optimize control concepts based on a large experimental data set. Integrating additional input variables could increase the flexibility of control concepts. For example, dynamic microwave adjustments could be implemented based on combined measurements of microwave reflections, sample temperature, and sample weight. Furthermore, process monitoring based on the microwave field could be investigated, as it was demonstrated that the drying state impacts microwave reflections.

Electromagnetic models can be used to efficiently identify advantageous control concepts despite the increase in the number of input variables and the adjustable microwave properties. Due to the limitations of electromagnetic models shown in this work, it is essential to experimentally validate the identified advantageous control concepts.

The design of the constructed MFD system enables future investigations with modified experimental setups. The installation of multiple SSGs would allow studies on the effects of phase shifts between the emitted microwaves. Using multiple SSGs would also enable the simultaneous application of several frequencies or varying power distributions between the SSGs. In addition, an extended sensor network could provide further input variables for process control. For example, infrared cameras would allow an observation of the locally resolved surface temperature distribution. Furthermore, the plant could be modified to enable hybrid FD techniques using microwaves and conventional heating simultaneously, which may have synergistic benefits and facilitate thermal control during drying.

The applicability of optimized MFD processes for drying industrially relevant products must be investigated to transfer the promising results to application. For example, the MFD of high-value foods or active pharmaceutical ingredients should be investigated. The scale-up of MFD is another major challenge for its industrial application, which must be addressed. Partial MFD could be used for time-efficient, product-specific process design in the scale-up process while enabling evaluation of drying homogeneity. However, attention must be paid to its limitations, as the behavior of the process parameters at the drying start may not be representative for the entire process.

A Appendix

A1 Supplementary material chapter 2

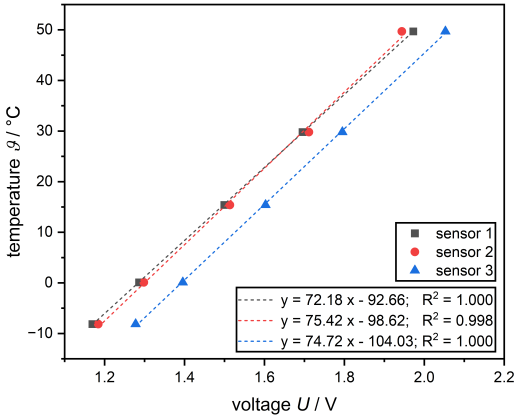

Figure A.1: Calibration curves of the three fiberoptic temperature sensors used in the FD commissioning experiments.

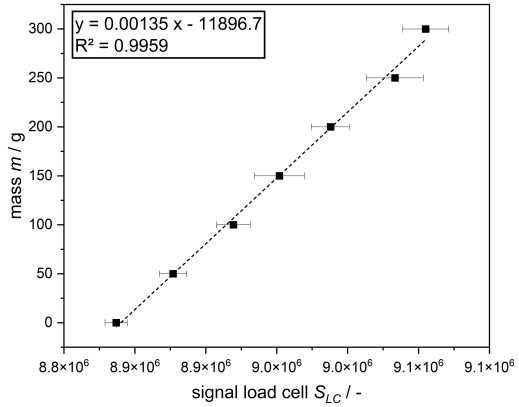

Figure A.2: Calibration curve of the load cell used in the MFD commissioning experiment.

A2 Supplementary material chapter 3

Table A.1: Frequencies utilized in the electromagnetic simulations depending on the drying state for the control concepts 1MF and 6EF.

	Frequency f / GHz						
	1MF	6EF					
Drying state z / %	f_1	f_1	f_2	f_3	f_4	f_5	f_6
0	2.4255	2.4000	2.4200	2.4400	2.4600	2.4800	2.5000
10	2.4263	2.4000	2.4200	2.4400	2.4600	2.4800	2.5000
20	2.4272	2.4000	2.4200	2.4400	2.4600	2.4800	2.5000
30	2.4283	2.4000	2.4200	2.4400	2.4600	2.4800	2.5000
40	2.4296	2.4000	2.4200	2.4400	2.4600	2.4800	2.5000
50	2.431	2.4000	2.4200	2.4400	2.4600	2.4800	2.5000
60	2.4326	2.4000	2.4200	2.4400	2.4600	2.4800	2.5000
70	2.4343	2.4000	2.4200	2.4400	2.4600	2.4800	2.5000
80	2.4362	2.4000	2.4200	2.4400	2.4600	2.4800	2.5000
90	2.4455	2.4000	2.4200	2.4400	2.4600	2.4800	2.5000
100	2.4418	2.4000	2.4200	2.4400	2.4600	2.4800	2.5000

Table A.2: Frequencies utilized in the electromagnetic simulations depending on the drying state for the control concepts 1RF and 6RF.

	Frequency f / GHz						
	1MF	6EF					
Drying state z / %	f_1	f_1	f_2	f_3	f_4	f_5	f_6
0	2.4133	2.4071	2.4133	2.4438	2.4541	2.4698	2.4789
10	2.4135	2.4100	2.4135	2.4444	2.4566	2.4701	2.4793
20	2.4127	2.4127	2.4452	2.4523	2.4587	2.4704	2.4797
30	2.4134	2.4012	2.4134	2.4459	2.4607	2.4706	2.4802
40	2.4627	2.4036	2.4141	2.4468	2.4627	2.4708	2.4806
50	2.4646	2.4063	2.4147	2.4478	2.4646	2.4710	2.4811
60	2.4664	2.4153	2.4490	2.4531	2.4664	2.4712	2.4813
70	2.4681	2.4158	2.4504	2.4531	2.4681	2.4714	2.4813
80	2.4698	2.4163	2.4521	2.4534	2.4698	2.4715	2.4818
90	2.4713	2.4002	2.4532	2.4542	2.4713	2.4717	2.4823
100	2.473	2.4014	2.4533	2.4566	2.4718	2.473	2.4829

Table A.3: Energy efficiencies of the frequencies utilized in the electromagnetic simulations in dependence on the drying state for the control concepts 1MF and 6EF.

	Energy efficiency η / %						
	1MF	**6EF**					
Drying state z / %	$\mathbf{f_1}$	$\mathbf{f_1}$	$\mathbf{f_2}$	$\mathbf{f_3}$	$\mathbf{f_4}$	$\mathbf{f_5}$	$\mathbf{f_6}$
0	13.22	59.52	17.43	28.55	39.93	57.71	28.51
10	11.93	58.71	17.19	22.29	53.54	56.26	23.10
20	10.90	62.66	18.35	17.83	75.28	54.74	18.62
30	10.03	53.56	19.52	14.64	82.91	52.86	15.46
40	9.20	40.05	18.58	12.50	58.88	50.48	12.97
50	8.39	33.48	21.87	12.01	35.96	47.66	11.07
60	7.53	33.69	27.30	15.29	24.10	43.92	9.51
70	6.57	43.18	16.36	12.16	18.54	39.10	8.19
80	5.48	71.91	11.52	6.57	16.53	33.44	7.14
90	4.28	96.18	8.31	4.36	17.81	26.76	5.93
100	3.05	41.30	6.35	3.10	26.52	18.92	4.43

Table A.4: Energy efficiencies of the frequencies utilized in the electromagnetic simulations in dependence on the drying state for the control concepts 1RF and 6RF.

	Energy efficiency η / %						
	1RF	**6RF**					
Drying state z / %	$\mathbf{f_1}$	$\mathbf{f_1}$	$\mathbf{f_2}$	$\mathbf{f_3}$	$\mathbf{f_4}$	$\mathbf{f_5}$	$\mathbf{f_6}$
0	99.27	93.43	99.27	80.95	77.68	54.47	60.12
10	98.88	96.01	98.88	76.01	78.50	54.36	57.20
20	99.96	99.96	70.58	28.40	81.91	54.78	54.86
30	96.49	56.19	96.49	64.91	85.63	55.26	52.94
40	89.11	48.31	87.68	59.54	89.11	56.30	51.35
50	92.20	41.04	79.15	55.75	92.20	57.49	50.35
60	94.81	72.90	54.73	38.04	94.81	59.63	50.08
70	96.93	67.92	58.42	35.98	96.93	63.72	52.55
80	98.46	61.95	69.35	39.48	98.46	74.28	60.23
90	98.93	98.31	88.95	81.37	98.93	98.78	73.71
100	99.72	91.67	58.94	98.89	57.39	99.72	91.68

Table A.5: Frequencies and respective energy efficiencies utilized in the control concepts in the experiments with the laboratory-scale MFD system. The respective energy efficiencies and frequencies were determined as the arithmetic means from the process characterization by a frequency sweep in triplicate.

	1MF	**6EF**					
	$\mathbf{f_1}$	$\mathbf{f_1}$	$\mathbf{f_2}$	$\mathbf{f_3}$	$\mathbf{f_4}$	$\mathbf{f_5}$	$\mathbf{f_6}$
Frequency f / GHz	2.4322	2.4000	2.4200	2.4400	2.4600	2.4800	2.5000
Energy efficiency η / %	23.93	23.70	60.57	63.22	61.00	62.53	58.17
	1RF	**6RF**					
	$\mathbf{f_1}$	$\mathbf{f_1}$	$\mathbf{f_2}$	$\mathbf{f_3}$	$\mathbf{f_4}$	$\mathbf{f_5}$	$\mathbf{f_6}$
Frequency f / GHz	2.4498	2.4498	2.4562	2.4652	2.4664	2.4725	2.4748
Energy efficiency η / %	94.15	94.15	71.66	91.52	92.5	83.15	85.81

A3 Supplementary material chapter 4

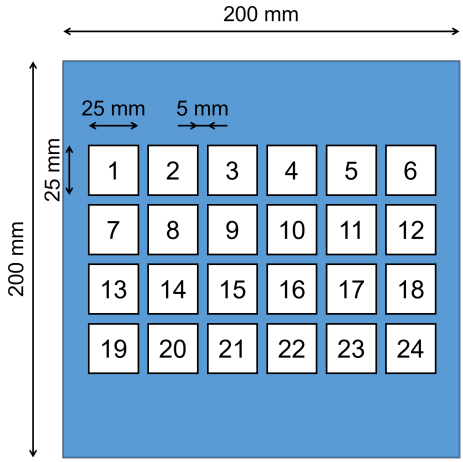

Figure A.3: Schematic top view of the arrangement of the 24 samples of tylose gel (white) on the product support (blue).

Table A.6: Average forward power and average chamber pressure in the experiments comparing termination criteria.

Experiment	Average forward power $\overline{P}_f$ / W	Average chamber pressure $\overline{p}_c$ / mbar
Partial drying - run 1	28.57	0.47
Partial drying - run 2	29.22	0.47
Partial drying - run 3	28.34	0.46
Complete drying	20.61	0.50

Table A.7: Average forward power and average chamber pressure in the experiments of the parameter study on chamber pressure.

Experiment	Average forward power $\overline{P}_f$ / W	Average chamber pressure $\overline{p}_c$ / mbar
$p_{c,set}$ = 0.2 mbar - run 1	16.86	0.19
$p_{c,set}$ = 0.2 mbar - run 2	13.52	0.19
$p_{c,set}$ = 0.2 mbar - run 3	15.03	0.19
$p_{c,set}$ = 0.5 mbar - run 1	17.36	0.47
$p_{c,set}$ = 0.5 mbar - run 2	18.02	0.47
$p_{c,set}$ = 0.5 mbar - run 3	17.90	0.47
$p_{c,set}$ = 1.0 mbar - run 1	14.26	0.87
$p_{c,set}$ = 1.0 mbar - run 2	16.17	0.87
$p_{c,set}$ = 1.0 mbar - run 3	14.59	0.87

Table A.8: Average forward power and average chamber pressure in the experiments of the parameter study on microwave power.

Experiment	Average forward power $\overline{P}_f$ / W	Average chamber pressure $\overline{p}_c$ / mbar
r_{on} = 0.25 - run 1	17.36	0.47
r_{on} = 0.25 - run 2	18.02	0.47
r_{on} = 0.25 - run 3	17.90	0.47
r_{on} = 0.50 - run 1	42.02	0.47
r_{on} = 0.50 - run 2	46.21	0.46
r_{on} = 0.50 - run 3	24.64	0.47
r_{on} = 0.75 - run 1	42.49	0.47
r_{on} = 0.75 - run 2	53.15	0.47
r_{on} = 0.75 - run 3	48.17	0.47
r_{on} = 0.75 - run 4	36.74	0.47
r_{on} = 1.00 - run 1	35.13	0.47
r_{on} = 1.00 - run 2	46.83	0.47
r_{on} = 1.00 - run 3	46.88	0.47
r_{on} = 1.00 - run 4	40.64	0.47

Table A.9: Average forward power and average chamber pressure in the experiments of the parameter study on microwave frequency.

Experiment	Average forward power $\overline{P}_f$ / W	Average chamber pressure $\overline{p}_c$ / mbar
1MF - run 1	19.00	0.46
1MF - run 2	18.14	0.47
1MF - run 3	18.31	0.46
1RF - run 1	27.53	0.45
1RF - run 2	28.05	0.47
1RF - run 3	26.59	0.47
6EF - run 1	28.57	0.47
6EF - run 2	29.22	0.47
6EF - run 3	28.34	0.46
6RF - run 1	32.95	0.47
6RF - run 2	33.31	0.47
6RF - run 3	31.25	0.47

Table A.10: Applied frequencies during the parameter studies on chamber pressure and microwave power.

Set chamber pressure $p_{c,set}$ / W	**0.2**	**0.5**	**1.0**
Frequency f_1 / MHz	2441.3	2449.6	2449.6
Frequency f_2 / MHz	2450.0	2456.2	2456.1
Frequency f_3 / MHz	2456.3	2467.3	2464.6
Frequency f_4 / MHz	2468.4	2470.7	2472.5
Frequency f_5 / MHz	2470.2	2475.1	2475.2
Frequency f_6 / MHz	2475.9	2497.2	2497.1

Table A.11: Applied frequencies during the parameter study on microwave frequency.

Control concept	**1MF**	**1RF**	**6EF**	**6RF**
Frequency f_1 / MHz	2432.0	2449.8	2400.0	2449.7
Frequency f_2 / MHz	-	-	2420.0	2456.2
Frequency f_3 / MHz	-	-	2440.0	2465.2
Frequency f_4 / MHz	-	-	2460.0	2466.4
Frequency f_5 / MHz	-	-	2480.0	2472.5
Frequency f_6 / MHz	-	-	2500.0	2474.8

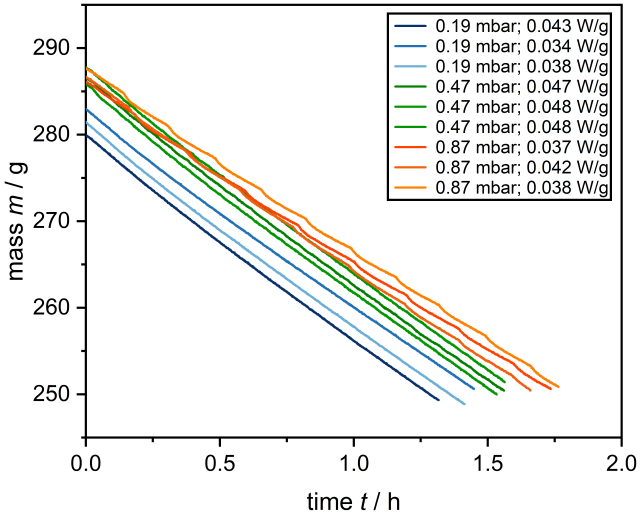

Figure A.4: Drying kinetics for experiments of the parameter study on chamber pressure. The values in the legend represent the average chamber pressure and the average specific dissipated power for the experiments.

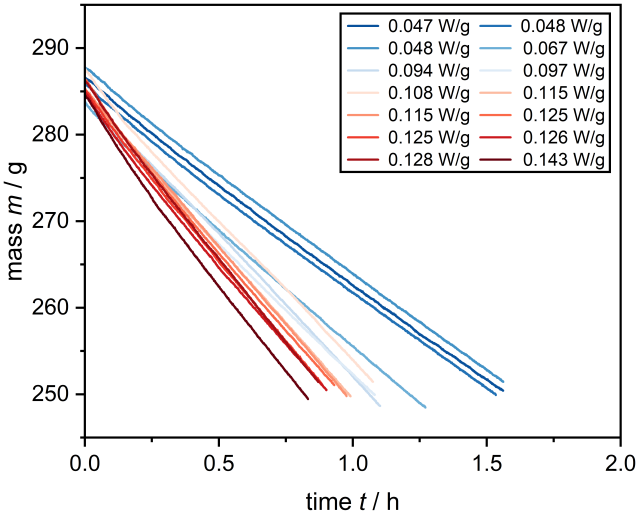

Figure A.5: Drying kinetics for experiments of the parameter study on microwave power. The powers in the legend are the average specific dissipated power for every experiment.

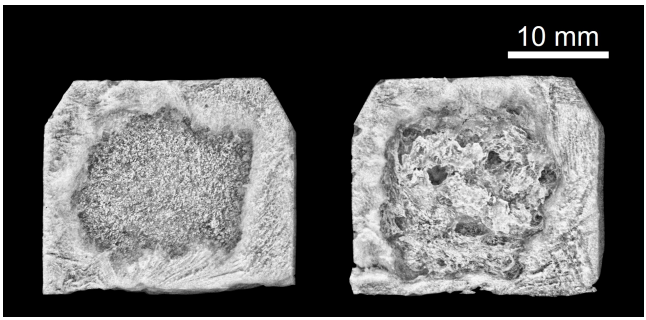

Figure A.6: Exemplary pictures of tylose gel samples in gray-scale: Intact sample (left), puffed sample (right). While both samples show a fine-pored structure in the dried outer layer, large pores in the center of the sample can only be observed for the puffed sample.

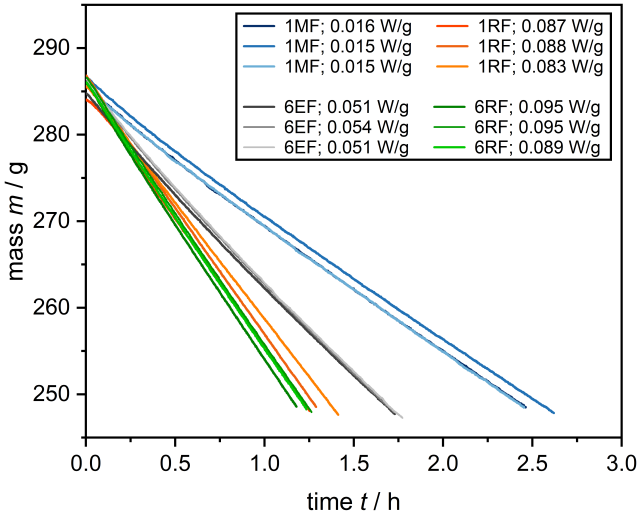

Figure A.7: Drying kinetics for the frequency-based control concepts in the parameter study on microwave frequency. The legend contains the frequency-based control concepts and the average specific dissipated powers for every experiment.

A4 Supplementary material chapter 5

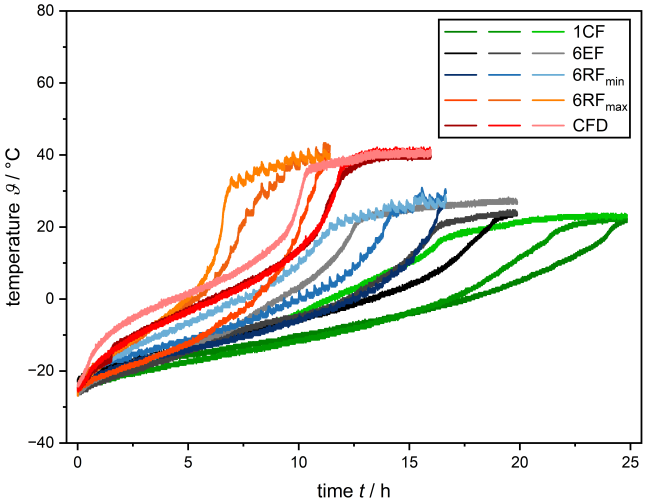

Figure A.8: Temperature of samples 4, 6, and 10 as a function of process time from MFD and CFD experiments depicted in Figure 5.6. For each color, the samples are displayed in the order 10, 4, and 6 from the darkest to the lightest shade.

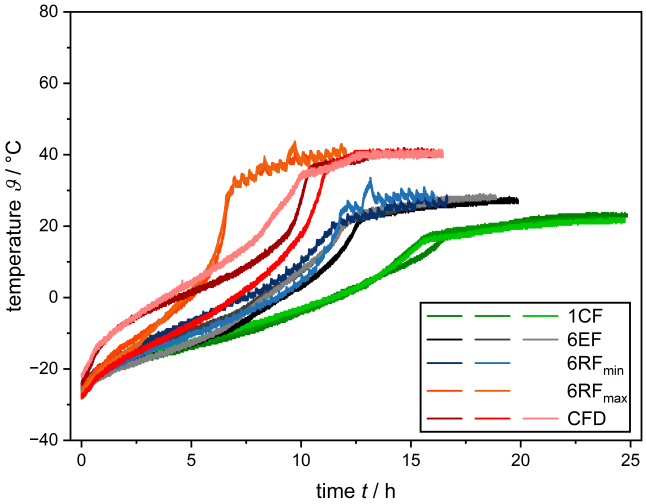

Figure A.9: Temperature of sample 6 as a function of process time for MFD and CFD experiments. The darkest shades of each color are the experiments shown in Figure 5.6.

List of figures

List of tables

List of publications

Publications (peer review)

T. Kaysan, X. Zhou, and V. Gaukel. Process intensification of microwave-assisted freeze-drying by frequency adjustment in real-time using solid-state technology. *Journal of Food Engineering*, 383:112221, 2024. ISSN 02608774. doi: 10.1016/j.jfoodeng.2024.112221.

T. Sickert, R. Bergmann, J. Christoph, and V. Gaukel. A time-saving approach to parameter studies in microwave-assisted freeze drying. *Processes*, 11(10):2886, 2023. doi: 10.3390/pr11102886.

T. Sickert, I. Kalinke, J. Christoph, and V. Gaukel. Microwave-assisted freeze-drying with frequency-based control concepts via solid-state generators: A simulative and experimental study. *Processes*, 11(2):327, 2023. doi: 10.3390/pr11020327.

Oral presentations

T. Kaysan, X. Zhou, N. Rudisile, and V. Gaukel. Potentials and constraints in the process intensification of microwave-assisted freeze-drying. *17th European PhD Workshop on Food Engineering and Technology*, 04/23/2024-04/24/2024, Aachen, Germany.

T. Sickert, X. Zhou, and V. Gaukel. Microwave-assisted freeze-drying of tylose gel through real-time frequency modulation. *57th Annual Microwave Power Symposium*, 06/27/2023-06/29/2023, Denver, USA.

T. Sickert, N. Rudisile, and V. Gaukel. Tracking of resonant frequencies in microwave-assisted drying: opportunities for process monitoring and optimization. *EuroPACT2023*, 05/07/2023-05/10/2023, Copenhagen, Denmark.

T. Sickert, X. Zhou, N. Rudisile, and V. Gaukel. Prozessoptimierung der mikrowellenunterstützten Gefriertrocknung durch Frequenzanpassung in Echtzeit. *Jahrestreffen 2023 der DECHEMA-Fachgruppen Abfallbehandlung und Wertstoffrückgewinnung und Trocknungstechnik*, 03/06/2023-03/07/2023, Dresden, Germany.

T. Sickert and V. Gaukel. Microwave-assisted freeze-drying of foodstuffs using a novel frequency-based control concept. *22nd International Drying Symposium*, 06/26/2022-06/29/2022, Worcester, Massachusetts, USA.

T. Sickert, M. Brunnenkant, J. Christoph, and V. Gaukel. Entwicklung eines Steuerungskonzeptes für die energieeffiziente und homogene mikrowellenunterstützte Gefriertrocknung von Lebensmitteln. *Jahrestreffen der ProcessNet-Fachgruppen Lebensmittelverfahrenstechnik und Trocknungstechnik*, 03/10/2022-03/11/2022, Frankfurt am Main, Germany.

Poster presentations

T. Sickert, X. Zhou, and V. Gaukel. Microwave-assisted freeze-drying of foodstuffs using a novel frequency-based control concept. *14th International Congress on Engineering and Food*, 06/20/2023-06/23/2023, Nantes, France.

T. Sickert, L. Richter, and V. Gaukel. Numerisch gestützte Untersuchung einer Mikrowellengefriertrocknung unter Verwendung der Solid State-Technologie. *Jahrestreffen der ProcessNet-Fachgruppen Lebensmittelverfahrenstechnik, Mischvorgänge, Grenzflächenbestimmte Systeme und Prozesse*, 03/11/2021-03/12/2021, Frankfurt am Main, Germany.

Bibliography

[1] C. Ratti. Hot air and freeze-drying of high-value foods: a review. *Journal of Food Engineering*, 49(4):311–319, 2001. ISSN 02608774. doi: 10.1016/S0260-8774(00)00228-4.

[2] S. Bhatta, T. Stevanovic Janezic, and C. Ratti. Freeze-drying of plant-based foods. *Foods*, 9(1), 2020. doi: 10.3390/foods9010087.

[3] F. Shishehgarha, J. Makhlouf, and C. Ratti. Freeze-drying characteristics of strawberries. *Drying Technology*, 20(1):131–145, 2002. doi: 10.1081/DRT-120001370.

[4] A. Reyes, A. Evseev, A. Mahn, V. Bubnovich, R. Bustos, and E. Scheuermann. Effect of operating conditions in freeze-drying on the nutritional properties of blueberries. *International Journal of Food Sciences and Nutrition*, 62(3):303–306, 2011. doi: 10.3109/09637486.2010.534078.

[5] X. Tang and M. J. Pikal. Design of freeze-drying processes for pharmaceuticals: practical advice. *Pharmaceutical Research*, 21(2):191–200, 2004. ISSN 0724-8741. doi: 10.1023/B:PHAM.0000016234.73023.75.

[6] Y. Miyamoto-Shinohara, J. Sukenobe, T. Imaizumi, and T. Nakahara. Survival of freeze-dried bacteria. *The Journal of General and Applied Microbiology*, 54(1):9–24, 2008. ISSN 0022-1260. doi: 10.2323/jgam.54.9.

[7] A. Ciurzyńska and A. Lenart. Freeze-drying - application in food processing and biotechnology - a review. *Polish Journal of Food and Nutrition Sciences*, 61(3):165–171, 2011. ISSN 1230-0322. doi: 10.2478/v10222-011-0017-5.

[8] X. Duan, M. Zhang, A. S. Mujumdar, and S. Wang. Microwave freeze drying of sea cucumber (stichopus japonicus). *Journal of Food Engineering*, 96(4): 491–497, 2010. ISSN 02608774. doi: 10.1016/j.jfoodeng.2009.08.031.

[9] T. Siebert, V. Gall, H. P. Karbstein, and V. Gaukel. Serial combination drying processes: A measure to improve quality of dried carrot disks and to reduce drying time. *Drying Technology*, 36(13):1578–1591, 2018. doi: 10.1080/07373937.2017.1418374.

[10] X. Cao, M. Zhang, A. S. Mujumdar, and Z. Wang. Effect of microwave freeze-drying on microbial inactivation, antioxidant substance and flavor quality of ashitaba leaves (angelica keiskei koidzumi). *Drying Technology*, 12: 1–8, 2018. doi: 10.1080/07373937.2018.1463245.

[11] S. Ambros, R. Mayer, B. Schumann, and U. Kulozik. Microwave-freeze drying of lactic acid bacteria: Influence of process parameters on drying behavior and viability. *Innovative Food Science & Emerging Technologies*, 48:90–98, 2018. ISSN 14668564. doi: 10.1016/j.ifset.2018.05.020.

[12] M. Ozcelik, A. Heigl, U. Kulozik, and S. Ambros. Effect of hydrocolloid addition and microwave-assisted freeze drying on the characteristics of foamed raspberry puree. *Innovative Food Science & Emerging Technologies*, 56: 102183, 2019. ISSN 14668564. doi: 10.1016/j.ifset.2019.102183.

[13] Z. Wang, X. Duan, L. Li, G. Ren, T. Wu, J. Chen, Y. Ang, J. Guo, and M. Zhao. Effects of freeze-drying and microwave vacuum freeze-drying on the activity of igy: From the perspective of protein structure. *Drying Technology*, 41(2):222–232, 2023. doi: 10.1080/07373937.2021.2015373.

[14] N. Härdter, R. Geidobler, I. Presser, and G. Winter. Accelerated production of biopharmaceuticals via microwave-assisted freeze-drying (mfd). *Pharmaceutics*, 15(5), 2023. ISSN 1999-4923. doi: 10.3390/pharmaceutics15051342.

[15] K. Schössler, H. Jäger, and D. Knorr. Novel contact ultrasound system for the accelerated freeze-drying of vegetables. *Innovative Food Science & Emerging Technologies*, 16:113–120, 2012. ISSN 14668564. doi: 10.1016/j.ifset.2012.05.010.

[16] N. L. Oliveira, S. H. Silva, J. d. A. Figueiredo, L. B. Norcino, and J. v. d. Resende. Infrared-assisted freeze-drying (irfd) of açai puree: Effects on the drying kinetics, microstructure and bioactive compounds. *Innovative Food Science & Emerging Technologies*, 74:102843, 2021. ISSN 14668564. doi: 10.1016/j.ifset.2021.102843.

[17] J. C. Atuonwu and S. A. Tassou. Quality assurance in microwave food processing and the enabling potentials of solid-state power generators: A review. *Journal of Food Engineering*, 234:1–15, 2018. ISSN 02608774. doi: 10.1016/j.jfoodeng.2018.04.009.

[18] Z. Tang, T. Hong, Y. Liao, F. Chen, J. Ye, H. Zhu, and K. Huang. Frequency-selected method to improve microwave heating performance. *Applied Thermal Engineering*, 131(2):642–648, 2018. ISSN 13594311. doi: 10.1016/j.applthermaleng.2017.12.008.

[19] S. Taghian Dinani, E. Feldmann, and U. Kulozik. Effect of heating by solid-state microwave technology at fixed frequencies or by frequency sweep loops on heating profiles in model food samples. *Food and Bioproducts Processing*, 127:328–337, 2021. ISSN 09603085. doi: 10.1016/j.fbp.2021.03.018.

[20] R. Yang and J. Chen. Dynamic solid-state microwave defrosting strategy with shifting frequency and adaptive power improves thawing performance. *Innovative Food Science & Emerging Technologies*, 81:103157, 2022. ISSN 14668564. doi: 10.1016/j.ifset.2022.103157.

[21] R. Yang, A. E. Fathy, M. T. Morgan, and J. Chen. Development of a complementary-frequency strategy to improve microwave heating of gellan gel in a solid-state system. *Journal of Food Engineering*, 314:110763, 2022. ISSN 02608774. doi: 10.1016/j.jfoodeng.2021.110763.

[22] R. Yang and J. Chen. Heating performance of dual-source microwave heating using different frequency shifting strategies in a solid-state system. *Food Research International*, 175:113781, 2024. doi: 10.1016/j.foodres.2023.113781.

[23] V. V. Yakovlev. Effect of frequency alteration regimes on the heating patterns in a solid-state-fed microwave cavity. *Journal of Microwave Power and Electromagnetic Energy*, 52(1):31–44, 2018. ISSN 0832-7823. doi: 10.1080/08327823.2017.1417105.

[24] I. Kalinke, F. Pusl, F. Häderle, and U. Kulozik. A comparative study of frequency-shifting strategies for uniform and energy-efficient microwave heating in solid-state microwave systems. *Innovative Food Science & Emerging Technologies*, 86:103388, 2023. ISSN 14668564. doi: 10.1016/j.ifset.2023.103388.

[25] L. Li, M. Zhang, and P. Yang. Suitability of lf-nmr to analysis water state and predict dielectric properties of chinese yam during microwave vacuum drying. *LWT - Food Science and Technology*, 105:257–264, 2019. ISSN 00236438. doi: 10.1016/j.lwt.2019.02.017.

[26] K. Nakagawa and S. Kono. Monitoring of primary drying in the freeze-drying process using an open-ended coaxial microwave resonator. *Journal of Food Engineering*, 289(2):110163, 2021. ISSN 02608774. doi: 10.1016/j.jfoodeng.2020.110163.

[27] M. Miyakawa, S. Kanamori, K. Hagihara, A. Itagaki, T. Nakamura, and M. Nishioka. Cylindrical resonator-type microwave heating reactor with real-time monitoring function of dielectric property applied to drying processes. *Industrial & Engineering Chemistry Research*, 60(25):9119–9127, 2021. ISSN 0888-5885. doi: 10.1021/acs.iecr.1c00569.

[28] G.-W. Oetjen. *Gefriertrocknen*. VCH, Weinheim, 1997. ISBN 352728821X.

[29] H.-J. Kretzschmar and W. Wagner. D2.1 thermophysikalische stoffwerte von wasser. In P. Stephan, S. Kabelac, M. Kind, D. Mewes, K. Schaber, and T. Wetzel, editors, *VDI-Wärmeatlas*, Springer Reference Technik, pages 201–218. Springer Berlin Heidelberg, Berlin, Heidelberg, 2019. ISBN 978-3-662-52988-1. doi: 10.1007/978-3-662-52989-8$\backslash$textunderscore.

[30] A. K. Konstantinidis, W. Kuu, L. Otten, S. L. Nail, and R. R. Sever. Controlled nucleation in freeze-drying: effects on pore size in the dried product layer, mass transfer resistance, and primary drying rate. *Journal of Pharmaceutical Sciences*, 100(8):3453–3470, 2011. doi: 10.1002/jps.22561.

[31] C. J. King. *Freeze Drying of Foods*. CRC monoscience series. CRC Press, Cleveland, 1971. ISBN 978-0878191055.

[32] A. I. Liapis, M. L. Pim, and R. Bruttini. Research and development needs and opportunities in freeze drying. *Drying Technology*, 14(6):1265–1300, 1996. doi: 10.1080/07373939608917146.

[33] F. Franks and T. Auffret. *Freeze-drying of Pharmaceuticals and Biopharmaceuticals*. The Royal Society of Chemistry, 2007. ISBN 978-0-85404-268-5. doi: 10.1039/9781847557704.

[34] H. D. Baehr and K. Stephan. *Wärme- und Stoffübertragung*. Springer Berlin Heidelberg, Berlin, Heidelberg, 10. aufl. 2019 edition, 2019. ISBN 3662584417. doi: 10.1007/978-3-662-58441-5.

[35] G. Assegehegn, E. La Brito-de Fuente, J. M. Franco, and C. Gallegos. Freeze-drying: A relevant unit operation in the manufacture of foods, nutritional products, and pharmaceuticals. *Advances in Food and Nutrition Research*, 93:1–58, 2020. ISSN 1043-4526. doi: 10.1016/bs.afnr.2020.04.001.

[36] H. P. Schuchmann and H. Schuchmann. *Lebensmittelverfahrenstechnik*. Wiley, 2005. ISBN 9783527312306. doi: 10.1002/9783527623549.

[37] F. Franks. Freeze-drying of bioproducts: putting principles into practice. *European Journal of Pharmaceutics and Biopharmaceutics*, 45(3):221–229, 1998. doi: 10.1016/S0939-6411(98)00004-6.

[38] D. Fissore, S. A. Velardi, and A. A. Barresi. In-line control of a freeze-drying process in vials. *Drying Technology*, 26(6):685–694, 2008. doi: 10.1080/07373930802046161.

[39] M. J. Pikal and S. Shah. The collapse temperature in freeze drying: Dependence on measurement methodology and rate of water removal from the glassy phase. *International Journal of Pharmaceutics*, 62(2-3):165–186, 1990. ISSN 03785173. doi: 10.1016/0378-5173(90)90231-r.

[40] Z. Irzyniec, J. Klimczak, and S. Michalowski. Freeze-drying of the black currant juice. *Drying Technology*, 13(1-2):417–424, 1995. doi: 10.1080/07373939508916961.

[41] D. E. Clark and W. H. Sutton. Microwave processing of materials. *Annual Review of Materials Science*, 26(1):299–331, 1996. doi: 10.1146/annurev.ms.26.080196.001503.

[42] D. M. Pozar. *Microwave engineering*. John Wiley & Sons Inc, Hoboken, NJ, fourth edition edition, 2012. ISBN 0470631554. URL `https://ebookcentral.proquest.com/lib/kxp/detail.action?docID=2064708`.

[43] M. Thumm and L. Feher. Millimeter-wave-sources development: Present and future. In M. Willert-Porada, editor, *Advances in Microwave and Radio Frequency Processing*, pages 15–23. Springer Berlin Heidelberg, Berlin, Heidelberg, 2006. ISBN 978-3-540-43252-4. doi: 10.1007/978-3-540-32944-2_2.

[44] A. C. Metaxas. Microwave heating. *Power Engineering Journal*, 5(5):237, 1991. ISSN 09503366. doi: 10.1049/pe:19910047.

[45] I. Kalinke and U. Kulozik. Enhancing microwave freeze drying: Exploring maximum drying temperature and power input for improved energy efficiency and uniformity. *Food and Bioprocess Technology*, 2024. ISSN 1935-5130. doi: 10.1007/s11947-024-03438-5.

[46] A. C. Metaxas and R. J. Meredith. *Industrial Microwave Heating*, volume 4 of *IET power and energy series*. IET, London, 1988. ISBN 978-1-84919-424-2. doi: 10.1049/PBPO004E.

[47] X. Duan, M. Zhang, A. S. Mujumdar, and R. Wang. Trends in microwave-assisted freeze drying of foods. *Drying Technology*, 28(4):444–453, 2010. doi: 10.1080/07373931003609666.

[48] V. Gaukel, T. Siebert, and U. Erle. Microwave-assisted drying. In *The Microwave Processing of Foods*, pages 152–178. Elsevier, 2017. ISBN 9780081005286. doi: 10.1016/B978-0-08-100528-6.00008-5.

[49] T. Ohlsson and N. Bengtsson. Microwave technology and foods. *Advances in Food and Nutrition Research*, 43:65–140, 2001. doi: 10.1016/s1043-4526(01)43003-8.

[50] A. R. von Hippel, editor. *Dielectric materials and applications*. Artech House microwave library. Artech House, Boston and London, [new ed., 2. ed.] edition, 1995. ISBN 9781580531238.

[51] S. Chandrasekaran, S. Ramanathan, and T. Basak. Microwave food processing—a review. *Food Research International*, 52(1):243–261, 2013. doi: 10.1016/j.foodres.2013.02.033.

[52] N. E. Bengtsson and P. O. Risman. Dielectric properties of foods at 3 ghz as determined by a cavity perturbation technique. *Review of Scientific Instruments*, 6(2):107–123, 1971. ISSN 0022-2739. doi: 10.1080/00222739.1971.11688789.

[53] Y. Llave, K. Mori, D. Kambayashi, M. Fukuoka, and N. Sakai. Dielectric properties and model food application of tylose water pastes during microwave thawing and heating. *Journal of Food Engineering*, 178(2):20–30, 2016. ISSN 02608774. doi: 10.1016/j.jfoodeng.2016.01.003.

[54] E. T. Thostenson and T.-W. Chou. Microwave processing: fundamentals and applications. *Composites Part A: Applied Science and Manufacturing*, 30(9):1055–1071, 1999. ISSN 1359835X. doi: 10.1016/S1359-835X(99)00020-2.

[55] R. E. Collin. *Foundations for microwave engineering*. IEEE Press series on electromagnetic wave theory. IEEE Press Wiley-Interscience and IEEE

Xplore, New York and Hoboken, New Jersey and Piscataway, New Jersey, second edition edition, 2001. ISBN 9780470544662. doi: 10.1109/9780470544662.

[56] T.V.C.T. Chan and H. C. Reader. *Understanding microwave heating cavities*. Artech House microwave library. Artech House, Boston, Mass., 2000. ISBN 1-58053-094-X.

[57] K. Yamamoto, H. Kuronuma, T. Koinuma, and N. Tashiro. A study of magnetron noise. *IEEE Transactions on Electron Devices*, 34(5):1223–1226, 1987. ISSN 0018-9383. doi: 10.1109/t-ed.1987.23071.

[58] D. Luan, Y. Wang, J. Tang, and D. Jain. Frequency distribution in domestic microwave ovens and its influence on heating pattern. *Journal of Food Science*, 82(2):429–436, 2017. doi: 10.1111/1750-3841.13587.

[59] J. C. Maxwell. Viii. a dynamical theory of the electromagnetic field. *Philosophical Transactions of the Royal Society of London*, 155:459–512, 1865. ISSN 0261-0523. doi: 10.1098/rstl.1865.0008.

[60] D. P. Hampshire. A derivation of maxwell's equations using the heaviside notation. *Philosophical Transactions of the Royal Society A: Mathematical, Physical and Engineering Sciences*, 376(2134):20170447, 2018.

[61] V. V. Yakovlev. Examination of contemporary electromagnetic software capable of modeling problems of microwave heating. In M. Willert-Porada, editor, *Advances in Microwave and Radio Frequency Processing*, volume 19, pages 178–190. Springer Berlin Heidelberg, Berlin, Heidelberg, 2006. ISBN 978-3-540-43252-4. doi: 10.1007/978-3-540-32944-2_20.

[62] W. Wang, S. Zhang, Y. Pan, J. Yang, Y. Tang, and G. Chen. Multiphysics modeling for microwave freeze-drying of initially porous frozen material assisted by wave-absorptive medium. *Industrial & Engineering Chemistry Research*, 59(47):20903–20915, 2020. ISSN 0888-5885. doi: 10.1021/acs.iecr.0c03852.

[63] Z. Tang, S. Zhang, T. Hong, H. Zhu, and K. Huang. Frequency–selected microwave heating: Its mathematical physics basis and characteristics. *International Journal of RF and Microwave Computer-Aided Engineering*, 30(4): 24, 2020. ISSN 1096-4290. doi: 10.1002/mmce.22131.

[64] A. Więckowski, P. Korpas, M. Krysicki, F. Dughiero, M. Bullo, F. Bressan, and C. Fager. Efficiency optimization for phase controlled multi-source microwave oven. *International Journal of Applied Electromagnetics and Mechanics*, 44(2):235–241, 2014. ISSN 13835416. doi: 10.3233/JAE-141764.

[65] S.-H. Ahn, C.-H. Jeong, D.-M. Lim, and W.-S. Lee. Kilowatt-level power-controlled microwave applicator with multiple slotted waveguides for improving heating uniformity. *IEEE Transactions on Microwave Theory and Techniques*, 68(7):2867–2875, 2020. ISSN 00189480. doi: 10.1109/TMTT.2020.2977645.

[66] Dassault Systèmes SE. Cst studio suite 2020 help, 2019.

[67] X. Cao, M. Zhang, A. S. Mujumdar, Q. Zhong, and Z. Wang. Effect of microwave freeze drying on quality and energy supply in drying of barley grass. *Journal of the Science of Food and Agriculture*, 98(4):1599–1605, 2018. doi: 10.1002/jsfa.8634.

[68] J. H. Gitter, R. Geidobler, I. Presser, and G. Winter. Significant drying time reduction using microwave-assisted freeze-drying for a monoclonal antibody. *Journal of Pharmaceutical Sciences*, 107(10):2538–2543, 2018. doi: 10.1016/j.xphs.2018.05.023.

[69] J. H. Gitter, R. Geidobler, I. Presser, and G. Winter. Microwave-assisted freeze-drying of monoclonal antibodies: Product quality aspects and storage stability. *Pharmaceutics*, 11(12), 2019. ISSN 1999-4923. doi: 10.3390/pharmaceutics11120674.

[70] H. Wang, X. Duan, L. Duan, and G. Ren. Mutual transformation of the water binding state and moisture diffusion characteristics of chinese yams during microwave freeze drying. *Drying Technology*, 39(1):66–76, 2020. doi: 10.1080/07373937.2019.1693400.

[71] J. Park, J. H. Cho, and R. D. Braatz. Mathematical modeling and analysis of microwave-assisted freeze-drying in biopharmaceutical applications. *Computers and Chemical Engineering*, 153:107412, 2021. doi: 10.1016/j.compchemeng.2021.107412.

[72] I. Kalinke and U. Kulozik. Irreversible thermochromic ink in the identification of over- and under-processed product segments in microwave-assisted freeze drying. *Journal of Food Engineering*, 349:111470, 2023. ISSN 02608774. doi: 10.1016/j.jfoodeng.2023.111470.

[73] S. Zhang, Y. Pan, W. Wang, and R. Lin. Microwave freeze-drying of coffee solution frozen with initial pores assisted by wave-absorbing medium. *Drying Technology*, 41(3):419–433, 2023. doi: 10.1080/07373937.2022.2095399.

[74] S. Abbasi and S. Azari. Novel microwave-freeze drying of onion slices. *International Journal of Food Science & Technology*, 44(5):974–979, 2009. ISSN 09505423. doi: 10.1111/j.1365-2621.2008.01774.x.

[75] S. A. Goldblith. Basic principles of microwaves and recent developments. *Advances in food research*, 15:277–301, 1966. ISSN 0065-2628. doi: 10.1016/s0065-2628(08)60082-8.

[76] C. Ratti. Freeze–drying process design. In *Ahmed, S. R. (Hg.) 2012 – Handbook of Food Process Design*, pages 621–647. Blackwell Publishing Ltd, 2012. doi: 10.1002/9781444398274.CH22.

[77] X. Duan, M. Zhang, X. Li, and A. S. Mujumdar. Microwave freeze drying of sea cucumber coated with nanoscale silver. *Drying Technology*, 26(4): 413–419, 2008. doi: 10.1080/07373930801929136.

[78] H. Feng, J. Tang, and R. P. Cavalieri. Dielectric properties of dehydrated apples as affected by moisture and temperature. *Transactions of the American Society of Agricultural Engineers*, 45(1), 2002. doi: 10.13031/2013.7855.

[79] A. E. Drouzas and H. Schubert. Microwave application in vacuum drying of fruits. *Journal of Food Engineering*, 28(2):203–209, 1996. ISSN 02608774. doi: 10.1016/0260-8774(95)00040-2.

[80] J. C. Atuonwu and S. A. Tassou. Energy issues in microwave food processing: A review of developments and the enabling potentials of solid-state power delivery. *Critical Reviews in Food Science and Nutrition*, 59(9):1392–1407, 2019. doi: 10.1080/10408398.2017.1408564.

[81] K. Knoerzer, M. Regier, and H. Schubert. Measuring temperature distributions during microwave processing. In *The Microwave Processing of Foods*, pages 327–349. Elsevier, 2017. ISBN 9780081005286. doi: 10.1016/B978-0-08-100528-6.00015-2.

[82] T. Durance and P. Yaghmaee. Microwave dehydration of food and food ingredients. In *Comprehensive Biotechnology*, volume 22, pages 617–628. Elsevier, 2011. ISBN 9780080885049. doi: 10.1016/B978-0-08-088504-9.00306-8.

[83] W. Chen, B. Gutmann, and C. O. Kappe. Characterization of microwave-induced electric discharge phenomena in metal-solvent mixtures. *ChemistryOpen*, 1(1):39–48, 2012. ISSN 2191-1363. doi: 10.1002/open.201100013.

[84] Friedrich Paschen. Ueber die zum funkenübergang in luft, wasserstoff und kohlensäure bei verschiedenen drucken erforderliche potentialdifferenz. *Annalen der Physik*, 273(5):69–96, 1889. ISSN 00033804. doi: 10.1002/andp.18892730505.

[85] Leonid Babich and Tat'yana V. Loiko. Generalized paschen's law for overvoltage conditions. *IEEE Transactions on Plasma Science*, 44(12):3243–3248, 2016. ISSN 0093-3813. doi: 10.1109/TPS.2016.2629022.

[86] J. Sun, W. Wang, Q. Yue, C. Ma, J. Zhang, X. Zhao, and Z. Song. Review on microwave–metal discharges and their applications in energy and industrial processes. *Applied Energy*, 175:141–157, 2016. ISSN 03062619. doi: 10.1016/j.apenergy.2016.04.091.

[87] N. Härdter, R. Geidobler, I. Presser, and G. Winter. Microwave-assisted freeze-drying: Impact of microwave radiation on the quality of high-concentration antibody formulations. *Pharmaceutics*, 15(12), 2023. ISSN 1999-4923. doi: 10.3390/pharmaceutics15122783.

[88] A. Abdelraheem, R. Tukra, P.. Kazarin, M. D. Sinanis, E. M. Topp, A. Alexeenko, and D. Peroulis. Statistical electromagnetics for industrial pharmaceutical lyophilization. *PNAS Nexus*, 1(3):pgac052, 2022. doi: 10.1093/pnasnexus/pgac052.

[89] Z. H. Wang and M. H. Shi. Microwave freeze drying characteristics of beef. *Drying Technology*, 17(3):434–447, 1999. doi: 10.1080/07373939908917544.

[90] R. Wang, M. Zhang, A. S. Mujumdar, and J.-C. Sun. Microwave freeze–drying characteristics and sensory quality of instant vegetable soup. *Drying Technology*, 27(9):962–968, 2009. doi: 10.1080/07373930902902040.

[91] H. Jiang, M. Zhang, and A. S. Mujumdar. Microwave freeze-drying characteristics of banana crisps. *Drying Technology*, 28(12):1377–1384, 2010. doi: 10.1080/07373937.2010.482702.

[92] H. Jiang, M. Zhang, Y. Liu, A. S. Mujumdar, and H. Liu. The energy consumption and color analysis of freeze/microwave freeze banana chips. *Food and Bioproducts Processing*, 91(4):464–472, 2013. ISSN 09603085. doi: 10.1016/j.fbp.2013.04.004.

[93] M. Mumenthaler and H. Leuenberger. Atmospheric spray-freeze drying: a suitable alternative in freeze-drying technology. *International Journal of Pharmaceutics*, 72(2):97–110, 1991. ISSN 03785173. doi: 10.1016/0378-5173(91)90047-R.

[94] E. Pert, Y. Carmel, A. Birnboim, T. Olorunyolemi, D. Gershon, J. Calame, I. K. Lloyd, and O. C. Wilson. Temperature measurements during microwave processing: The significance of thermocouple effects. *Journal of the American Ceramic Society*, 84(9):1981–1986, 2001. ISSN 0002-7820. doi: 10.1111/j.1151-2916.2001.tb00946.x.

[95] R. Pisano. Automatic control of a freeze-drying process: Detection of the end point of primary drying. *Drying Technology*, 40(1):140–157, 2020. doi: 10.1080/07373937.2020.1774891.

[96] S. M. Patel, T. Doen, and M. J. Pikal. Determination of end point of primary drying in freeze-drying process control. *AAPS PharmSciTech*, 11(1):73–84, 2010. doi: 10.1208/s12249-009-9362-7.

[97] A. Kharaghani, E. Tsotsas, C. Wolf, T. Beutler, M. Guttzeit, and G.-W. Oetjen. Freeze-drying. In *Ullmann's Encyclopedia of Industrial Chemistry*, volume 14, pages 1–47. Wiley-VCH Verlag GmbH & Co. KGaA, Weinheim, Germany, 2000. ISBN 9783527306732. doi: 10.1002/14356007.h12_h01.pub2.

[98] I. C. Hunter. *Theory and design of microwave filters*, volume 48 of *IET electromagnetic waves series*. Institution of Engineering and Technology, London, reprint with new cover edition, 2006. ISBN 0852967772.

[99] K. Jousten. On the gas species dependence of pirani vacuum gauges. *Journal of Vacuum Science & Technology A: Vacuum, Surfaces, and Films*, 26(3): 352–359, 2008. ISSN 0734-2101. doi: 10.1116/1.2897314.

[100] F. Martín. *Artificial transmission lines for RF and microwave applications*. Wiley series in microwave and optical engineering. Wiley, Hoboken, New Jersey, 2015. ISBN 1118487605.

[101] C. S. Song, J. H. Nam, C.-J. Kim, and S. T. Ro. Temperature distribution in a vial during freeze-drying of skim milk. *Journal of Food Engineering*, 67 (4):467–475, 2005. ISSN 02608774. doi: 10.1016/j.jfoodeng.2004.04.041.

[102] A. Wexler. Vapor pressure formulation for ice. *Journal of Research of the National Bureau of Standards. Section A, Physics and Chemistry*, 81A(1): 5–20, 1977. doi: 10.6028/jres.081A.003.

[103] W. J. Coumans, P.J.A.M. Kerkhof, and S. Bruin. Theoretical and practical aspects of aroma retention in spray drying and freeze drying. *Drying Technology*, 12(1-2):99–149, 1994. doi: 10.1080/07373939408959951.

[104] X. Duan, X. Yang, G. Ren, Y. Pang, L. Liu, and Y. Liu. Technical aspects in freeze-drying of foods. *Drying Technology*, 34(11):1271–1285, 2016. doi: 10.1080/07373937.2015.1099545.

[105] T. M. Lin, T. D. Durance, and C. H. Scaman. Characterization of vacuum microwave, air and freeze dried carrot slices. *Food Research International*, 31(2):111–117, 1998. doi: 10.1016/S0963-9969(98)00070-2.

[106] S. A. Velardi and A. A. Barresi. Development of simplified models for the freeze-drying process and investigation of the optimal operating conditions. *Chemical Engineering Research and Design*, 86(1):9–22, 2008. doi: 10.1016/j.cherd.2007.10.007.

[107] R. Wang, M. Zhang, and A. S. Mujumdar. Effects of vacuum and microwave freeze drying on microstructure and quality of potato slices. *Journal of Food Engineering*, 101(2):131–139, 2010. ISSN 02608774. doi: 10.1016/j.jfoodeng.2010.05.021.

[108] Y. H. Ma and P. R. Peltre. Freeze dehydration by microwave energy: Part i. theoretical investigation. *AIChE Journal*, 21(2):335–344, 1975. doi: 10.1002/aic.690210215.

[109] Y. H. Ma and P. R. Peltre. Freeze dehydration by microwave energy: Part ii. experimental study. *AIChE Journal*, 21(2):344–350, 1975. doi: 10.1002/aic.690210216.

[110] Y. Wang, M. Zhang, A.. S. Mujumdar, and K. J. Mothibe. Microwave-assisted pulse-spouted bed freeze-drying of stem lettuce slices—effect on product quality. *Food and Bioprocess Technology*, 6(12):3530–3543, 2013. ISSN 1935-5130. doi: 10.1007/s11947-012-1017-0.

[111] H. Jiang, M. Zhang, A. S. Mujumdar, and R.-X. Lim. Drying uniformity analysis of pulse-spouted microwave–freeze drying of banana cubes. *Drying Technology*, 34(5):539–546, 2016. doi: 10.1080/07373937.2015.1061000.

[112] W. Wang, S. Zhang, Y. Pan, Y. Tang, and G. Chen. Wave-absorbing material aided microwave freeze-drying of vitamin c solution frozen with preformed pores. *Drying Technology*, 51:1–14, 2020. doi: 10.1080/07373937.2020.1752229.

[113] K. Witkiewicz and J. F. Nastaj. Simulation strategies in mathematical modeling of microwave heating in freeze-drying process. *Drying Technology*, 28(8):1001–1012, 2010. doi: 10.1080/07373937.2010.497090.

[114] Z. Y. Li, R. F. Wang, and T. Kudra. Uniformity issue in microwave drying. *Drying Technology*, 29(6):652–660, 2011. doi: 10.1080/07373937.2010.521963.

[115] C. Bianchi, P. Bonato, F. Dughiero, and P. Canu. Enhanced power density uniformity for microwave catalytic reactions adopting solid-state generators: Comparison with magnetron technology. *Chemical Engineering and Processing: Process Intensification*, 120:286–300, 2017. doi: 10.1016/j.cep.2017.07.006.

[116] J. Zhou, Y. Li, N. Li, S. Liu, L. Cheng, S. Sui, and J. Gao. A multi-pattern compensation method to ensure even temperature in composite materials during microwave curing process. *Composites Part A: Applied Science and Manufacturing*, 107(3):10–20, 2018. ISSN 1359835X. doi: 10.1016/j.compositesa.2017.12.017.

[117] L. C. Capozzi, A. A. Barresi, and R. Pisano. Supporting data and methods for the multi-scale modelling of freeze-drying of microparticles in packed-beds. *Data in Brief*, 22:722–755, 2019. doi: 10.1016/j.dib.2018.12.061.

[118] V. Chaurasiya and J. Singh. An analytical study of coupled heat and mass transfer freeze-drying with convection in a porous half body: A moving boundary problem. *Journal of Energy Storage*, 55(100664):105394, 2022. doi: 10.1016/j.est.2022.105394.

[119] P. G. Huray. *Maxwell's equations*. Wiley, Hoboken, N.J, online-ausg edition, 2010. ISBN 978-0-470-54276-7. URL `http://site.ebrary.com/lib/alltitles/Doc?id=10512895`.

[120] Y. Guan and Y. Nikawa. Measurement of temperature-dependent complex permittivity for materials using cylindrical resonator under microwave irradiation. *Electronics and Communications in Japan*, 90(11):1–8, 2007. ISSN 8756663X. doi: 10.1002/ecjb.20346.

[121] S. Curet, O. Rouaud, and L. Boillereaux. Microwave tempering and heating in a single-mode cavity: Numerical and experimental investigations. *Chemical Engineering and Processing: Process Intensification*, 47(9-10):1656–1665, 2008. doi: 10.1016/j.cep.2007.09.011.

[122] L. Riedel. A test substance for freezing experiments. *Kältetechnik*, 12(8): 222–225, 1960.

[123] C. Deep, A. K. Pratihar, and M. K. Sharma. Freezing time-temperature behavior and parametric study of cylindrical shaped tylose gel samples: A numerical and experimental study. *Thermal Science and Engineering Progress*, 24:100933, 2021. ISSN 24519049. doi: 10.1016/j.tsep.2021.100933.

[124] U. Kaatze and V. Uhlendorf. The dielectric properties of water at microwave frequencies. *Zeitschrift für Physikalische Chemie*, 126(2):151–165, 1981. ISSN 0942-9352. doi: 10.1524/zpch.1981.126.2.151.

[125] C. Matzler and U. Wegmuller. Dielectric properties of freshwater ice at microwave frequencies. *Journal of Physics D: Applied Physics*, 20(12):1623–1630, 1987. ISSN 0003-6935. doi: 10.1088/0022-3727/20/12/013.

[126] M. Chamchong and A. K. Datta. Thawing of foods in a microwave oven: I. effect of power levels and power cycling. *Journal of Microwave Power and Electromagnetic Energy*, 34(1):9–21, 1999. ISSN 0832-7823. doi: 10.1080/08327823.1999.11688384.

[127] R. Wang, M. Zhang, A. S. Mujumdar, and H. Jiang. Effect of salt and sucrose content on dielectric properties and microwave freeze drying behavior of re-structured potato slices. *Journal of Food Engineering*, 106(4):290–297, 2011. ISSN 02608774. doi: 10.1016/j.jfoodeng.2011.05.015.

[128] J. Marti and K. Mauersberger. A survey and new measurements of ice vapor pressure at temperatures between 170 and 250k. *Geophysical Research Letters*, 20(5):363–366, 1993. ISSN 00948276. doi: 10.1029/93GL00105.

[129] Z. Du, Z. Wu, W. Gan, G. Liu, X. Zhang, J. Liu, and B. Zeng. Multiphysics modeling and process simulation for a frequency-shifted solid-state

source microwave oven. *IEEE Access*, 7:184726–184733, 2019. doi: 10.1109/ACCESS.2019.2960317.

[130] K. Pitchai, S. L. Birla, J. Subbiah, D. Jones, and H. Thippareddi. Coupled electromagnetic and heat transfer model for microwave heating in domestic ovens. *Journal of Food Engineering*, 112(1-2):100–111, 2012. ISSN 02608774. doi: 10.1016/j.jfoodeng.2012.03.013.

[131] I. Polaert, A. Ledoux, L. Estel, R. Huyghe, and M. Thomas. Microwave assisted regeneration of zeolite. *International Journal of Chemical Reactor Engineering*, 5(1):A117, 2007. doi: 10.2202/1542-6580.1436.

[132] C. Antonio and R. T. Deam. Comparison of linear and non-linear sweep rate regimes in variable frequency microwave technique for uniform heating in materials processing. *Journal of Materials Processing Technology*, 169(2): 234–241, 2005. ISSN 09240136. doi: 10.1016/j.jmatprotec.2005.03.024.

[133] L. Ma, D.-L. Paul, N. Pothecary, C. Railton, J. Bows, L. Barratt, J. Mullin, and D. Simons. Experimental validation of a combined electromagnetic and thermal fdtd model of a microwave heating process. *IEEE Transactions on Microwave Theory and Techniques*, 43(11):2565–2572, 1995. ISSN 00189480. doi: 10.1109/22.473179.

[134] F. Bressan, F. Dughiero, M. Bullo, and P. Di Barba. Efficiency optimization of a two-port microwave oven: a robust automated procedure. *The International Journal for Computation and Mathematics in Electrical and Electronic Engineering*, 34(4):1213–1228, 2015. ISSN 0332-1649. doi: 10.1108/COMPEL-05-2014-0109.

[135] R. Yang, A. E. Fathy, M. T. Morgan, and J. Chen. Development of online closed-loop frequency shifting strategies to improve heating performance of foods in a solid-state microwave system. *Food Research International*, 154: 110985, 2022. doi: 10.1016/j.foodres.2022.110985.

[136] L.-l. Huang, M. Zhang, A. S. Mujumdar, and R.-X. Lim. Comparison of four drying methods for re-structured mixed potato with apple chips. *Journal*

of Food Engineering, 103(3):279–284, 2011. ISSN 02608774. doi: 10.1016/j.jfoodeng.2010.10.025.

[137] T. Sickert, I. Kalinke, J. Christoph, and V. Gaukel. Microwave-assisted freeze-drying with frequency-based control concepts via solid-state generators: A simulative and experimental study. *Processes*, 11(2):327, 2023. doi: 10.3390/pr11020327.

[138] H. Feng, J. Tang, R. P. Cavalieri, and O. A. Plumb. Heat and mass transport in microwave drying of porous materials in a spouted bed. *AIChE Journal*, 47(7):1499–1512, 2001. doi: 10.1002/aic.690470704.

[139] F. Yang, W. Wang, B. Yan, T. Hong, Y. Yang, H. Zhu, L. Wu, and K. Huang. Sweep frequency heating based on injection locked magnetron. *Processes*, 7 (6):341, 2019. doi: 10.3390/pr7060341.

[140] X. Zhou, Z. Tang, P. D. Pedrow, S. S. Sablani, and J. Tang. Microwave heating based on solid-state generators: New insights into heating pattern, uniformity, and energy absorption in foods. *Journal of Food Engineering*, 357:111650, 2023. ISSN 02608774. doi: 10.1016/j.jfoodeng.2023.111650.

[141] M. K. Krokida, V. T. Karathanos, and Z. B. Maroulis. Effect of freeze-drying conditions on shrinkage and porosity of dehydrated agricultural products. *Journal of Food Engineering*, 35(4):369–380, 1998. ISSN 02608774. doi: 10.1016/S0260-8774(98)00031-4.

[142] S. Rambhatla and M. J. Pikal. Heat and mass transfer scale-up issues during freeze-drying, i: atypical radiation and the edge vial effect. *AAPS PharmSciTech*, 4(2):E14, 2003. doi: 10.1208/pt040214.

[143] S. P. Morgan. Effect of surface roughness on eddy current losses at microwave frequencies. *Journal of Applied Physics*, 20(4):352–362, 1949. ISSN 0021-8979. doi: 10.1063/1.1698368.

[144] A. E. Drouzas, E. Tsami, and G. D. Saravacos. Microwave/vacuum drying of model fruit gels. *Journal of Food Engineering*, 39(2):117–122, 1999. ISSN 02608774. doi: 10.1016/S0260-8774(98)00133-2.

[145] J. Dumpler and C. I. Moraru. Microwave vacuum drying of dairy cream: processing, reconstitution, and whipping properties of a novel dairy product. *Journal of Dairy Science*, 2023. doi: 10.3168/jds.2023-23657.

[146] X. Zhou, S. Zhang, Z. Tang, J. Tang, and P. S. Takhar. Microwave frying and post-frying of french fries. *Food Research International*, 159:111663, 2022. doi: 10.1016/j.foodres.2022.111663.

[147] Y. Hasegawa, K. Nakamura, D. Lubomirsky, S. Park, S. Kobayashi, and H. Sugai. Microwave plasma generation by the fast rotation and slow pulsation of resonant fields in a cylindrical cavity. *Japanese Journal of Applied Physics*, 56(4):046203, 2017. ISSN 0021-4922. doi: 10.7567/JJAP.56.046203.

[148] S. Tsubaki, Y. Nakasako, N. Ohara, M. Nishioka, S. Fujii, and Y. Wada. Ultra-fast pyrolysis of lignocellulose using highly tuned microwaves: synergistic effect of a cylindrical cavity resonator and a frequency-auto-tracking solid-state microwave generator. *Green Chemistry*, 22(2):342–351, 2020. ISSN 1463-9262. doi: 10.1039/c9gc02745a.

[149] R. Yang, M. Morgan, A. Fathy, C. Luckett, Z. Wang, and J. Chen. A comprehensive evaluation of microwave reheating performance using dynamic complementary-frequency shifting strategy in a solid-state system. *Food and Bioprocess Technology*, 16(5):1061–1075, 2023. ISSN 1935-5130. doi: 10.1007/s11947-022-02974-2.

[150] T. Sickert, R. Bergmann, J. Christoph, and V. Gaukel. A time-saving approach to parameter studies in microwave-assisted freeze drying. *Processes*, 11(10):2886, 2023. doi: 10.3390/pr11102886.

[151] C. Straube, J. Meyer, and A. Dittler. Identification of deposited oil structures on thin porous oil mist filter media applying µ-ct imaging technique. *Separations*, 8(10):193, 2021. doi: 10.3390/separations8100193.

[152] R. Ballentine. Determination of ascorbic acid in citrus fruit juices. *Industrial & Engineering Chemistry Analytical Edition*, 13(2):89, 1941. ISSN 0096-4484. doi: 10.1021/i560090a011.

[153] W. Wang, C. Zhao, J. Sun, X. Wang, X. Zhao, Y. Mao, X. Li, and Z. Song. Quantitative measurement of energy utilization efficiency and study of influence factors in typical microwave heating process. *Energy*, 87:678–685, 2015. ISSN 03605442. doi: 10.1016/j.energy.2015.05.036.

[154] T. Siebert, M. Zuber, E. Hamann, T. Baumbach, H. P. Karbstein, and V. Gaukel. Micro-ct visualization of structure development during freeze-drying processes. *Drying Technology*, 38(3):376–384, 2020. doi: 10.1080/07373937.2019.1572619.

[155] T. Gulati and A. K. Datta. Coupled multiphase transport, large deformation and phase transition during rice puffing. *Chemical Engineering Science*, 139: 75–98, 2016. ISSN 00092509. doi: 10.1016/j.ces.2015.08.057.

[156] K. Zou, J. Teng, L. Huang, X. Dai, and B. Wei. Effect of osmotic pretreatment on quality of mango chips by explosion puffing drying. *LWT - Food Science and Technology*, 51(1):253–259, 2013. ISSN 00236438. doi: 10.1016/j.lwt.2012.11.005.

[157] I. Saguy, I. J. Kopelman, and S. Mizrahi. Simulation of ascorbic acid stability during heat processing and concentration of grapefruit juice. *Journal of Food Process Engineering*, 2(3):213–225, 1978. ISSN 01458876. doi: 10.1111/j.1745-4530.1978.tb00208.x.

[158] H. Jiang, M. Zhang, A. S. Mujumdar, and R.-X. Lim. Comparison of drying characteristic and uniformity of banana cubes dried by pulse-spouted microwave vacuum drying, freeze drying and microwave freeze drying. *Journal of the Science of Food and Agriculture*, 94(9):1827–1834, 2014. doi: 10.1002/jsfa.6501.

[159] M. Szultka, M. Buszewska-Forajta, R. Kaliszan, and B. Buszewski. Determination of ascorbic acid and its degradation products by high-performance liquid chromatography-triple quadrupole mass spectrometry. *Electrophoresis*, 35(4):585–592, 2014. doi: 10.1002/elps.201300439.

[160] B. Gómez Ruiz, S. Roux, F. Courtois, and C. Bonazzi. Kinetic modelling of ascorbic and dehydroascorbic acids concentrations in a model solution at different temperatures and oxygen contents. *Food Research International*, 106:901–908, 2018. doi: 10.1016/j.foodres.2018.01.051.